UNIVERSITY OF TURKU

EVALUATION OF ^{68}GA-LABELED PET RADIOPHARMACEUTICALS FOR IMAGING OF $\alpha_V\beta_3$ INTEGRIN AND VASCULAR ADHESION PROTEIN-1 IN INFLAMMATION AND CANCER

Riikka Viitanen née Siitonen

TURUN YLIOPISTON JULKAISUJA – ANNALES UNIVERSITATIS TURKUENSIS
SARJA - SER. D OSA - TOM. 1533 | MEDICA - ODONTOLOGICA | TURKU 2021

UNIVERSITY OF TURKU

EVALUATION OF ^{68}GA-LABELED PET RADIOPHARMACEUTICALS FOR IMAGING OF $\alpha_v\beta_3$ INTEGRIN AND VASCULAR ADHESION PROTEIN-1 IN INFLAMMATION AND CANCER

Riikka Viitanen née Siitonen

TURUN YLIOPISTON JULKAISUJA – ANNALES UNIVERSITATIS TURKUENSIS
SARJA – SER. D OSA – TOM. 1533 | MEDICA – ODONTOLOGICA | TURKU 2021

University of Turku

Faculty of Medicine
Department of Clinical Physiology and Nuclear Medicine
Drug Research Doctoral Programme
Turku PET Centre

Supervised by

Professor Anne Roivainen, PhD
Turku PET Centre and
Turku Center for Disease Modeling
University of Turku
Turku, Finland

Academician Sirpa Jalkanen, MD, PhD
MediCity Research Laboratory
University of Turku
Turku, Finland

Reviewed by

Assistant Professor Olof Eriksson, PhD
Department of Medicinal Chemistry
Uppsala University, Sweden

Adjunct Professor Mirkka Sarparanta, PhD
Department of Chemistry
University of Helsinki, Finland

Opponent

Head Physician Johanna Huhtakangas, MD, PhD
Department of Rheumatology
Kuopio University Hospital, Finland

ISBN 978-951-29-8359-9 (PRINT)
ISBN 978-951-29-8360-5 (PDF)
ISSN 0355-9483 (Print)
ISSN 2343-3213 (Online)
Painosalama Oy, Turku, Finland 2021

To my family

UNIVERSITY OF TURKU
Faculty of Medicine
Clinical Physiology and Nuclear Medicine
RIIKKA VIITANEN née SIITONEN: Evaluation of ^{68}Ga-labeled PET radiopharmaceuticals for imaging of $\alpha_v\beta_3$ integrin and vascular adhesion protein-1 in inflammation and cancer
Doctoral Dissertation, 134 pp.
Drug Research Doctoral Programme (DRDP)
February 2021

ABSTRACT

Inflammation is involved in the pathogenesis of several chronic diseases as well as in the development of cancer. Vascular adhesion protein-1 (VAP-1) is an inflammation inducible endothelial adhesion molecule that participates in the leukocyte extravasation from blood to sites of inflammation. Under normal conditions, VAP-1 is absent on the surface of endothelium but, upon inflammation, is rapidly translocated from intracellular storage granules to the endothelial cell surface. Sialic acid-binding immunoglobulin-like lectin 9 (Siglec-9) is a leukocyte ligand of VAP-1 and the [^{68}Ga]Ga-DOTA-Siglec-9 is a promising positron emission tomography (PET) radiopharmaceutical for the imaging of inflammation. Another adhesion molecule, $\alpha_v\beta_3$ integrin, is overexpressed in angiogenic endothelial cells, and is therefore considered a target for the imaging of angiogenesis in tumors and inflammatory diseases.

The aim of the studies included in this thesis was 1) to evaluate the feasibility of [^{68}Ga]Ga-DOTA-Siglec-9 for the imaging of inflammation in mouse models of arthritis and melanoma, and 2) to explore its safety, whole-body distribution, and radiation dosimetry in healthy subjects as well as its ability to detect arthritis in a patient with rheumatoid arthritis. In mouse melanoma studies, in addition to VAP-1, $\alpha_v\beta_3$ integrin activation was studied using [^{68}Ga]Ga-DOTA-E[c(RGDfK)]$_2$. The *in vivo* PET imaging, *ex vivo* gamma counting, tissue autoradiography, and histological and immunohistochemical stainings were utilized in these studies. Dynamic PET/computed tomography (CT) imaging with concurrent blood sampling clarified the whole-body distribution kinetics, targeting, and radiation exposure of [^{68}Ga]Ga-DOTA-Siglec-9 in humans.

The results showed that [^{68}Ga]Ga-DOTA-Siglec-9 clearly detected inflammation in the mouse arthritis and melanoma models, and longitudinal PET/CT allowed the monitoring of disease development over time. In mouse melanoma, [^{68}Ga]Ga-DOTA-E[c(RGDfK)]$_2$ detected changes of $\alpha_v\beta_3$ integrin expression and activity. In humans, the [^{68}Ga]Ga-DOTA-Siglec-9 was safe and well-tolerated, and capable of detecting arthritic joints. In conclusion, these preclinical and clinical studies indicate that [^{68}Ga]Ga-DOTA-Siglec-9 is a promising new PET radiopharmaceutical for imaging inflammation. In the future, [^{68}Ga]Ga-DOTA-Siglec-9 PET may have potential for imaging various inflammatory diseases besides rheumatoid arthritis.

KEYWORDS: inflammation, cancer, positron emission tomography, VAP-1, Siglec-9

TURUN YLIOPISTO
Lääketieteellinen tiedekunta
Kliininen fysiologia ja isotooppilääketiede
RIIKKA VIITANEN o.s. SIITONEN: ^{68}Ga-leimattujen PET radiolääkeaineiden arviointi $\alpha_v\beta_3$ integriinin ja VAP-1 molekyylin kuvantamiseksi tulehduksessa ja syövässä
Väitöskirja, 134 s.
Lääketutkimuksen tohtoriohjelma (DRDP)
Helmikuu 2021

TIIVISTELMÄ

Tulehdus liittyy useiden kroonisten sairauksien sekä syövän kehittymiseen. Verisuonen endoteelisolujen pinnalla esiintyvä VAP-1 on tulehduksen indusoima tartuntamolekyyli, joka osallistuu valkosolujen siirtämiseen verenkierrosta tulehduspaikoille. Normaali olosuhteissa VAP-1 puuttuu verisuonen pinnalta, mutta tulehduksen seurauksena se siirtyy solunsisäisistä säilytysjyväsistä endoteelisolun pinnalle. Siglec-9 on valkosolujen pinnalla oleva VAP-1:n vastinmolekyyli ja [^{68}Ga]Ga-DOTA-Siglec-9 peptidi on lupaava merkkiaine tulehduksen kuvantamiseen positroniemissiotomografialla (PET). Toinen tartuntamolekyyli, $\alpha_v\beta_3$-integriini, yli-ilmentyy uudisverisuonten endoteelisoluissa, jonka vuoksi sitä voidaan käyttää uudisverisuonten muodostumisen kuvantamiseen kasvaimissa ja tulehdussairauksissa.

Väitöskirjatutkimuksen tarkoituksena oli 1) tutkia [^{68}Ga]Ga-DOTA-Siglec-9:n soveltuvuutta tulehduksen kuvantamiseen hiiren niveltulehdus- ja melanoomamalleissa sekä 2) tutkia [^{68}Ga]Ga-DOTA-Siglec-9:n turvallisuutta, kokokehojakaumaa ja säteilyaltistumista terveillä vapaaehtoisilla ja kykyä havaita niveltulehdus nivelreumapotilaalla. Lisäksi hiiren melanoomatutkimuksissa tutkittiin $\alpha_v\beta_3$ integriiniaktiivisuutta [^{68}Ga]Ga-DOTA-E[c(RGDfK)]$_2$:lla. Tutkimusmenetelminä käytettiin *in vivo* PET-kuvantamista, *ex vivo* -gammamittausta, autoradiografiaa sekä histologisia ja immunohistokemiallisia värjäyksiä. PET/tietokonetomografia (TT) -kuvantamisella selvitettiin [^{68}Ga]Ga-DOTA-Siglec-9:n kokokehojakautumista, VAP-1 molekyyliin kohdentumista ja säteilyaltistumista ihmisillä.

Tutkimustulokset osoittivat, että [^{68}Ga]Ga-DOTA-Siglec-9 pystyi havaitsemaan tulehduksen hiiren niveltulehdus- ja melanoomamalleissa, ja PET/TT-pitkäaikaisseuranta mahdollisti sairauden kehityksen seuraamisen. [^{68}Ga]Ga-DOTA-E[c(RGDfK)]$_2$ pystyi havaitsemaan $\alpha_v\beta_3$ integriinin ilmentymisen ja aktiivisuuden muutoksia melanoomamallissa. Ihmisillä [^{68}Ga]Ga-DOTA-Siglec-9 osoittautui turvalliseksi ja hyvin siedetyksi, ja se kykeni havaitsemaan niveltulehdukset. Yhteenvetona voidaan todeta, että nämä prekliiniset ja kliiniset tutkimukset osoittivat, että [^{68}Ga]Ga-DOTA-Siglec-9 on lupaava uusi PET-merkkiaine tulehduksen kuvantamiseen. Tulevaisuudessa [^{68}Ga]Ga-DOTA-Siglec-9 PET voi olla lupaava menetelmä kuvantamaan muitakin tulehduksellisia sairauksia nivelreuman lisäksi.

AVAINSANAT: tulehdus, syöpä, positroniemissiotomografia, VAP-1, Siglec-9

Table of Contents

Abbreviations

AOC	Amine oxidase copper containing
ARG	Autoradiography
CAO	Copper-containing amine oxidase
CD	Cluster of differentiation
CT	Computed tomography
DAMP	Damaged-associated molecular pattern
DIP	Distal interphalangeal joint
FAP	Fibroblast activation protein
FAPI	Fibroblast activation protein inhibitor
GMP	Good manufacturing practice
HE	Hematoxylin and eosin
HEPES	2-[4-(2-hydroxyethyl)piperazin-1-yl]ethanesulfonic acid
HEV	High endothelial venule
HIF1α	Hypoxia-inducible factor 1α
HPLC	High-performance liquid chromatography
ICAM-1	Intracellular adhesion molecule-1
IFNγ	Interferon-γ
IL	Interleukin
i.v.	Intravenous
JAM	Junctional adhesion molecule
LA	Lyme arthritis
LB	Lyme borreliosis
LFA-1	Lymphocyte function associated antigen-1
mAb	Monoclonal antibody
MAC-1	Macrophage-1 antigen
MEM	Modified Eagle medium
MRI	Magnetic resonance imaging
mRNA	Messenger RNA
NF-κB	Nuclear factor kappa-light-chain-enhancer of activated B cells
NK	Natural killer cell
PAMP	Pathogen-associated molecular pattern

PBS	Phosphate-buffered saline
PECAM-1	Platelet endothelial cell adhesion molecule-1
PET	Positron emission tomography
PID	Proximal interphalangeal joint
PSGL1	P-selectin glycoprotein ligand 1
RA	Rheumatoid arthritis
RGD	Arginyl-glycyl-aspartic acid
ROI	Region of interest
s.c.	Subcutaneous
SHARPIN	Shank-associated RH domain-interacting protein
Siglec	Sialic acid-binding immunoglobulin-like lectin
SPECT	Single photon emission computed tomography
SSAO	Semicarbazide-sensitive amine oxidase
SSTR	Somatostatin receptor
STAT3	Signal transducer and activator of transcription 3
SUV	Standardized uptake value
sVAP-1	Soluble vascular adhesion protein-1
T_{reg}	Regulatory T cell
TAM	Tumor-associated macrophage
TAN	Tumor-associated neutrophil
TIL	Tumor infiltrating lymphocyte
TME	Tumor microenvironment
TNF	Tumor necrosis factor
TPQ	Topaquinone
TSPO	Translocator protein
VAP-1	Vascular adhesion protein-1
VCAM-1	Vascular cell adhesion molecule-1
VLA-4	Very late antigen-4
VOI	Volume of interest
WBC	White blood cell

List of Original Publications

This dissertation is based on the following original publications, which are referred to in the text by their Roman numerals:

I Riikka Siitonen, Annukka Pietikäinen, Heidi Liljenbäck, Meeri Käkelä, Mirva Söderström, Sirpa Jalkanen, Jukka Hytönen, Anne Roivainen. Targeting of vascular adhesion protein-1 by positron emission tomography visualizes sites of inflammation in *Borrelia burgdorferi* -infected mice. *Arthritis Research & Therapy* 2017;19(1):254.

II Riikka Siitonen, Emilia Peuhu, Anu Autio, Heidi Liljenbäck, Elina Mattila, Olli Metsälä, Meeri Käkelä, Tiina Saanijoki, Ingrid Dijkgraaf, Sirpa Jalkanen, Johanna Ivaska, Anne Roivainen. ^{68}Ga-DOTA-E[c(RGDfK)]$_2$ PET imaging of SHARPIN-regulated integrin activity in mice. *Journal of Nuclear Medicine* 2019;60(10):1380–1387.

III Riikka Viitanen, Olli Moisio, Petteri Lankinen, Xiang-Guo Li, Mikko Koivumäki, Sami Suilamo, Tuula Tolvanen, Kirsi Taimen, Markku Mali, Ia Kohonen, Ilpo Koskivirta, Vesa Oikonen, Helena Virtanen, Kristiina Santalahti, Anu Autio, Antti Saraste, Laura Pirilä, Pirjo Nuutila, Juhani Knuuti, Sirpa Jalkanen, Anne Roivainen. First-in-human study of ^{68}Ga-DOTA-Siglec-9, PET ligand targeting vascular adhesion protein 1. *Journal of Nuclear Medicine* 2020 Aug 17. Published online ahead of print.

1 Introduction

Inflammation, including leukocyte infiltration, vascular changes, and increased blood flow, plays an important role during acute defense against pathogens and other inflammatory stimuli. However, uncontrolled and long-lasting inflammation can eventually lead to pathologic changes in tissues. Inflammation contributes to the pathogenesis of chronic diseases, such as rheumatoid arthritis, inflammatory bowel disease, and cardiovascular disease, and is involved in various steps of tumor development (Elinav et al., 2013; Guo et al., 2018; Libby, 2006; Zhang & Li, 2014). Many of these diseases are global health problems with increasing morbidity, which often leads to disability, increases both health care and non-health care related costs, and contributes to mortality (Jacobs et al., 2011). Early detection of inflammatory lesions is important for proper diagnosis and better opportunities for cost-effective treatment of these diseases.

Positron emission tomography (PET) provides a non-invasive method to explore inflammation in humans *in vivo* at molecular and cellular levels. Upon inflammatory stimuli, the release of proinflammatory mediators, increased vascular permeability with infiltrating leukocytes, increased tissue destruction, and attempts to heal are among the potential targets for visualizing inflammation. Glucose analog 2-deoxy-2-[^{18}F]-fluoro-*D*-glucose ([^{18}F]FDG) is the most extensively studied PET tracer in the field of oncology, which has shown to be a valuable tool for tumor detection, staging, restaging, radiation therapy planning, and therapy response monitoring (Boellaard et al., 2015). In addition to tumor detection, [^{18}F]FDG imaging is feasible for the detection of inflammation and infection, for example, in rheumatoid arthritis and chronic osteomyelitis, because the uptake of [^{18}F]FDG is based on increased glucose metabolism of inflammatory cells (Chaudhari et al., 2010; Guhlmann et al., 1998; Kubota et al., 2009). However, the major disadvantage of [^{18}F]FDG is that it is unable to distinguish metabolically active cells from each other (inflammatory cell vs. tumor cell) and can then cause false-positive results. The possibility to give false-positive results affects its usability. Additionally, the high background uptake in the heart and brain impairs the ability of [^{18}F]FDG to detect inflammatory lesions or tumors near these tissues. (Wu et al., 2013)

There are several approaches for PET imaging of immune cells, but novel inflammation specific imaging agents are needed. Leukocyte extravasation from blood to inflamed tissues is a crucial step in both acute and chronic inflammation. Targeting of endothelial adhesion molecules, which mediate leukocyte extravasation may provide a solution for a more inflammation specific PET tracer. Vascular adhesion protein-1 (VAP-1) is an endothelial adhesion molecule that contributes to leukocyte extravasation. A beneficial property of VAP-1 is that it is absent on the surface of endothelium under normal conditions but is rapidly translocated upon inflammation from intracellular storage granules to the endothelial cell surface. VAP-1 has also enzymatic activity that catalyzes the oxidative deamination of primary amines, and the end products of this reaction act as inflammation mediators (Salmi & Jalkanen, 2005). It is known that sialic acid-binding immunoglobulin-like lectin 9 (Siglec-9) is a leukocyte ligand of VAP-1 (Aalto et al., 2011). Moreover, several preclinical studies have shown that gallium-68-radiolabeled Siglec-9 motif containing peptide ([^{68}Ga]Ga-DOTA-Sigle-9) can be used for PET imaging of inflammation and cancer (Aalto et al., 2011; Ahtinen et al., 2014; Elo et al., 2018; Retamal et al., 2016; Silvola et al., 2016; Virtanen et al., 2015, 2017).

Integrins, cell adhesion molecules consisting of α and β subunits, are essential for cell migration and invasion. Integrins mediate adhesion to the extracellular matrix and regulate intracellular signaling pathways that control cytoskeletal organization, force generation and survival. Regulation of integrin activity is fundamentally important during development and in many physiological processes in adults. Shank-associated RH domain-interacting protein (SHARPIN) is an endogenous inhibitor of β_1-integrin activity that binds to integrin α-subunits and prevents interaction of activators to β-subunits. In addition, SHARPIN controls β_1-integrin dependent cell adhesion and migration in several normal and malignant cell types. (Bouvard et al., 2013; Desgrosellier &Cheresh, 2010; Rantala et al., 2011) The integrin $\alpha_v\beta_3$-targeting PET tracers, arginyl-glycyl-aspartic acid (RGD) peptides, provides information of $\alpha_v\beta_3$ integrin expression on the tumor vasculature because angiogenic endothelial cells express high levels of $\alpha_v\beta_3$ integrin whereas its expression is low in normal tissues (Dijkgraaf et al., 2007, 2011).

For this thesis, the novel VAP-1 targeting PET tracer, [^{68}Ga]Ga-DOTA-Siglec-9, was investigated for its feasibility to detect inflammation at an early stage of the disease and to monitor the progression of the disease in mouse models of arthritis and melanoma. In the SHARPIN deficient mouse model, we investigated how [^{68}Ga]Ga-DOTA-E[c(RGDfK)]$_2$ accumulated in inflamed areas and melanoma tumors, and how stromal SHARPIN regulated tumor growth, metastasis, and vascularization. In addition, the safety, whole-body distribution, metabolism, and radiation dosimetry of [^{68}Ga]Ga-DOTA-Siglec-9 was assessed, for the first time, in healthy subjects.

2 Review of the Literature

2.1 Inflammation

The hallmarks of acute inflammation are increased blood flow and vascular permeability, vasodilation, and infiltration of leukocytes to the inflamed tissue. (Kumar et al., 2017; Serhan et al., 2010) Inflammation is a biological response of human body to harmful stimuli, such as tissue damage or pathogens. As early as the first century CE, the classic four symptoms of inflammation were defined as *rubor* (redness), *calor* (heat), *dolor* (pain), and *tumor* (swelling). The fifth symptom of inflammation, *functio laesa* (loss of function), was later added to the list to improve the definition of inflammation. Today, we are well aware of the beneficial effects of inflammation and the required interaction of different molecular and cellular factors (Cavaillon & Singer, 2018). Every day human body is exposed to potentially harmful organisms that activate host defense mechanism. Immune response can be divided into innate and adaptive immune system. Innate immune system is activated immediately after recognition of pathogens by innate immune cells, such as neutrophils, and it leads to production of cytokines. If innate immune system fails to destroy the pathogen, adaptive immune system is activated. Adaptive immune system uses antigen-specific reactions through lymphocytes and forms immunological memory. This immunological memory provides long-lasting protection, which produce more robust response for subsequent exposure. (Parkin & Cohen, 2001)

The pathogenesis of inflammation is a complex system comprised of a wide range of biological processes, which needs inducers, sensors, mediators, and effectors to eliminate the original cause of cell injury and to initiate the tissue repair (Medzhitov, 2008). Inducers initiate the inflammation response and they can be divided into two categories: exogenous and endogenous. Exogenous inducers can be categorized as microbial and non-microbial factors. Microbial inducers include pathogen-associated molecular patterns (PAMPs), which originate from microorganisms, and virulence factors. Non-microbial inducers include allergens, irritants, foreign bodies, and toxic compounds. (Medzhitov, 2008; Varela et al., 2018) Endogenous inducers of inflammation are damage-associated molecular patterns (DAMPs) that are released by stressed, injured, or improperly functioning

tissue cells. These exogenous and endogenous signals stimulate the cells of the innate immune system, which then elicits the production and secretion of cytokines and other proinflammatory mediators. (Vestweber, 2015) Inflammatory mediators affect the vasculature and the recruitment of leukocytes by altering the functioning of many tissues. Generally, mediators are derived from plasma proteins or secreted by cells (Kumar et al., 2017). In some cases, mediators can be produced directly in response to specific stimulation by inflammatory inducers (Medzhitov, 2008).

Once initiated, the main purpose of the inflammatory response is to remove the source of disturbance, allow the host to adapt to the abnormal conditions, and finally, resolve the inflammation and restore the state of homeostasis in the tissue. Inflammation is divided into two types: acute and chronic inflammation. Acute inflammation involves a temporary source of disturbance and a rapid immune response. At an initial phase of acute inflammation, edema is formed by increased blood flow and leakage of water, salt and proteins from vasculature. Later, neutrophils migrate to the inflamed tissue, as a result of interactions between adhesion molecules on the vascular endothelium. The main purpose of acute inflammatory response is to restore the tissue to its preinjury state. (Kumar et al., 2017) Chronic inflammation refers to a slow, long-term inflammation lasting from several weeks or months to years. Generally, the chronic state follows when the inflammatory response fails to eliminate the initial stimuli, or chronic inflammation may begin without any signs of a prior acute reaction (Varela et al., 2018). Different from the hallmarks of acute inflammation, chronic inflammation is associated with infiltration of mononuclear cells (macrophages, lymphocytes and plasma cells), tissue damage and repair, vascular proliferation, and fibrosis (Kumar et al., 2017).

2.1.1 Leukocyte extravasation across inflamed endothelium

Normal immune responses are required in order to move the circulating leukocytes from blood into tissues. Leukocyte trafficking across the endothelium in inflamed or damaged tissues happens in veins (Nourshargh et al., 2010). Transmigration is an extremely controlled multistep process that utilizes adhesive interactions between leukocytes and endothelial cells. Several adhesion molecules have been identified from the surface of endothelial cells, and they are key factors in this process. Initially, leukocyte extravasation was described as a three-step process, but nowadays, it includes several steps. These steps are tethering, rolling, arrest, adhesion, crawling and transmigration. (Ley et al., 2007; Nourshargh & Alon, 2014; Vestweber, 2015)

The whole cascade begins when endo- or exogenous inducers stimulate the cells of the innate immune system to release cytokines and other pro-inflammatory mediators, which activate the endothelial cells of post-capillary venules in the inflamed tissue. The first interaction between circulating leukocytes and the

endothelium are mediated by P-, E-, and L-selectins via their counterpart P-selectin glycoprotein ligand 1 (PSGL1). PSGL1 is a ligand for all of these three selectins even though it was first described as a P-selectin ligand. The selectin-mediated capture of leukocytes leads to the rolling of leukocytes along the endothelium and slows down the rolling process. (Chavakis et al., 2009; Vestweber, 2015) Additionally, vascular adhesion protein-1 (VAP-1), an inflammation inducible adhesion molecule expressed on the surface of endothelial cells, participates in the capture and rolling steps of the leukocyte extravasation cascade (Salmi & Jalkanen, 2019).

In addition to the selectin-mediated rolling, integrins are involved in the slow rolling step and the arrest of leukocytes firmly on the endothelium. The endothelial cells express chemokines on their surface, which initiate leukocyte arrest during the rolling step. First, the rolling leukocytes get activated by chemokines and this leads to the activation of integrins on the surface of leukocytes. Then, activated integrins can interact with their counterparts, intercellular adhesion molecule-1 (ICAM-1) and vascular cell adhesion molecule-1 (VCAM-1), on the surface of the endothelium. The most important integrins involved in leukocyte extravasation are lymphocyte function associated antigen-1 (LFA-1), macrophage-1 antigen (MAC-1), and very late antigen-4 (VLA-4). (Vestweber, 2015)

Following the firm adhesion, the next step is crawling, where leukocytes are seeking appropriate places for transmigration into the tissue. During crawling, the same leukocyte integrins as in the firm adhesion step generate interactions with their endothelial ligands VCAM-1, ICAM-1 and ICAM-2. Transmigration is the final step in the leukocyte extravasation process. This step is mediated by several different adhesion molecules and receptors including integrins, platelet endothelial cell adhesion molecule-1 (PECAM-1), junctional adhesion molecules (JAMs), VAP-1 and cluster of differentiation 99 (CD99). (Nourshargh & Alon, 2014; Salmi & Jalkanen, 2019; Vestweber, 2015) Transmigration can happen either through the tight junctions between adjacent endothelial cells (paracellular route) or through an individual endothelial cell (transcellular route). Granulocytes mainly use the paracellular route to migrate through the endothelium. The transcellular route is mainly used by lymphocytes and, especially in the thin parts of endothelium, with the help of vesiculo-vascuolar organelles. (Ley et al., 2007; Nieminen et al., 2006) The multistep leukocyte extravasation process is illustrated in Figure 1.

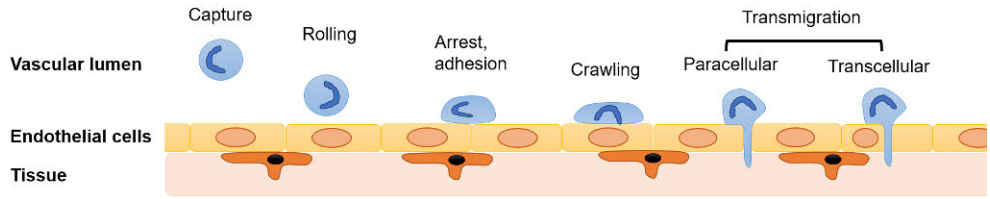

Leukocyte ligands	L-selectin	PSGL1	ICAM-1	ICAM-1/2	JAMs	ICAM-1
		Siglec-9/10	VCAM-1	VCAM-1	Siglec-9/10	JAMA
					PECAM1	PECAM-1
					CD99	CD99
Endothelial cell molecules	PSGL1	P-, E-selectin	LFA-1	MAC-1	LFA-1, MAC-1, VLA-4	LFA-1
		VAP-1	VLA-4		VAP-1	PECAM1
					PECAM1	CD99
					CD99	

Figure 1. An overview of the leukocyte extravasation cascade and leukocyte-endothelial cell interactions. The key leukocyte ligands for each step and their endothelial cell counterparts are shown.

2.1.2 Link between inflammation and cancer

Inflammation is recognized as a critical component that greatly contributes to the development and progression of tumors. This phenomenon is not a novel finding, since already in the mid-19th century Rudolf Virchow suggested that the origin of cancers resides in the sites of chronic inflammation (Virchow, 1881). Cancer-related inflammation shares the same hallmarks with chronic inflammation: infiltration of inflammatory cells and mediators into the tumor tissue, angiogenesis, and attempts to heal. Epidemiological studies have shown that chronic inflammatory diseases and conditions precede the development of certain malignant cancers, including bladder, cervical, gastric, intestinal, esophageal, ovarian, prostate, and thyroid cancers. (Mantovani et al., 2008) Knowledge of the cancer promoting activity of microbial infections and oncoviruses is growing. The strongest association of microbial infection with malignancy is identified in gastric cancer arising from *Helicobacter pylori* infection. Hepatitis C infection is associated with liver carcinoma, while an increased risk of bladder and colon carcinoma is associated with parasites called schistosomes. Human papilloma virus, hepatitis B virus, and Epstein-Barr virus may develop virus-associated malignant tumors where these viruses can directly add active oncogenes to the human genome. (Coussens & Werb, 2002; Elinav et al., 2013)

The mechanisms of cancer-related inflammation are complex because tumors can induce different kinds of inflammatory responses, which vary depending on the context. The inflammatory response is mediated by the crosstalk between two

pathways: intrinsic and extrinsic. In the intrinsic pathway, genetic alterations including the activation of oncogenes or inactivation of tumor suppressors may trigger inflammatory cascade. Malignantly transformed cells are able to induce the expression and production of inflammatory mediators into the tumor microenvironment (TME), even in the absence of an inflammatory condition. Oncogenes *ras* and *myc* are the most frequently mutated or overexpressed in many human cancers. In contrast, the extrinsic pathway is mediated by leukocytes and environmental factors, such as hypoxia, which establish inflammatory conditions, thus increasing the risk of developing cancers. The crossroads for these two pathways to meet is provided by the activation of transcription factors. The transcription factors, including nuclear factor kappa-light-chain-enhancer of activated B cells (NF-κB), signal transducer and activator of transcription 3 (STAT3), and hypoxia-inducible factor 1α (HIF1α), coordinate the production of cytokines and chemokines. This will result in an endless cycle that strengthens the inflammation in TME, where cytokines and chemokines recruit various leukocytes to tissues and the recruited leukocytes activate the same transcription factors to produce inflammatory mediators. This cycle promotes many tumor promoting effects: cell survival and proliferation, angiogenesis, tumor invasion and metastasis, and immunosuppression. (Mantovani et al., 2008; Nakamura & Smyth, 2017)

Integrins are cell adhesion molecules, which play an important role in how cells interact with surrounding environment and other cells. Circulating leukocytes express their integrins in an inactive or non-ligand binding state. Activation of integrins are needed for wide range of cellular events, such as platelet aggregation and leukocyte trafficking. Dysregulated ability to activate integrins associates with various human diseases, including cancer and bleeding disorders. (Bouvard et al., 2013; Evans et al., 2009; Hynes, 2002) Tumor growth depends on the formation of new blood vessels called angiogenesis. Invasion and migration of endothelial cells in response to vascular growth factor signaling and integrin-mediated cell adhesion play a central role in the angiogenic process. Several endothelial cell integrins, for example, $\alpha_v\beta_3$ integrin, regulate angiogenesis by promoting endothelial cell migration and survival. Furthermore, certain integrins promote monocyte trafficking to tumors in response to tumor-secreted chemokines and cytokines, and subsequent angiogenesis. (Avraamides et al., 2008; Desgrosellier & Cheresh, 2010)

Generally, carcinogenesis has been regarded as a multistep process of genetic and epigenetic changes occurring in cancer cells only. However, nowadays many studies have indicated that TME plays an important role in tumor transformation. The TME consists of different cell types: stromal cells (fibroblasts and macrophages), endothelial cells, immune cells (myeloid cells and lymphocytes),

bone marrow-derived precursor cells, and circulating platelets. (Kim & Bae, 2016) Malignant cells utilize the stromal and immune cells of the TME to produce inflammatory mediators. As a result, adaptive immune response is suppressed and the primary tumor continues to grow toward its uncontrolled spread into distant tissues. (Garner & de Visser, 2020)

2.1.2.1 Tumor-associated macrophages

Macrophages are differentiated from monocytes and constitute the best-known immune cell population in tumors. Tumor-associated macrophages (TAMs) are recruited to tumors by cytokines and chemokines. TAMs have a complex dual function in the TME because they can either destroy cancer cells by secreting cytokines or produce potential mediators to induce angiogenesis and boost tumor progression. (Coussens & Werb, 2002; Kim & Bae, 2016) Macrophages in human cancers have traditionally been divided into two groups: classically activated M1 and alternatively activated M2 macrophages. The classically activated M1 macrophages secrete high amounts of pro-inflammatory cytokines like interleukin-12 (IL-12) and tumor necrosis factor (TNF) in response to the stimulation of interferon-γ (IFNγ). The M1 macrophages have an anti-tumoral function because they initiate tumor rejection. In contrast, alternatively activated M2 macrophages are protumoral because they stimulate tumor progression. The M2 macrophages are activated by cytokines IL-4 and IL-13, and they mostly secrete high levels of IL-10 in the TME. (Caronni et al., 2015; Garner & de Visser, 2020; Mantovani et al., 2002) However, the growing knowledge of TAMs has raised questions about oversimplification in terms of the division into M1 and M2 macrophages. Different signals from the TME are influencing the activation of TAMs, and as a result, TAMs constitute a heterogeneous mixture of different macrophage phenotypes (Garner & de Visser, 2020; Kim & Bae, 2016). Today, a new nomenclature for macrophages has been discussed and suggested to be more specifically related to their activators (Murray et al., 2014).

2.1.2.2 Tumor-associated neutrophils

Neutrophils are crucial during acute inflammation as they form a barrier against infection or inflammation. However, a large meta-analysis concerning different human malignancies has shown that an increased number of tumor-associated neutrophils (TANs) are associated with a poorer outcome in patients (Gentles et al., 2015). Within the TME, numerous signals activate TANs to differentiate as anti- or pro-tumorigenic phenotypes. Similarly to the M1 and M2 division, TANs are classified as N1 (anti-tumor neutrophil) or N2 (pro-tumor neutrophil) neutrophils. The N1 neutrophils are more cytotoxic to malignant cells by expressing pro-

inflammatory chemokines and cytokines. In contrast, the N2 neutrophils express more pro-tumoral factors and induce immunosuppression in the TME. (Fridlender et al., 2009)

2.1.2.3 Tumor infiltrating lymphocytes

Tumor mass consists of tumor cells but also a range of other cell types, including leukocytes, fibroblasts, and endothelial cells. Together with TAMs, tumor infiltrating lymphocytes (TILs) are the major subpopulations that infiltrate inside the tumors. TILs are a diverse group of lymphocytes that is mainly comprised of effector T cells, regulatory T cells (T_{reg}), natural killer (NK) cells, macrophages, dendritic cells, and myeloid derived suppressor cells. (Mantovani et al., 2008) Numerous publications have demonstrated that increased infiltration of lymphocytes in tumors is associated with improved survival in, for instance, melanoma, lung, prostate, and colorectal cancer patients (Clemente et al., 1996; Dieu-Nosjean et al., 2008; Tosolini et al., 2011; Vesalainen et al., 1994). In the following, the focus is on CD8, CD4, T_{reg} and NK cells.

Similarly to innate immune response, cytotoxic $CD8^+$ T and $CD4^+$ helper T cells play an important role during the immune defense against cancers (Speiser et al., 2016). $CD8^+$ T cells are activated by antigen presenting cells via major histocompatibility complex molecules. Differentiated cytotoxic $CD8^+$ T cells find and attack directly the tumor cells, resulting in the destruction of the tumor. Unlike cytotoxic $CD8^+$ T cells, anti-tumoral response of $CD4^+$ helper T cells is indirect. $CD4^+$ helper T cells organize and promote other immune cells, such as macrophages, NK cells and cytotoxic $CD8^+$ T cells, to fight against tumor cells by secretion of TNF, IFNγ and IL-2. (Gonzalez et al., 2018) Regulatory T cells are a subpopulation of T cells and play a crucial role in maintaining the homeostasis of the immune system by suppressing the function of cytotoxic $CD8^+$ T cells, $CD4^+$ helper T cells, macrophages, and NK cells (Garner & de Visser, 2020; Gonzalez et al., 2018). However, T_{reg} cells can inhibit anti-tumoral immune response by accumulating in primary tumors and lymph nodes. An increased number of T_{reg} cells has been shown to correlate with a poor prognosis. (Sasada et al., 2003)

NK cells are a subpopulation of innate lymphoid cells that participate in mediating the adaptive immune response. NK cells express numerous receptors on the cell surface, and these receptors are responsible for the activation, inhibition, and adhesion effects. The name ‘natural killer cells’ comes from their ability to recognize and destroy defective cells, including tumor cells and infected cells. (Vivier et al., 2012) Some publications have shown that the infiltration of NK cells into tumors is associated with a good prognosis in human non-small cell lung cancer, renal cell carcinoma, and colorectal carcinoma (Carrega et al., 2008; Eckl et al., 2012; Halama et al., 2011).

2.2 Vascular adhesion protein-1

In the early 1990s, Salmi and Jalkanen discovered novel adhesion molecule. The discovery was made by producing several monoclonal antibodies (mAbs) against purified synovial vessels from patients suffering from rheumatoid arthritis (RA). In immunohistochemical stainings, a particular mAb (1B2) stained high endothelial venules (HEV) in inflamed synovial membranes as well as in human peripheral lymph nodes and tonsils. The antigen of 1B2 antibody differed from other known adhesion molecules for several details, and this new antigen was named as vascular adhesion protein-1,VAP-1 (Salmi & Jalkanen, 1992).

The expression of VAP-1 is not limited to synovial endothelial cells. VAP-1 is also found in various other cell and tissue types. It is expressed in the HEVs of lymphoid tissues, such as tonsils and peripheral lymph nodes, where VAP-1 controls leukocyte trafficking. (Salmi & Jalkanen, 1992; Salmi et al., 1993) In larger vessels, such as aorta and vena cava, VAP-1 is detected in smooth muscle cells of the vessel wall. However, VAP-1 is not present in skeletal or cardiac muscle cells. (Jaakkola et al., 1999; Salmi et al., 1993) In human heart, VAP-1 is detected in the endothelial cells of endocardium and to a limited extent in the small vessels of myocardium. In human kidney, VAP-1 is present in intratubular vessels, but not in arterial endothelium of glomeruli. (Salmi et al., 1993) In adipocytes, VAP-1 is detected in intracellular glucose transporter type 4 positive vesicles (Enrique-Tarancón et al., 1998). The human liver is another VAP-1 positive tissue, and VAP-1 is constantly expressed in the sinusoidal and vascular endothelium (McNab et al., 1996). In addition to these tissues, VAP-1 is detected in some occasional venules in brain and skin, but the surface of leukocytes, fibroblasts, and epithelial cells are VAP-1 negative (Salmi et al., 1993).

2.2.1 Structure of VAP-1

VAP-1 is a membrane-bound endothelial cell surface molecule. It is composed of a short N-terminal cytoplasmic tail, a single transmembrane domain, and a large extracellular domain. Structurally, VAP-1 consists of two identical 90 kDa monomeric subunits, which form a dimeric structure. (Salmi & Jalkanen, 1992; Smith et al., 1998) VAP-1 is heavily sialylated and the cloning of VAP-1 revealed that O- and N-linked glycans can be found, as decorations, on the top of the VAP-1 structure (Salmi & Jalkanen, 1996; Smith et al., 1998). There are six N-linked glycosylation sites on the surface of the VAP-1 molecule. These sugar units are necessary for the adhesion process, and mutations in these glycosylation sites have resulted in reduced lymphocyte binding properties. (Maula et al., 2005) The determination of the crystal structure of VAP-1 revealed that the molecule is a heart-shaped protein and the monomeric subunit consists of domains D1, D2, D3, and D4.

The D4 domain of VAP-1 contains an active site, which is located deep inside the molecule, forming a circular shape cavity for the substrate. One crucial amino acid, leucine 469, functions as a gatekeeper that blocks the entrance of the active site for potential substrates. The heart of the active site includes the topaquinone (TPQ) cofactor with tyrosine modification, the catalytic base, and the copper ion with histidines coordinating its place. (Airenne et al., 2005)

2.2.2 VAP-1 as an enzyme

Cloning of VAP-1 and the subsequent biochemical analyses in 1998 revealed that VAP-1 is an enzyme. It shares significant homology with the enzymes called semicarbazide-sensitive amine oxidases (SSAOs). (Smith et al., 1998) Currently, VAP-1 is officially called amine oxidase copper-containing 3 (AOC3) and the correct enzyme name for VAP-1 is primary amine oxidase (EC.1.4.3.21). SSAOs, also known as primary amine oxidases, differ from other amine oxidases, such as monoamine oxidases A and B, in terms of their sensitivity of substrates and inhibitors, subcellular localization, cofactors, and function (Salmi & Jalkanen, 2001).

VAP-1 (AOC3) belongs to the human copper-containing amine oxidase (CAO) family, which includes three other genes: AOC1, AOC2, and AOC4 (Finney et al., 2014). All CAOs catalyze the oxidative deamination of primary amines but differ from each other for substrate specificities. The AOC1 gene encodes an enzyme called diamine oxidase, which is responsible for metabolizing ingested histamine and maintaining normal pregnancy (Elmore et al., 2002; Finney et al., 2014). The AOC2 gene encodes retina-specific amine oxidase. The protein has only been found in the retina although the messenger RNA (mRNA) is detected in many tissues (Imamura et al., 1997; Kaitaniemi et al., 2009). The AOC4 gene is found in the human genome but it is a pseudogene. This means that the AOC4 gene does not form a functional protein since the sequence contains a premature stop codon. (Schwelberger, 2007) The AOC3 gene encodes VAP-1, which is the most studied of the three CAOs and physiologically an essential protein (Finney et al., 2014; Smith et al., 1998). The natural substrates of VAP-1 are methylamine and aminoacetone, whereas AOC2 prefers phenylethylamine, tryptamine and *p*-tyramine as its substrates (Kaitaniemi et al., 2009; Smith et al., 1998). Moreover, proteins encoded by AOC2 and VAP-1 share 65% sequence homology, whereas the protein encoded by AOC1 shares 38% similarity with VAP-1 (Finney et al., 2014). The human AOC3 gene has four exons and it is located in chromosome 17 (17q21.31) (Pannecoeck et al., 2015; Schwelberger, 2007).

VAP-1 catalyzes the oxidative deamination of primary amines to generate aldehyde while releasing hydrogen peroxide and ammonium. The overall reaction of

SSAO is written as $R\text{-}CH_2\text{-}NH_3^+ + H_2O + O_2 \rightarrow R\text{-}COH + H_2O_2 + NH_4^+$ (Vakal et al., 2020). As mentioned earlier, the TPQ cofactor is required for the enzymatic reaction. The SSAO reaction is divided into two half-reactions, a reductive and an oxidative reaction. In the reductive half-reaction, the amine substrate first reacts with TPQ in the active site and forms a Schiff base. Next, the aldehyde product is released by hydrolysis and the remaining TPQ is reduced. In the oxidative half-reaction, molecular oxygen reoxidizes the reduced TPQ, and hydrogen peroxide and ammonium are released. (Lopes de Carvalho et al., 2019; Salmi & Jalkanen, 2019) These end products of the primary amines act as inflammation mediators and contribute to leukocyte extravasation.

2.2.3 VAP-1 as an adhesion molecule

VAP-1 participates in leukocyte extravasation across the inflamed endothelium. As an adhesion molecule, VAP-1 is an inflammation inducible molecule. In normal conditions, VAP-1 is absent on the surface of endothelium and is stored in intracellular storage granules. Upon inflammation, VAP-1 is rapidly translocated from the intracellular storage granules to the endothelial cell surface. VAP-1 contributes to leukocyte extravasation during the tethering, rolling, and transmigration steps.

Initial evidence of the adhesive properties of VAP-1 was demonstrated in inhibition studies: using *in vitro* assays and intravital imaging, the anti-VAP-1 monoclonal antibodies have been shown to inhibit the binding of leukocytes to endothelium in different tissues and to reduce the rolling, adhesion, and transmigration of leukocytes (Arvilommi et al., 1996; Koskinen et al., 2004; Kurkijärvi et al., 2001; Lalor et al., 2002; McNab et al., 1996; Salmi & Jalkanen, 1992). To date, several experimental animal models have been utilized to acquire further evidence of the adhesive role of VAP-1. It has been shown to mediate the migration of monocytes to an air pouch inflammation (Merinen et al., 2005). In peritonitis models of rabbits and mice, VAP-1 mediates the migration of granulocytes (Merinen et al., 2005; Tohka et al., 2001). Moreover, VAP-1 is expressed in pancreas during the development of type 1 diabetes, and anti-VAP-1 antibody treatment prevents its development (Merinen et al., 2005). In mouse atherosclerotic plaques, VAP-1 is expressed on the luminal surface of endothelial cells, and small molecular inhibitor treatment reduces the macrophage density in plaques (Silvola et al., 2016). In a rat experimental autoimmune encephalomyelitis model, VAP-1 is present in vascular lesions, and small molecular inhibitor treatment reduces the accumulation of lymphocytes into lesions during the acute phase (Elo et al., 2018). In a rat liver allograft rejection model, VAP-1 mediates the binding of lymphocytes to the rejected organ (Martelius et al., 2004). In addition to

inflammatory diseases, it has been shown that, in tumors, anti-VAP-1 inhibit the binding of NK cells, tumor infiltrating lymphocytes (TILs) and lymphokine-activated killer cells to VAP-1 positive vessels of cancer tissue (Irjala et al., 2001). In melanomas and lymphomas, VAP-1 regulates tumor growth and enhances the migration of Gr-1$^+$CD11b$^+$ myeloid cells into tumors (Marttila-Ichihara et al., 2009). Furthermore, anti-VAP-1 mAbs have been shown to attenuate the accumulation of CD3$^+$ and CD8$^+$ T cells into melanomas (Marttila-Ichihara et al., 2010).

As mentioned before, VAP-1 is both an enzyme and an adhesion molecule. In addition to mAbs, the adhesive function of VAP-1 can be inhibited by specific inhibitors of its enzyme activity. The SSAO inhibitors have been shown to reduce the number of lymphocytes rolling on and adhering to endothelium by *in vitro* flow assays (Salmi et al., 2001). Additionally, in the same experiments, it has been detected that the lymphocyte tethering to endothelium is not dependent on the SSAO activity of VAP-1. Inhibition of the SSAO activity of VAP-1 reduces adhesion and transmigration of lymphocytes to endothelium as shown by *in vitro* flow assays of hepatic endothelial cells (Lalor et al., 2002). Using *in vitro* assays and *in vivo* models, SSAO inhibitors also reduce the number of granulocytes during the rolling, adhesion, and transmigration steps (Koskinen et al., 2004). In the same experiments, anti-VAP-1 mAbs do not hamper the SSAO activity of VAP-1 and vice versa. Therefore, VAP-1 is a dual function molecule that affects leukocyte extravasation both depending on and independently of the enzyme activity (Salmi & Jalkanen, 2011).

It has been earlier shown that the CD4$^+$ and CD8$^+$ T cells, B lymphocytes, monocytes, and granulocytes use the VAP-1 dependent adhesion to vasculature (Salmi & Jalkanen, 2019). The T_{reg} cells and CD16$^+$ monocytes also use the VAP-1 mediated adhesion to vasculature (Aspinall et al., 2010; Shetty et al., 2011). The leukocyte ligands of VAP-1 are sialic acid-binding immunoglobulin-like lectin (Siglec) 9 on the surface of granulocytes and Siglec-10 on the surface of a subpopulation of lymphocytes (Aalto et al., 2011; Kivi et al., 2009). Cell-mediated binding assay and docking studies revealed that Siglec-9 binds to the enzymatic groove of VAP-1 and the interaction involves enzyme activity-dependent as well as independent mechanisms (Aalto et al., 2011). The SSAO activity of VAP-1 catalyzes primary amines and its end product, hydrogen peroxidase, promotes leukocyte extravasation. Hydrogen peroxidase produced during the VAP-1 mediated amine oxidation regulates the synthesis of other adhesion molecules, including ICAM-1, mucosal addressin cell adhesion molecule 1 (MadCAM-1), E-selectin, and P-selectin (Jalkanen et al., 2007; Lalor et al., 2007; Liaskou et al., 2011). Furthermore, the SSAO activity of VAP-1 activates transcription factors, such as NF-κB and tumor suppression factor p53, and induces the secretion of chemokine CXCL8 (Lalor et al., 2007; Solé et al., 2008).

2.2.4 Soluble form of VAP-1

Besides its transmembrane form, VAP-1 is found in a soluble form in the blood circulation (Kurkijärvi et al., 1998). Soluble VAP-1 (sVAP-1) is formed through the cleavage of the membrane-bound form by a metalloproteinase dependent process (Abella et al., 2004). In humans, liver sinusoidal endothelial cells (Kurkijarvi et al., 2000) and adipocytes are the sources of sVAP-1, and the level of sVAP-1 is partly regulated by insulin (Abella et al., 2004). In healthy human plasma, the concentration of sVAP-1 is stable and normally about 820 ng/ml (Aalto et al., 2014). For the most part, an increased sVAP-1 level has been associated with several diseases with an inflammatory component, such as diabetes, liver diseases, and psoriasis (Kurkijärvi et al., 1998; Salmi & Jalkanen, 2019). Inflammatory bowel disease is an exception to other inflammatory diseases because no elevated concentration of sVAP-1 has been found in relation to it (Koutroubakis et al., 2002).

Increased and decreased sVAP-1 levels are also found in cancer patients. Several studies have reported that circulating sVAP-1 levels in serum samples were higher in gastric, colorectal, and hepatocellular cancer patients as compared to the controls (Kemik et al., 2010; Y. I. Li et al., 2014; Toiyama et al., 2009; Yasuda et al., 2011). Patients with low sVAP-1 levels have a notably worse prognosis of gastric and colorectal cancers. Moreover, sVAP-1 correlated negatively with lymph node and hepatic metastasis, and this suggests that sVAP-1 could be a good prognostic marker for metastasis. (Toiyama et al., 2009; Yasuda et al., 2011) In contrast to increased sVAP-1 levels in different cancers, decreased circulating sVAP-1 levels have only been reported in thyroid cancer patients. The sVAP-1 levels correlated negatively with serum thyroglobulin levels and provide an additional tool for diagnosing thyroid cancer. (Hu et al., 2016)

2.2.5 VAP-1 in arthritis

Rheumatoid arthritis is a chronic inflammatory disease, which mainly affects joints with cartilage and bone destructions, but also involves extra-articular manifestations (Smolen et al., 2016). Additionally, it is a systemic inflammatory disease in which RA patients suffer from comorbid conditions, such as cardiovascular disease, renal disease, and depression (Anders & Vielhauer, 2011; Bruce, 2008; Nurmohamed et al., 2015). Joint swelling in RA is a reflection of an inflamed synovial membrane, which is a result from the activation of the immune system. Leukocyte extravasation from blood to the joints is involved in the pathogenesis of arthritis. This process is mediated by adhesive interactions between the blood leukocytes and endothelium, and several adhesion molecules and chemokines are involved. (Pannecoeck et al., 2015) As stated earlier, VAP-1 is one of these adhesion molecules, participating in the leukocyte extravasation cascade.

In humans, the first evidence of VAP-1 on the vasculature of inflamed synovia was found when the VAP-1 molecule was discovered (Salmi & Jalkanen, 1992). Following the initial discovery, it has been shown that VAP-1 is expressed on the surface of synovial blood vessels in RA patients (Salmi et al., 1997). In arthritis models, the VAP-1 deficiency and inhibition of SSAO activity have been shown to attenuate the clinical inflammation scores of arthritis and disease progression (Marttila-Ichihara et al., 2006). In addition, high expression of VAP-1 has been reported in inflamed synovial vessels of patients with treatment-resistant Lyme arthritis (LA) (Akin et al., 2001). However, increased serum levels of sVAP-1 have not been indicated in RA patients (Kurkijärvi et al., 1998).

The involvement of VAP-1 in leukocyte extravasation across inflamed endothelium and the inhibition of adhesive properties have made the VAP-1 molecule an interesting drug target for anti-inflammatory therapy. Several drug companies are developing antibodies and inhibitors to block the VAP-1 function in different disease indications (Vakal et al., 2020). One of the drug companies is Biotie Therapies (currently known as Acorda), which developed a fully human anti-VAP-1 antibody (BTT1023 or Timolumab). In early clinical trials it has been shown to be safe, well tolerated, and efficient for patients with RA and psoriasis. However, the phase II clinical trial with primary sclerosing cholangitis patients showed lack of efficacy and this trial was discontinued. (Arndtz et al., 2017)

2.2.6 VAP-1 in melanoma

Melanoma is responsible for the majority of deaths in skin cancers (Miller & Mihm, 2006). A few malignant melanoma cells may dissociate from the primary tumor, enter blood circulation or lymphatic vessels, adhere to the vascular wall of distant organs, and generate metastasis. Common sites for melanoma metastases are lungs, liver, and brain. (Braeuer et al., 2014) Similarly to inflammatory cells, tumor cells need adhesion molecules and their counter receptors to facilitate the invasion and spread of primary tumors (Kobayashi et al., 2007; Miller & Mihm, 2006).

Some cancer studies have investigated the role of VAP-1 in tumor progression and metastasis. Initially, adhesion molecules VAP-1 and ICAM-1 were shown to participate in the recruitment of TILs and to support the adhesion of TILs to tumor vascular wall in human hepatocellular carcinoma (Yoong et al., 1998). Thereafter, VAP-1 has been shown to mediate the adhesion of TILs, lymphokine activated killer cells, and NK cells to the tumor endothelium in squamous cell carcinoma of the head and neck cancer (Irjala et al., 2001), and the recruitment of myeloid cells in experimental lung metastasis model (Ferjančič et al., 2013). In human melanoma samples, immunofluorescence staining of VAP-1 has indicated that intratumoral vessels exhibit lower expression of VAP-1 compared to the border region of

melanoma (Forster-Horváth et al., 2004). Experimental *in vivo* studies have confirmed the role of VAP-1 in melanoma progression. VAP-1 regulates the growth of melanoma by increasing the recruitment of myeloid cells, especially Gr-$1^{+}CD11b^{+}$, into tumors (Marttila-Ichihara et al., 2009). Additionally, VAP-1 enhances angiogenesis, for which the oxidative activity of VAP-1 is necessary. In subsequent studies with SSAO inhibitors, it was proved that angiogenesis was dependent on the oxidative activity of VAP-1 (Marttila-Ichihara et al., 2010). To this day, no studies have reported elevated or decreased levels of sVAP-1 in melanoma patients.

2.3 Imaging of inflammation in arthritis and melanoma

The classical symptoms of inflammation, i.e. redness, heat, pain, and swelling, are easily recognized by clinical examination. In addition to clinical examination, laboratory tests and imaging methods are usually required to confirm the diagnosis of different inflammatory diseases. The clinical picture and suspicion of the disease type influence the choice of imaging methods. The purpose of imaging, for example, in RA, is to confirm the inflammatory findings and to verify seriously damaged tissues. In addition, imaging may detect the ongoing disease process at an early stage, allowing for timely intervention and possibly prevention of disease progression. Inflammation imaging methods can be divided into two groups: anatomical and molecular imaging. Anatomical imaging methods provide information of the structural changes in adjacent tissues and morphology of lesion (Cavaillon & Singer, 2018; Histed et al., 2012). Molecular imaging methods detect biological and biochemical processes at cellular or molecular level. Molecular imaging helps to understand the mechanism behind the disease and provides a potential tool for detecting inflammatory foci at an early stage of the disease. (Cavaillon & Singer, 2018; MacRitchie et al., 2020) Molecular imaging is a valuable tool in the clinical context because it can be used in the early diagnosis of diseases, monitoring of therapy response, and identifying of new drug targets (MacRitchie et al., 2020). However, it is unlikely that a single imaging method would be useful to fulfill all desired features for clinical molecular imaging. Therefore, molecular imaging is usually combined with an anatomical imaging method, and this is called hybrid imaging modality.

2.3.1 Anatomical imaging

Conventional radiography is based on X-rays, which pass through the body and are arrested by a detector. This imaging modality has been considered as a gold standard

for imaging of RA for many years and is routinely used in clinical diagnosing. Although new imaging modalities have been developed, conventional radiography is still used because of its reliability, long-term of experience, easy availability, good spatial resolution, and low cost. Conventional radiography provides important knowledge of bone erosions in specific sites, bone deformities, and cartilage loss, which are key factors in the diagnosis of RA. On the other hand, conventional radiography causes radiation exposure and it has a low sensitivity to certain distinct early signs of joint manifestations. (Bansal, 2006; Kgoebane et al., 2018; Llopis et al., 2017; Narayan et al., 2017) In oncology, chest radiography is also used for the investigation of lung metastases in patients with melanoma. This is a reasonable examination approach since melanoma tends to metastasize into the lungs. Chest radiograph is not routinely performed for all melanoma patients, but it is recommended for those who are symptomatic or whose melanoma has not yet metastasized into sentinel lymph nodes. (Dancey et al., 2008)

Computed tomography (CT) imaging is based on X-rays and a detector in a similar manner as conventional radiography. The difference between these two imaging methods is that CT combines many X-ray measurements taken from different projections and creates cross-sectional images of the scanned area using mathematical algorithms. CT detects tumors and metastases based on changes in the organ structures and the angiogenesis of malignant neoplasms. However, small metastases are difficult to accurately detect by CT. (Dancey et al., 2008; Histed et al., 2012; MacRitchie et al., 2020) Non-targeted ionized contrast agents are used to visualize blood vessels. Increased blood flow in abnormally vascularized tissues may indicate tumor and inflammation (Histed et al., 2012). A liver metastasis of melanoma is highly vascularized, and a contrast agent is often used in abdominal CT imaging to detect liver metastases. However, the correct timing between contrast enhancement and scanning calls for further evaluation. (Dancey et al., 2008) CT provides an excellent spatial resolution, fast scanning times, and whole-body imaging. On the other hand, its use exposes patients to radiation and it lacks functional information. The use of ionized contrast agents is also limited due to possible allergy or renal insufficiency of the patient. (Gotthardt et al., 2010; MacRitchie et al., 2020)

Ultrasound technique is used for many purposes in the field of medicine. It is based on high frequency sound impulses, which a transducer generates and detects as returning echoes from the tissues (Dancey et al., 2008). The ultrasound method can be used for clinical examination of patients with RA and melanoma. In patients with RA, ultrasound is utilized in the assessment of soft tissues. It can visualize synovial hypertrophy, accumulation of fluid in joints and tendons, and small alterations in the structure of tendons and ligaments (Sudoł-Szopińska et al., 2012). A special ultrasound technique called color Doppler ultrasound gives further

information of the blood flow in the inflamed synovium. In patients with RA, this method could be used to monitor the efficiency of therapy responses (Kgoebane et al., 2018). In patients with melanoma, ultrasound imaging visualizes skin lesions and it is also used to investigate the formation of metastases in different tissues, for example, in the abdominal and pelvic area. The color Doppler ultrasound method is used to detect vasculature of skin lesions to enhance the accuracy in imaging. (Dancey et al., 2008) The ultrasound imaging method is useful because it has a good spatial resolution (below 1 millimeter), good availability, and affordable price, it enables functional imaging (Doppler), and does not expose patients to ionizing radiation. The limitations of ultrasound imaging are its high dependence on the experience of the operator, low tissue penetration, and reflection of sound impulses, which can be obstructed by gas bubbles from the bowel. (Gotthardt et al., 2010; Kgoebane et al., 2018)

Magnetic resonance imaging (MRI) is a technique that uses a powerful magnetic field and radio waves to form a detailed image of the inside of the body. Hydrogen nucleus has magnetic properties and it is naturally abundant in human body in water and fat. The external magnetic field of the MRI scanner aligns the dipoles of hydrogen atoms and the pulse of radio waves can rotate polarization. After the pulse of radio waves, the hydrogen nucleus emits a radiofrequency signal simultaneously with its magnetization returning to the normal orientation, and this can be detected with the MRI scanner. (Dancey et al., 2008; Grover et al., 2015) In patients with RA, MRI detects sensitively all changes occurring in the soft tissue, cartilage and bone, and even at an early phase. Furthermore, it allows the detection of enhanced vascularization in areas of active inflammation by means of a gadolinium contrast agent. (Kgoebane et al., 2018) In patients with melanoma, MRI is not routinely used in clinics due to the long imaging times, but melanoma deposits have been shown to produce high tissue contrast (Dancey et al., 2008). The MRI method is feasible at the clinical level because it provides functional, anatomical, and molecular imaging data with high resolution and without radiation exposure (Gotthardt et al., 2010; MacRitchie et al., 2020). Long imaging times, loud noise, and artifacts resulting from respiratory and cardiac movements limit the use of MRI. Additionally, patients suffering from claustrophobia and patients with pacemakers, implants, and other devices cannot be imaged with MRI without limitations. (Dancey et al., 2008; Gotthardt et al., 2010)

2.3.2 Targeted molecular imaging

Targeted molecular imaging aims to non-invasively visualize and detect biological processes at molecular or cellular level in the body. To detect these biological processes, it utilizes molecules as probes, which can be either endogenous molecules

or exogenous probes depending on the selected imaging modality. It is unlikely that single imaging technique offers all desired features from a high spatial resolution to deep tissue imaging. Hence, different imaging modalities are combined to provide hybrid imaging methods. The most commonly fused imaging modalities are CT, MRI, positron emission tomography (PET), and single photon emission computed tomography (SPECT) for clinical molecular imaging. (MacRitchie et al., 2020) The molecular imaging methods can be used for the purpose of the early diagnosing of the disease, monitoring therapy response, identifying and/or validating new drug targets, and revealing an unknown pathway that underlies the disease.

The latest and emerging new technology approach is based on indocyanine green (ICG)-enhanced fluorescence optical imaging (FOI), which has shown promising results for imaging of inflammation. In experimental animal model of arthritis, ICG-FOI was able to detect inflamed joints, and these results corresponded to histological findings (Meier et al., 2010). In humans with arthritis, this approach revealed its feasibility to detect inflammatory changes with a good sensitivity (Werner et al., 2012). However, further investigations are needed for better image interpretation and analysis until it can be used as an imaging tool in clinics.

The ultrasound technique can serve both as an anatomical and targeted molecular imaging method. In contrast-enhanced ultrasound imaging, targeted microbubble contrast agents are applied to enhance the ultrasound signal. Microbubbles are injected intravenously, and they are composed of gas bubbles stabilized with a shell. An encapsulated shell consisting of albumin was used as the first-generation microbubble contrast agent, but today the encapsulated shell may consist of proteins, lipids, and polymers. The choice of shell material plays an important role since it affects the target binding properties, prevents diffusion of gas-filled microbubbles, and affects the compatibility of the material and the host without toxicity. Microbubbles can be targeted to the vascular endothelium affected by the disease, using an angiogenesis marker $\alpha_v\beta_3$ integrin or inflammatory markers, such as ICAM-1. Currently, microbubble contrast agents for ultrasound imaging are mainly approved for clinical indications of cardiovascular imaging. In some circumstances, contrast-enhanced ultrasound is used to detect liver lesions in the clinic. (Martin & Dayton, 2013; Perera et al., 2015)

Nuclear imaging modalities, SPECT and PET, facilitate the acquisition of both functional and molecular information. Additionally, these imaging modalities provide the possibility to image the dimensions of the body in their entirety in the same manner as CT and MRI. (MacRitchie et al., 2020) SPECT is a non-invasive and sensitive imaging method based on gamma-ray emitting radionuclides. The SPECT camera rotates around the patient and the detectors detect the emitted gamma rays from several different projections. The collected data are reconstructed into three-dimensional images. The commonly used SPECT radionuclides are

Technetium-99m (^{99m}Tc), Indium-111 (^{111}In), and Iodine-123 (^{123}I), which are intermediate-lived radionuclides [half-lives range from 6.0067 hours (^{99m}Tc) to 2.8047 days (^{111}In)]. (Khalil et al., 2011; Rahmim & Zaidi, 2008) Radiolabeling of the patient´s own white blood cells (WBC) has been used for many years as the gold standard for SPECT imaging of inflammation and infection. Radiolabeled WBCs accumulate in the inflamed tissue through leukocyte transmigration, where they first adhere to the vascular endothelium and then migrate to inflammatory foci. Before radiolabeling, WBCs must be isolated from the patient. The isolated WBCs are labeled either with ^{111}In-oxine or ^{99m}Tc-hexamethylpropylene (^{99m}Tc-HMPAO). ^{99m}Tc is the most frequently used radionuclide for the labeling of WBCs because it provides more of optimal physical characteristics and a lower radiation exposure than ^{111}In. (Connolly & Donohoe, 2017) Other clinically used SPECT tracers for the imaging of inflammations and infections are ^{67}Ga-citrate, ^{99m}Tc- or ^{111}In-labeled liposomes, antibodies or antibody fragments, cytokines, and chemotactic peptides (Boerman et al., 2001; Gotthardt et al., 2010; Signore & Glaudemans, 2011). Furthermore, SPECT imaging allows simultaneous imaging with two different radionuclides in different energy windows. The method is called dual tracer imaging, and it reduces study times and patient discomfort, and provides concurrent information of two distinct body functions, but its use is mainly limited to research purposes. Dual tracer imaging is not possible to perform with PET since all PET tracers emit positrons that are converted to photons in the same energy window (≈511 kEv). (Rahmim & Zaidi, 2008) In addition to dual tracer imaging, the advantages of SPECT include the wide availability of SPECT cameras and long-lived radionuclides that permit the flexible scheduling and delivery of tracers to distant research centers or hospitals. However, the spatial resolution of clinical SPECT cameras is around 10 mm, which limits their usability to detect lesions of small size. (Khalil et al., 2011)

PET is a minimally invasive and very sensitive molecular imaging method, which has multiple functional imaging applications in medicine. It is utilized to detect and measure changes in physiological functions like blood flow, metabolism, and absorption. For the imaging of biochemical processes, PET uses radioactive tracers that are labeled with positron emitting radionuclides. When PET radionuclides decay, they emit a positron that moves a short distance until it encounters an electron. The kinetic energy of positron affects the distance it travels in the tissue and impact on spatial resolution. The collision between a positron and an electron leads to annihilation, which produces two 511 kiloelectron volt gamma rays traveling to opposite directions. The PET camera detects these gamma rays with detectors, which are surrounding the patient. The collected data of the location and energy of gamma rays are then reconstructed into three-dimensional images with computational algorithms. (Rahmim & Zaidi, 2008) PET radionuclides can be

produced either with a cyclotron or with a generator. The most commonly utilized cyclotron produced PET radionuclides are Fluorine-18 (^{18}F, physical half-life 109.77 min), Carbon-11 (^{11}C, 20.364 min), and Oxygen-15 (^{15}O, 122.24 s). These three classical PET radionuclides are short-lived, routinely used and have favorable physical features for the production of high quality PET images. (Synowiecki et al., 2018) The most commonly used short-lived and generator produced PET radionuclide is Gallium-68 (^{68}Ga, physical half-life 67.71 min). The generator facilitates the production of PET tracers in a radiochemical laboratory and does not require a large space. (Dash & Chakravarty, 2019) PET imaging has many advantages over SPECT imaging. Most importantly, PET has higher sensitivity to detect functional and molecular information between nanomolar and picomolar concentrations. Furthermore, the spatial resolution of clinical PET cameras is around 4-6 mm, which is higher than that of SPECT cameras. PET imaging modality differs from other imaging modalities in that it allows the quantification of the imaging data. (Gotthardt et al., 2010; Khalil et al., 2011; MacRitchie et al., 2020) Properties of different imaging modalities are summarized in Table 1.

Table 1. Properties of different imaging modalities.

Imaging modality	Spatial resolution	Provided information	References
Conventional radiography	0.1 mm	Anatomical	(Bansal, 2006)
CT	15–50 µm	Anatomical	(MacRitchie et al., 2020)
Ultrasound	> 1 mm	Anatomical	(Gotthardt et al., 2010)
MRI	0.5–1.5 mm (1.5 T) 10–200 µm (> 3 T)	Anatomical, functional and molecular	(Gotthardt et al., 2010; MacRitchie et al., 2020)
SPECT	8–12 mm (clinical) ≤ 1 mm (preclinical)	Functional and molecular	(Khalil et al., 2011)
PET	4–6 mm (clinical) 1–2 mm (preclinical)	Functional and molecular	(Gotthardt et al., 2010; Khalil et al., 2011; MacRicthie et al. 2020)

2.4 PET imaging of inflammation biomarkers

The field of PET imaging of inflammation has been active during the past decades. Several radiopharmaceuticals have been developed to target various inflammatory molecules in order to acquire more information of the disease pathology on tissue level. Upon inflammatory stimuli, the release of pro-inflammatory mediators, increased vascular permeability with infiltrating leukocytes, increased tissue destruction, and attempts to heal are potential targets to visualize inflammation. In addition, PET imaging of inflammation is a feasible method for the purposes of

providing essential information of an inflammatory disease at an early phase, monitoring the disease progression, and validating anti-inflammatory drug targets.

2.4.1 Tracer targeting glucose metabolism

The most commonly used PET tracer is an ^{18}F-labeled glucose analog known as 2-deoxy-2-[^{18}F]fluoro-*D*-glucose ([^{18}F]FDG). The uptake of [^{18}F]FDG is based on the high metabolic activity in tissues where cells are using glucose as an energy source. [^{18}F]FDG is taken up in cells in a similar manner as glucose via glucose transporters. Once inside the cell, [^{18}F]FDG is phosphorylated by *hexokinase* to [^{18}F]FDG-6-phosphate. After phosphorylation, [^{18}F]FDG-6-phosphate cannot enter into glycolysis and further metabolize like glucose-6-phosphate because the hydroxyl group in C2 position is replaced with ^{18}F. Hence, [^{18}F]FDG-6-phosphate is trapped in the cells. In 1980, [^{18}F]FDG PET was first described as a potential biomarker in tumor imaging (Som et al., 1980). Based on the European Association of Nuclear Medicine (EANM) guideline, [^{18}F]FDG PET is a valuable imaging modality tool for tumor detection, staging, restaging, radiation therapy planning, and therapy response monitoring in the field of oncology (Boellaard et al., 2015). Besides tumor imaging, [^{18}F]FDG PET/CT imaging is used for detection of inflammation and infection. During inflammatory condition, [^{18}F]FDG is taken up by inflammatory cells, neutrophils and macrophages in particular, that express high levels of glucose transporters 1 and 3 (Chrapko et al., 2016). Based on the EANM and Society of Nuclear Medicine and Molecular Imaging (SNMMI) guidelines, major indications for [^{18}F]FDG PET/CT imaging of inflammation and infection include vasculitis, fever of unknown origin, sarcoidosis, peripheral bone osteomyelitis, suspected spinal infection, metastatic infection, and high-risk patients with bacteremia (Jamar et al., 2013). Although [^{18}F]FDG has many advantages, such as high sensitivity and fast accumulation, it has limitations as well. [^{18}F]FDG PET is not specific for inflammation imaging because it is a marker of glucose metabolism in several cell types and may thus cause false-positive results. In addition, [^{18}F]FDG has high physiological uptake in the heart and brain. High physiological uptake limits the detection of inflammatory foci near to these tissues.

2.4.2 Tracers targeting integrins

Integrins are heterogenic transmembrane receptors that mediate both cell-extracellular matrix and cell-cell interactions. These receptors consist of an α- and a β-subunit, which mediate signals from cell surface to cytoplasm. The best-known integrin is $\alpha_v\beta_3$, which is overexpressed in angiogenic endothelial cells, cancer cells, and inflammatory cells, such as macrophages. This makes $\alpha_v\beta_3$ integrin an interesting

target for the imaging of different inflammatory and oncologic diseases. $\alpha_v\beta_3$ integrin recognizes and binds to the arginyl-glycyl-aspartic acid (RGD) tripeptide motif. (Antonov et al., 2011; Bouvard et al., 2013; Brooks et al., 1994; Desgrosellier & Cheresh, 2010; Kapp et al., 2017) The first successfully tested RGD-targeting PET tracer in humans was [^{18}F]-Galacto-RGD, which provided a good tumor-to-background ratio (Haubner et al., 2005). Later on in the clinical use, [^{18}F]-Galacto-RGD has been evaluated in a wide variety of cancers, such as melanoma, sarcoma, glioblastoma, head and neck cancer, and breast cancer, with promising results (Beer et al., 2006, 2008; Haubner et al., 2005; Schnell et al., 2009). Apart from tumor imaging, another $\alpha_v\beta_3$ integrin targeting tracer, [^{68}Ga]Ga-PRGD2, has been utilized to image neovascularization and treatment response in patients with RA. [^{68}Ga]Ga-PRGD2 showed high uptakes in the affected joints and tendons, and the changes in tracer uptake correlated with the disease activity (Zhu et al., 2014). In experimental animal models, several ^{68}Ga-labeled RGD peptide-based PET tracers have been developed and tested to improve the pharmacokinetic properties while maintaining the high receptor affinity and selectivity to $\alpha_v\beta_3$ (Beer & Schwaiger, 2008; Eo & Jeong, 2016; Wu et al., 2013). In a mouse renal cell carcinoma model, Dijkraaf and co-workers have demonstrated that the multimerization of RGD peptide improved tumor targeting for $\alpha_v\beta_3$ integrin (Dijkgraaf et al., 2011). Additionally, changing the bifunctional chelating agent between ^{68}Ga and RGD peptide to 1,4,7-triazacyclononane-1,4,7-triacetic acid (NOTA) or 1,4,7-triazacyclononane,1-glutaric acid-4,7-acetic acid (NODAGA) shows better tumor-to-background ratios than the pioneer 1,4,7,10-tetraazacyclododecane-N,N′,N′′,N′′′-tetraacetic acid (DOTA)-RGD peptide in mouse prostate and glioblastoma models (Dumont et al., 2011; Israel et al., 2014).

2.4.3 Tracers targeting membrane molecules of inflammatory cells

Somatostatin receptors (SSTRs) are well-known and much investigated imaging targets for diagnosing and monitoring the therapy response of neuroendocrine tumors. There are three somatostatin analogs DOTANOC, DOTATOC, and DOTATATE, which differ from each other for binding affinity to SSTR subtypes (Reubi et al., 2000). In addition to neuroendocrine tumors, high SSTRs expression is also found in human monocytes and macrophages (Dalm et al., 2003). This makes SSTRs a potential target for imaging inflammation. ^{68}Ga-labeled DOTA-conjugated somatostatin analog, [^{68}Ga]Ga-DOTANOC, is predominantly used for neuroendocrine tumor imaging and binds to SSTR2, SSTR3 and SSTR5 (Wild et al., 2003, 2005). Besides neuroendocrine tumor imaging, Ambrosini and coworkers have demonstrated that [^{68}Ga]Ga-DOTANOC can detect fibrotic lungs in patients

with idiopathic pulmonary fibrosis (Ambrosini et al., 2010). Another somatostatin analog, SSTR2- and SSTR5-targeting [^{68}Ga]Ga-DOTATOC, has been successfully demonstrated to detect carcinoid lesions and neuroendocrine tumors with lung and bone metastases (Buchmann et al., 2007; Hofman et al., 2015; Hofmann et al., 2001). Additionally, a pilot study with sarcoidosis patients has illustrated that [^{68}Ga]Ga-DOTATOC can visualize lymph node, uvea, and muscle lesions (Nobashi et al., 2016). The third somatostatin analog, SSTR2-targeting [^{68}Ga]Ga-DOTATATE, has been approved for detecting neuroendocrine tumors in the clinic (MacRitchie et al., 2020). Recently, Tarkin and coworkers have detected high [^{68}Ga]Ga-DOTATATE uptake in atherosclerotic plaques and the uptake correlated with macrophage-rich areas (Tarkin et al., 2017). However, further studies are needed to validate the feasibility of somatostatin analogs for inflammation imaging.

Translocator protein (TSPO), formerly known as benzodiazepine receptor, is a mitochondrial membrane protein, which is widely distributed in peripheral tissues. TSPO is mainly overexpressed in macrophages, monocytes, activated microglia cells, and astrocytes. Therefore, TSPO-targeted PET imaging has been mostly evaluated in neuroinflammatory diseases, such as multiple sclerosis. (Canat et al., 1993; Oh et al., 2011; Papadopoulos & Lecanu, 2009) Imaging of synovitis using selective TSPO ligand [^{11}C]PK11195 has also been reported. PET studies in patients with RA revealed high [^{11}C]PK11195 uptakes in the inflamed joints, and the increased uptake correlated with the number of macrophages (Gent et al., 2015; van der Laken et al., 2008). Furthermore, TSPO-targeted [^{11}C]PK11195 has been used to image vascular inflammation in patients with systemic inflammatory disorders, and it has shown to be feasible for imaging intraplaque inflammation in patients with a carotid stenosis (Gaemperli et al., 2012; Lamare et al., 2011; Pugliese et al., 2010). The second generation TSPO tracers [^{11}C]DPA-713 and [^{18}F]DPA-714 had better target-to-background ratio than [^{11}C]PK11195 in an experimental rat arthritis model, and [^{11}C]DPA-713 has shown similar results in a proof-of-principle study in patients with RA (Bruijnen et al., 2019; Gent et al., 2014).

2.4.4 Tracers targeting other potential inflammatory markers

Targeting cytokines or enzymes in an inflamed environment is a potential new strategy to image inflammatory diseases. Interleukin 2 (IL-2) is a small cytokine (15 kDa) with pleiotropic effects on immune system. IL-2 binds to an IL-2 receptor complex, which leads to the activation and differentiation of T lymphocytes. Activation of T lymphocytes takes place in many inflammatory diseases, including autoimmune diseases, tumor inflammation, and graft rejection. (Boyman & Sprent, 2012; Mizui, 2019) Previously, IL-2 has been radiolabeled with ^{123}I and ^{99m}Tc and used to image tumor infiltrating lymphocytes and chronic inflammatory diseases,

such as autoimmune diseases, by using SPECT imaging technique (Loose et al., 2008; Signore et al., 2003; Signore et al., 2000, 2004). However, PET imaging offers better resolution than SPECT imaging, and various IL-2-targeting PET tracers have been developed during the past years. ^{18}F-labeled IL-2 ([^{18}F]FB-IL-2) was capable of detecting activated T lymphocytes in a mouse and rat xenograft model of inflammation (Di Gialleonardo, Signore, Glaudemans, et al., 2012; Di Gialleonardo, Signore, Willemsen, et al., 2012). Recently, Hartimath and coworkers have shown that [^{18}F]FB-IL-2 can detect tumor infiltrating T lymphocytes and can be used to monitor therapy response in a mouse tumor model (Hartimath et al., 2017). Two new radiolabeled IL-2 variants, [^{68}Ga]Ga-NODAGA-IL-2 and [^{18}F]AlF-RESCA-IL-2, have been developed, and they showed high uptake in lymphoid tissue and activated T lymphocytes in a mouse xenograft model of inflammation (van der Veen et al., 2020).

Rituximab, a monoclonal antibody targeting B lymphocyte antigen CD20, is a widely used drug to treat lymphomas and autoimmune diseases. This antibody can be radiolabeled with Zirconium-89 (^{89}Zr) and used for the imaging of CD20-positive B cell lymphomas (Muylle et al., 2015). Subsequently, [^{89}Zr]Zr-rituximab has been used for imaging patients with RA. [^{89}Zr]Zr-rituximab showed increased uptake in the affected joints, and the uptake correlated with response to rituximab treatment (Bruijnen et al., 2016). Imaging of B cells with ^{64}Cu-labeled rituximab ([^{64}Cu]Cu-rituximab) has been utilized to image multiple sclerosis in an experimental autoimmune encephalomyelitis (EAE) model. James and coworkers have demonstrated that [^{64}Cu]Cu-rituximab has higher uptake in lumbar spinal cord of an EAE mouse model expressing human CD20 on B cells than in the spinal cord of the control mouse group (James et al., 2017). Recently, next generation anti-CD20 antibodies, such as obinutuzumab and ofatumumab, have been developed and their antibody fragments have been radiolabeled with ^{89}Zr and ^{124}I. ^{89}Zr-labeled antibody fragments of obinutuzumab showed better tumor uptake than ^{124}I-labeled compounds in a murine lymphoma tumor model expressing human CD20 (Zettlitz et al., 2017). Additionally, ^{89}Zr-labeled obinutuzumab and ofatumumab detected human lymphoma xenografts in mice and the tumor uptake of these PET tracers was slightly higher than that of [^{89}Zr]Zr-rituximab (Yoon et al., 2018). The promising results with these radiolabeled humanized anti-CD20 antibodies can be directly translated to the clinic, and CD20 may prove to be a potential target for the imaging of autoimmune diseases.

Fibroblast activation protein (FAP) is a transmembrane glycoprotein and cell surface serine protease. FAP is upregulated in cancer-related fibroblasts of human epithelial cancers and at sites of tissue remodeling, such as fibrosis, arthritis, and wound healing. (Bauer et al., 2006; Garin-Chesa et al., 1990; Levy et al., 1999; Rettig et al., 1993) Imaging of FAP expression has been utilized using radiolabeled FAP

antibody and inhibitors (FAPIs). FAP-targeting antibody 28H1 has been used both in PET and SPECT imaging of RA. In studies with an animal model of RA, antibody 28H1 radiolabeled with ^{111}In, ^{89}Zr or ^{99m}Tc has been shown to accumulate in the inflamed synovium, and the increased uptake in inflamed joints correlated with the arthritis score (Laverman et al., 2015; van der Geest et al., 2017). Preclinical studies with radiolabeled FAPI compounds have been utilized in myocardial infarction, human pancreatic xenograft, and FAP-positive tumor models, and the results have shown good target-to-background ratios (Lindner et al., 2018; Loktev et al., 2018; Toms et al., 2020; Varasteh et al., 2019; Watabe et al., 2020). Clinically, the most potential ^{68}Ga-labeled FAPI compounds ([^{68}Ga]Ga-FAPI-2/4) have effective dose and tumor-to-background ratios comparable with the oncologic standard [^{18}F]FDG (Giesel et al., 2019). Recently, [^{68}Ga]Ga-FAPI-4 has been reported to show high tumor uptake in 28 different kinds of FAP-positive cancers including breast, head and neck, pancreatic, and salivary gland cancer (Kratochwil et al., 2019). New ^{68}Ga-labeled FAPI compounds have been developed, and they have improved intratumoral uptake and tumor-to-background ratio *in vivo* and in the first diagnostic trials of cancer patients (Loktev et al., 2019).

2.4.5 Tracer targeting adhesion molecules

Adhesion molecules are upregulated in various diseases, for example, RA, and are therefore potential targets for inflammation imaging. VCAM-1 and ICAM-1 are members of immunoglobulin superfamily that are endothelial adhesion proteins. VCAM-1 plays an important role in the initiation and development of atherosclerotic plaques (Cybulsky et al., 2001). A synthetic VCAM-1 targeting peptide was identified and labeled with ^{18}F ([^{18}F]4V) to evaluate expression of VCAM-1 in atherosclerosis. In atherosclerotic mice, [^{18}F]4V showed high uptake in atherosclerotic plaques and the uptake correlated to mRNA levels of VCAM-1. Furthermore, increased VCAM-1 mRNA levels and high uptake of [^{18}F]4V were detected during myocardial ischemia and transplanted hearts. (Nahrendorf et al., 2009) ICAM-1 targeting tracers have shown promising results in studies concerning pulmonary diseases. In rats, ^{111}In-labeled ICAM-1 antibody showed high uptakes in injured lungs in two different experimental lung injury models, and the expression of ICAM-1 remained upregulated after lung injury (Weiner et al., 2001; Weiner et al., 1998). In addition, radiolabeled ICAM-1 targeting nanoparticles have been used to monitor the drug delivery properties of nanoparticles to lung endothelium. Copper-64 (^{64}Cu)- and ^{123}I-labeled ICAM-1 targeting nanoparticles have shown favorable properties as drug delivery carriers to lung endothelium in mice (Rossin et al., 2008; Zern et al., 2013), and are therefore potential PET tracers to image pulmonary diseases.

Another adhesion molecule, VAP-1, was for the first time shown to be a promising target for *in vivo* imaging of inflammation in animal models of skin inflammation and arthritis by Jaakkola and co-workers (Jaakkola et al., 2000). To date, several preclinical studies using radiolabeled synthetic peptides based on the crystal structure of human VAP-1 or selected from phage display libraries have proven VAP-1 to be a potential target for imaging inflammation in animal models (Aalto et al., 2011; Autio et al., 2010, 2011; Lankinen et al., 2008; Silvola et al., 2010; Ujula et al., 2009). Using a molecular model of VAP-1, the linear GGGGKGGGG peptide was designed to bind to the active site of VAP-1 and interacts with TPQ residue of VAP-1 thereby inhibiting SSAO enzyme activity (Yegutkin et al., 2004). The first generation radiolabeled VAP-1 targeting PET tracer was a linear nine amino acid peptide GGGGKGGGG containing DOTA-chelator and labeled with ^{68}Ga, [^{68}Ga]Ga-DOTAVAP-1 (Ujula et al., 2009). The *in vivo* specificity of [^{68}Ga]Ga-DOTAVAP-1 has been shown in an osteomyelitis rat model and turpentine oil-induced acute sterile inflammation rat model (Autio et al., 2010; Lankinen et al., 2008). Following the first VAP-1 specific imaging candidate, a 8-amino-3,6-diooxaoctanoyl linker (polyethylene glycol, PEG derivative) was attached to the peptide to improve its imaging properties. In turpentine oil-induced sterile skin inflammation model, [^{68}Ga]Ga-DOTAVAP-PEG-1 showed enhanced pharmacokinetic properties and higher target-to-background ratios compared to the original [^{68}Ga]Ga-DOTAVAP-1 (Autio et al., 2011). Sialic acid-binding immunoglobulin-like lectins (Siglecs) are transmembrane cell surface receptors that bind sialylated glycoconjugates. These interactions mediate cell-cell communication. (Bornhöfft et al., 2018) Siglec-9, a member of the Siglec family, is found with varying expressions in monocytes, neutrophils, B cells, NK cells, $CD4^+$ T cells and $CD8^+$ T cells (Zhang et al., 2000). To further develop second generation VAP-1 targeting PET tracer, a phage display method discovered a novel VAP-1 binding peptide with similarities to the amino acid sequence of Siglec-9 and this peptide revealed to act as a natural leukocyte ligand for VAP-1. Surface plasmon resonance assay revealed that the found phage peptide binds selectively to recombinant VAP-1. A cyclic peptide (CARLSLSWRGLTLCPSK) containing enriched amino acids 283-297 from Siglec-9 was stabilized with a PEG derivative, 8-amino-3,6-diooxaoctanoyl linker, between the peptide and DOTA-chelator and radiolabeled with ^{68}Ga, resulting in [^{68}Ga]Ga-DOTA-Siglec-9. In skin inflammation and melanoma models, [^{68}Ga]Ga-DOTA-Siglec-9 was able to detect inflammation. (Aalto et al., 2011) Later on, several publications have shown that ^{68}Ga-labeled Siglec-9 can be used for imaging of inflammation in bone infection, synovitis, atherosclerosis, and lung injury models (Ahtinen et al., 2014; Retamal et al., 2016; Silvola et al., 2016; Virtanen et al., 2015).

In summary, our previous studies have demonstrated the feasibility of VAP-1-targeted PET imaging of inflammation in several experimental models. However, further studies with [^{68}Ga]Ga-DOTA-Siglec-9 peptide in a model of bacterial infection-induced arthritis and its response to treatment are warranted because only chemically induced arthritis has been previously studied. In addition, the *in vitro* assays of human tissue samples provide only limited information on the suitability of [^{68}Ga]Ga-DOTA-Siglec-9 peptide for PET imaging of inflammation. Therefore, the biodistribution, metabolism, pharmacokinetics, and safety issues of [^{68}Ga]Ga-DOTA-Siglec-9 as well as its ability to detect inflammation must be studied in humans.

3 Aims

The purpose of this study was to investigate the feasibility of targeting VAP-1 with radiolabeled Siglec-9 peptide for PET imaging of inflammation in arthritis and melanoma models. In melanoma study, the purpose was to investigate the role of SHARPIN in inflammation, tumorigenesis, and vasculature using [^{68}Ga]Ga-DOTA-E[c(RGDfK)]$_2$ and [^{68}Ga]Ga-DOTA-Siglec-9. The ultimate goal was to study the biodistribution, metabolism, pharmacokinetics and safety issues of [^{68}Ga]Ga-DOTA-Siglec-9 as well as its ability to detect inflammation in humans.

The specific aims of the study were to:

1. Delineate the feasibility of [^{68}Ga]Ga-DOTA-Siglec-9 for detecting *Borrelia burgdorferi* infection-induced inflammation.
2. Explore the possible effects of SHARPIN deficiency on the [^{68}Ga]Ga-DOTA-E[c(RGDfK)]$_2$ peptide distribution with or without melanoma tumor allografts, tumor microenvironment and tumor-associated inflammation detected by [^{68}Ga]Ga-DOTA-Siglec-9 peptide.
3. Assess the safety, tolerability, metabolism, pharmacokinetics, whole-body distribution and radiation dosimetry of [^{68}Ga]Ga-DOTA-Siglec-9 peptide in healthy subjects, and the ability to detect arthritis.

4 Materials and Methods

4.1 Animal models

All animal experiments were performed in compliance with the European Union directive relating to the conduct of animal experimentation. Study protocols were approved by the National Animal Experiment Board in Finland and the regional State Administrative Agency for Southern Finland (license numbers ESAVI/3116/04.10.07/2017, ESAVI/9339/04.10.07/2016, and ESAVI/5239/04.10.07/2017). The animals were housed under standardized conditions in the Central Animal Laboratory of University of Turku with a 12 hour light-dark cycle and they had access to water and food *ad libitum*.

4.1.1 Animal model of Lyme borreliosis (I)

Twenty-six 4-week-old female C3H/HeNhsd mice (Envigo, Horst, The Netherlands) weighing 23 ± 1.8 g were utilized in Study I. To induce Lyme borreliosis, twenty-two mice were intracutaneously injected with 10^6 bacteria of a wild-type *Borrelia burgdorferi* sensu stricto N40 strain (abbreviated *B. burgdorferi*) in phosphate-buffered saline (PBS) solution into lower back. Four uninfected control mice were injected with an equal volume of PBS into lower back. Four weeks after *B. burgdorferi* infection, eight of *B. burgdorferi*-infected mice were subcutaneously (s.c.) treated with 25 mg/kg ceftriaxone (Rocephalin®, Roche, Grenzach-Wyhlen, Germany) twice a day for five days.

4.1.2 Sharpin-deficient mouse model (II)

Sixteen 6-week-old (weight 19 ± 1.8 g) mice harboring a spontaneous null mutation in the *Sharpin* gene (C57BL/KaLawRij-SHARPIN^{cpdm}/RiJ-SunJ, strain 007599, Jackson Laboratory, Bar Harbor, MA, USA; abbreviated hereafter *Sharpin^{cpdm}*) and their nine littermate wild-type (wt) mice (weight 20 ± 2.8 g) were utilized. *Sharpin^{cpdm}* mice suffer from progressive multi-organ inflammation with chronic eosinophilic hyperproliferative dermatitis starting at 3-5 weeks of age, and limiting the lifespan of the mice to 7 weeks of age (HogenEsch et al., 1993; Seymour et al., 2007).

4.1.3 Animal model of melanoma (II)

For Study II, B16 murine melanoma cells with high metastatic potential (Fidler & Nicolson, 1977) (B16-F10-luc-2G5) were grown in modified Eagle medium (MEM) supplemented with 10% fetal calf serum, MEM vitamin solution (Gibco; Invitrogen, Carlsbad, CA, USA), L-glutamine, sodium pyruvate, and penicillin-streptomycin (Sigma-Aldrich, Saint Louis, MO, USA) at 37°C in the presence of 5% carbon dioxide. For the B16 melanoma model, female and male *Sharpin*^{cpdm} and their littermate wt mice were utilized. At the age of five and a half weeks, 10^6 B16 melanoma cells were s.c. injected into the neck area of the *Sharpin*^{cpdm} (n = 12, weight 20 ± 2.5 g) and wt (n = 12, weight 22 ± 2.0 g) mice, and tumors were allowed to grow for seven days before PET studies. For the B16 melanoma footpad tumor model, right hind leg footpads were sterilized with alcohol and 10^6 B16 melanoma cells mixed with Matrigel were injected into the right hind leg of the *Sharpin*^{cpdm} and wt mice. The tumors were allowed to grow for fourteen days.

4.2 Subject characteristics in the first-in-human study (III)

Study III included six healthy male subjects (age 37 ± 9 years) and one 49-year-old male patient with newly diagnosed RA. The study protocol was reviewed and approved by the joint Ethics Committee of the University of Turku and Turku University Hospital, and by the Finnish Medicines Agency. This first-in-human study was conducted in accordance with the principles of the Declaration of Helsinki. All participants provided their written informed consent before the PET studies. The study has been registered as a clinical trial on ClinicalTrials.gov (NCT03755245).

All subjects were screened for medical, neurological, and psychiatric history, and the history of alcohol or drug abuse was determined using questionnaires. Before the PET/CT imaging, routine blood tests, electrocardiography, and a clinical examination were performed for all subjects. During imaging, vital signs were monitored, and blood and urine samples were taken during and after the PET/CT imaging.

4.3 Tracer radiosyntheses

All tracers utilized in these studies were synthesized in the Radiopharmaceutical Chemistry Laboratory of the Turku PET Centre. For the first-in-human study, [^{68}Ga]Ga-DOTA-Siglec-9 was synthesized and produced according to the good manufacturing practice (GMP) standard. [^{18}F]FDG was synthesized as previously described (Hamacher et al., 1986). The radiochemical purity of the tracers was over 95% in each synthesized batch.

4.3.1 [^{68}Ga]Ga-DOTA-Siglec-9

^{68}Ga was obtained from a ^{68}Ge/^{68}Ga generator (Eckert & Ziegler, Valencia, CA, USA) by elution with 0.1 M HCl. ^{68}Ga eluate (0.5 mL, 220 ± 47 MBq) was mixed with 2-[4-(2-hydroxyethyl)piperazin-1-yl]ethanesulfonic acid (HEPES) to give a pH of approximately 4.1, and thereafter DOTA-Siglec-9 peptide (3-6 nmol, 7.3-14.5 µg dissolved in deionized water; Peptide Specialty Laboratories GmbH, Heidelberg, Germany) was added to the mixture. The reaction mixture was then heated at 100°C for 15 minutes. After cooling down with an ice bath to approximately room temperature, 1 M NaOH solution was used to adjust the pH to neutral. The radiochemical purity of [^{68}Ga]Ga-DOTA-Siglec-9 was determined using radio detector-coupled reversed-phase high-performance liquid chromatography (radio-HPLC). The radio-HPLC system consisted of LaChrom instruments (Hitachi, Merck, Darmstadt, Germany), and a Radiomatic 150TR radioisotope detector (Packard, Meriden, CT, USA). Jupiter C18 column (4.6 × 150 mm, 300 Å, 5 µm; Phenomenex, Torrance, CA, USA) was used and the HPLC conditions were as follows: flow rate 1 mL/min; λ = 215 nm; A = 0.1% trifluoroacetic acid (TFA) in water; B = 0.1% TFA in acetonitrile (ACN); gradient: during 0-2 min 82% A and 18% B; during 2-11 min from 82% A and 18% B to 40% A and 60% B; during 11-15 min from 40% A and 60% B to 82% A and 18% B; during 15-20 min 82% A and 18% B. Molecular structure of DOTA-Siglec-9 peptide is shown in Figure 2.

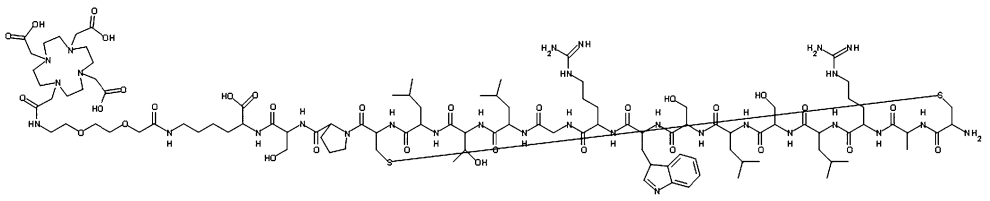

Figure 2. Molecular structure of DOTA-Siglec-9 peptide. Modified and reprinted with permission from Virtanen et al., 2015.

4.3.2 GMP-grade [^{68}Ga]Ga-DOTA-Siglec-9

The radiosynthesis of GMP-grade [^{68}Ga]Ga-DOTA-Siglec-9 was performed using a fully automated synthesis device (Modular Lab PharmTracer, Eckert & Ziegler). ^{68}Ga was obtained from a ^{68}Ge/^{68}Ga generator (Eckert & Ziegler, Valencia, CA, USA) by elution with 0.1 M HCl and passing the eluate through a Strata-XC cation exchange cartridge. Bound $^{68}GaCl_3$ (766 ± 148 MBq) was eluated with acidified acetone (0.6 mL, containing 3.25% water and 0.02 M HCl) into a reaction vial. The reaction vial contained GMP-grade DOTA-Siglec-9 precursor (30 µg, 12 nmol in 60

µL water; ABX Advanced Biomedical Compounds GmbH, Radeberg, Germany), 0.2 M sodium acetate buffer, and absolute ethanol, and the reaction mixture was incubated at 65°C for 6 min. After incubation time, the reaction mixture was diluted with physiological saline and purified by loading onto a C18 cartridge (SepPak Light C18, Waters) and washing the cartridge twice with physiological saline. Purified [^{68}Ga]Ga-DOTA-Siglec-9 was eluted with ethanol through a 0.22 µm filter into the sterile end product vial and formulated into physiological saline. The radiochemical purity of GMP-grade [^{68}Ga]Ga-DOTA-Siglec-9 was evaluated by radio-HPLC (LC-20A Prominence HPLC System, Shimadzu, Kyoto, Japan; on-line radioactivity detector Flow-Count, Bioscan Inc.) using an analytical Kinetex C18 column (2.6 µm, 100 Å, 75 × 4.6 mm; Phenomenex). Solvent A was 0.16% TFA in water and solvent B was 0.16% TFA in ACN, and linear gradient from 18% B to 50% B over 12 min was used. Flow rate was 1 mL/min and λ = 220 nm.

4.3.3 [^{68}Ga]Ga-DOTA-E[c(RGDfK)]$_2$ and [^{68}Ga]Ga-DOTA-E[c(RGEfK)]$_2$

^{68}Ga was obtained from a ^{68}Ge/^{68}Ga generator (Eckert & Ziegler) as previously described (Chapter 4.3.1). DOTA-E[c(RGDfK)]$_2$ precursor (3 nmol, 5 µg dissolved in deionized water) was added to the mixture. The reaction mixture was then heated at 100°C for 15 min. The radiochemical purity of [^{68}Ga]Ga-DOTA-E[c(RGDfK)]$_2$ was determined by radio-HPLC. Jupiter C18 column was used and the HPLC conditions were as follows: flow rate 1 mL/min; λ = 220 nm; A = 0.1% TFA in water; B = 0.1% TFA in ACN. The A/B gradient was as follows: during 0-2 min 82%/18%; during 2-11 min from 82%/18% to 40%/60%; during 11-14 min 40%/60%; during 14-15 min from 40%/60% to 82%/18%; and during 15-20 82%/18%. Molecular structure of DOTA-E[c(RGDfK)]$_2$ is shown in Figure 3. DOTA-E[c(RGEfK)]$_2$ control peptide precursor (3 nmol, 5 µg dissolved in deionized water) was radiolabeled in same reaction conditions as [^{68}Ga]Ga-DOTA-E[c(RGDfK)]$_2$. Additionally, the radiochemical purity of [^{68}Ga]Ga-DOTA-E[c(RGEfK)]$_2$ was determined as described above.

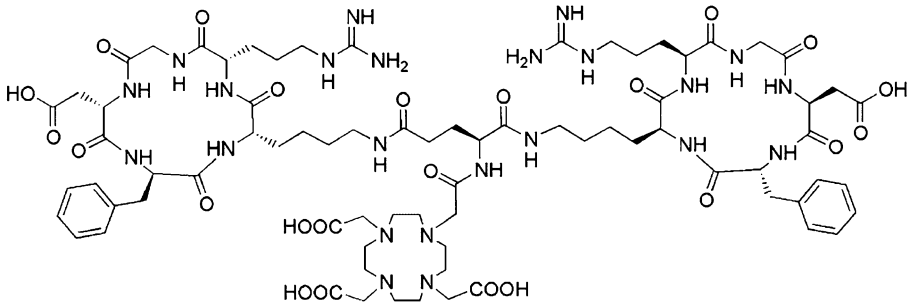

Figure 3. Molecular structure of DOTA-E[c(RGDfK)]$_2$. Modified and reprinted with permission from Dijkgraaf et al., 2011.

4.4 Small animal PET studies

4.4.1 PET studies of Lyme borreliosis (I)

The swelling of hind tibiotarsal joint of each mouse was measured once a week using a metric caliper and followed up for seven weeks. Six mice (two *B. burgdorferi*-infected, two uninfected controls, and two ceftriaxone-treated *B. burgdorferi*-infected mice) were followed up and imaged weekly with Inveon Multimodality PET/CT scanner (Siemens Medical Solutions, Knoxville, TN, USA) for seven weeks starting at four days post-infection. In addition, two *B. burgdorferi*-infected and/or ceftriaxone-treated *B. burgdorferi*-infected mice were imaged with PET/CT and killed each week from two weeks up to seven weeks post-infection. The mice were i.v. injected with 9.9 ± 1.1 MBq (1.2 ± 0.53 µg) of [^{68}Ga]Ga-DOTA-Siglec-9 via a tail vein under isoflurane anesthesia and a 30-min dynamic PET imaging was performed based on our previous study (Aalto et al., 2011). The PET data were acquired in a list mode and iteratively reconstructed with an ordered subset expectation maximization three-dimensional algorithm (OSEM3D). The quantitative analysis of *in vivo* PET/images was performed using Inveon Research Workplace 4.1 software (Siemens Medical Solutions, Malvern, PA, USA). Regions of interest (ROIs) were defined in hind tibiotarsal joints and other main tissues based on CT. The results were expressed as standardized uptake values (SUVs) calculated as (average radioactivity within the ROI) / (injected radioactivity/animal weight).

After the last PET/CT imaging, the mice were sacrificed, various tissue samples were excised using sterile techniques and weighed, and radioactivity was measured using a gamma counter (Triathler 3″, Hidex, Turku, Finland). *Ex vivo* radioactivity measurements were corrected for radionuclide decay from the time of injection and

for the weight of tissue and animal. The tissue uptake results were reported as percentage of injected radioactivity dose per gram of tissue (%ID/g).

After gamma counting, samples of ear, heart, tibiotarsal joint, and urinary bladder were collected using sterile techniques to assess the *B. burgdorferi* infection status. Samples were cultured in BSK II medium supplemented with phosphomycin (50 µg/mL, Sigma-Aldrich) at 33°C for six weeks, and the growth was monitored every two weeks with a microscope. Furthermore, one tibiotarsal joint of each animal was collected for histological analysis.

4.4.2 PET studies of *Sharpin*^{cpdm} mice with and without melanoma tumors (II)

Study II consisted of two experimental study designs. The first study design involved *Sharpin*^{cpdm} and wt mice without B16 melanoma tumors. Seven *Sharpin*^{cpdm} (weight 20 ± 1.3 g) and nine wt (weight 20 ± 2.8 g) were i.v. injected with 10 ± 1.0 MBq (0.56 ± 0.22 µg) of [^{68}Ga]Ga-DOTA-E[c(RGDfK)]$_2$ and a 30-min dynamic PET/CT imaging was performed. The PET data were reconstructed with an ordered subset expectation maximization two-dimensional algorithm. Two different competition studies were performed to verify the specificity of [^{68}Ga]Ga-DOTA-E[c(RGDfK)]$_2$ uptake. *Sharpin*^{cpdm} mice (n = 4, weight 18 ± 0.77 g) were injected with an 18 mg/kg dose of non-labeled DOTA-E[c(RGDfK)]$_2$ peptide 10 min before PET/CT imaging. Subsequently, [^{68}Ga]Ga-DOTA-E[c(RGDfK)]$_2$ (9.1 ± 0.90 MBq, 0.63 ± 0.33 µg) was injected and imaged as described above. In another competition study, *Sharpin*^{cpdm} mice (n = 5, weight 17 ± 2.0 g) were i.v. injected with 9.1 ± 0.60 MBq (0.51 ± 0.20 µg) of control peptide [^{68}Ga]Ga-DOTA-E[c(RGEfK)]$_2$ and imaged as described above. After PET/CT imaging, the mice were sacrificed, various tissues were excised, weighed, and measured with a gamma counter (Triathler 3″, Hidex). The results of *ex vivo* biodistribution were expressed as %ID/g.

In the second study design, *Sharpin*^{cpdm} and wt mice with B16 melanoma tumors were utilized. The growth of B16 melanoma cells was verified with bioluminescence imaging (IVIS Spectrum, Perkin Elmer, Waltham, MA, USA) one day after cell inoculation. Using ultrasound imaging (Vevo 2100, VisualSonics Inc., Toronto, Ontario, Canada), the growth of tumors was monitored and measured at 1, 4, 6, 7, 8, and 9 days after inoculation under isoflurane anesthesia. To measure the blood flow in tumors, the non-targeted contrast agent consisting of phospholipid shell microbubbles filled with nitrogen and perfluorobutane (5×10^7 microbubbles; Vevo MicroMarker, VisualSonics) was i.v. injected via a tail vein catheter. ROIs were defined around the entire tumor and time to peak was determined from the graph and used as a measure of blood flow. PET/CT imaging studies with [^{68}Ga]Ga-DOTA-E[c(RGDfK)]$_2$ and [^{68}Ga]Ga-DOTA-Siglec-9 were performed seven, nine, and ten

days after the B16 melanoma cell inoculation. The mice were first i.v. injected with 5.5 ± 0.72 MBq (0.32 ± 0.15 µg) of [^{68}Ga]Ga-DOTA-Siglec-9 and a 30-min dynamic PET/CT imaging was performed. After radioactive decay, the mice were i.v. injected with 9.6 ± 2.3 MBq (0.65 ± 0.34 µg) of [^{68}Ga]Ga-DOTA-E[c(RGDfK)]$_2$ and a 60-min dynamic PET/CT imaging was performed. The PET data were reconstructed with OSEM3D. Using Carimas 2.9 software (Turku PET Centre), quantitative PET analysis was done by defining the ROI within tumor. Time frames 45-60 min post-injection were used for the [^{68}Ga]Ga-DOTA-E[c(RGDfK)]$_2$ PET image analysis and time frames 20-30 min post-injection were used for the [^{68}Ga]Ga-DOTA-Siglec-9 PET image analysis. The *in vivo* results were expressed as SUV_{mean}.

During the last [^{68}Ga]Ga-DOTA-E[c(RGDfK)]$_2$ PET/CT imaging, the mice were i.v. injected with anti-VAP-1 antibody (clone 7-88, 1 mg/kg) ten minutes before being sacrificed. After the last PET/CT, the radioactivity of excised tissues was measured with a gamma counter (Triathler 3″, Hidex). The *ex vivo* results were expressed as SUV. The distribution of [^{68}Ga]Ga-DOTA-E[c(RGDfK)]$_2$ in tumors was studied in more detail with digital autoradiography (ARG). After gamma counting, the B16 melanoma tumors were frozen in isopentane, cut into 20 and 8 µm cryosections, and apposed to an imaging plate (Fuji Imaging Plate BAS-TR2025, Fuji Photo Film Co., Tokyo, Japan). After the end of the exposure time, the plates were scanned with a Fuji Analyzer BAS-5000 (internal resolution 25 µm). The ARG data were analyzed using Tina 2.1 software (Raytest Isotopenmessgeräte, GmbH, Straubenhardt, Germany). According to hematoxylin-eosin staining, ROIs were drawn in tumor, tumor border, tumor periphery, skin, and muscle. The results from ARG analysis were reported as photostimulated luminescence per square millimeter (PSL/mm^2). The background count was subtracted from the image data, and PSL/mm^2 values were normalized for the injected radioactivity dose, weight of the mouse, and radioactivity decay.

4.5 Human radiation dosimetry study (III)

This study was performed using a Discovery 690 whole-body PET/CT scanner (General Electric Medical Systems). In healthy subjects, 162 ± 4 MBq (13.6 ± 3.0 µg) of [^{68}Ga]Ga-DOTA-Siglec-9 was i.v. injected and the PET imaging started at 1, 10, 20, 40, 100, and 200 min after injection. Scanning at 100 min after injection covered the whole range from head to toes, whereas other scans covered the range from head to mid thighs. The patient with RA was first imaged with [^{18}F]FDG. After fasting of 6 h, 198 MBq of [^{18}F]FDG was i.v. injected and a PET scan from head to toes was performed at 46 min after injection. The next day, the patient was i.v. injected with 175 MBq (15 µg) of [^{68}Ga]Ga-DOTA-Siglec-9 and a 30-min dynamic PET/CT imaging was performed on hands, followed by a whole-body scan. PET

images were reconstructed with three-dimensional VUE Point algorithm. During PET imaging, venous blood samples were collected at 2, 3, 5, 6, 7, 10, 15, 20, 30, 60, 90, 180, and 240 min after the injection of [^{68}Ga]Ga-DOTA-Siglec-9. The radioactivity of whole blood and plasma was measured with an automated gamma counter (1480 Wizard 3″, Perkin Elmer/Wallac, Turku, Finland), and then plasma proteins were precipitated with acetonitrile. The percentage of radioactivity bound to plasma proteins was calculated and expressed as previously described (Jensen et al., 2017). The stability of [^{68}Ga]Ga-DOTA-Siglec-9 *in vivo* was examined from plasma samples. Plasma proteins were precipitated with 10% sulfosalicylic acid and the protein-free plasma supernatants were analyzed with radio-HPLC. The radio-HPLC was performed using a semi-preparative Kinetex C18 column (5 µm, 300 Å, 150 × 10 mm; Phenomenex) at flow rate 5 min/mL and gradient A = 0.16% TFA/water and B = 0.16% TFA/ACN as follows: during 0-11 min solvent B from 0% to 50%; during 11-12 min solvent B from 50% to 100%; during 12-14 min solvent B 100%; and during 14-15 min solvent B from 100% to 0%. The same HPLC procedure was used for the analysis of urine samples.

Distribution kinetics and dose estimates were quantified from the whole-body image data of healthy subjects according to the Radiation Dose Assessment Resource method for internal dose estimation (Stabin & Siegel, 2003). Volumes of interests (VOIs) were defined using Hermes 2.7 software (Hermes Medical Solutions, Stockholm, Sweden). The VOIs covered the whole organ or a representative volume of the organ, and the following source organs were identified: brain, bone (cortical and trabecular), left ventricle of heart, heart wall, kidneys, liver, muscle, pancreas, red bone marrow, salivary glands, spleen, and urinary bladder. Urinary clearance and biological half-life were estimated using measurements of urinary voids. Time-activity curves were determined for each source organ. The resultant kinetic data were modeled using the sums of exponentials to determine residence times of the source organs. A urinary bladder voiding interval of 3.5 h was used in the calculation of the bladder residence time. Radiation absorbed doses were calculated using these residence times and the Organ Level INternal Dose Assessment/EXponential Modeling (OLINDA/EXM) version 2.2 software (Stabin & Siegel, 2018). The adult male (~70 kg) reference model was used. OLINDA/EXM 2.2 uses the International Commission on Radiological Protection (ICRP) Publication 103 (ICRP 103) recommendation for calculating the effective dose (ICRP, 2007).

In the patient with RA, VOIs were drawn in the area of three inflamed finger joints [proximal interphalangeal (PIP) joints 2 and 3, and distal interphalangeal (DIP) joint 3] of the right hand using Carimas 2.10 software (Turku PET Centre, Turku, Finland). The average radioactivity concentrations of VOIs were used for further analyses and the uptake of [^{68}Ga]Ga-DOTA-Siglec-9 and [^{18}F]FDG was expressed as SUV.

4.6 Histology and immunohistochemistry

In Study I, one tibiotarsal joint of each mouse was collected, formalin-fixed, demineralized, paraffin-embedded, and cut into 5 µm sections. The 5 µm sections were stained with hematoxylin and eosin (HE) for basic histology. From HE stainings, joint inflammation was analyzed by a pathologist blinded to the infection status of the mouse. Synovial proliferation, chronic inflammation, and active inflammation were scored on a scale from 0 to 6. Furthermore, the diameters of the joints were also measured. In Study II, the 20 µm tumor cryosections were stained with HE for basic histology and scanned with a digital slide scanner (Pannoramic 250 Flash, 3DHistech Ltd., Budapest, Hungary). The morphology of each tumor was examined using Pannoramic Viewer v. 1.15 software (3DHistech Ltd.).

For immunohistochemistry, VAP-1 stainings were performed on the tibiotarsal joint and B16 melanoma tumor sections. In Study I, the 5 µm formalin-fixed, decalcified, paraffin-embedded tibiotarsal joints were stained with a monoclonal TK10-79 antibody recognizing mouse VAP-1 (1 µg/mL). Antigen retrieval with 0.01 M citric acid and removal of endogenous peroxidase with 1% hydrogen peroxidase were performed for the sections. The primary antibody was detected with a VECTASTAIN Elite ABC rat immunoglobulin G kit (PK-6104, Vector Laboratories, Burlingame, CA, USA), followed by a horseradish peroxidase-conjugated avidin. Diaminobenzidine (K3468, DAKO, Glostrup, Denmark) was used as a chromogen, and hematoxylin was used for counterstaining. In Study II, the mice were i.v. injected with a monoclonal rat anti-mouse VAP-1 antibody (clone 7-88, 1 mg/kg) before being sacrificed. The 8 µm B16 melanoma tumor sections were stained with a secondary Alexa Fluor 488-conjugated goat anti-rat IgG (A11006, Invitrogen, Carlsbad, CA, USA).

To study vascularization, CD31 stainings were performed on the 8 µm B16 melanoma tumor cryosections. The sections were incubated overnight with anti-CD31 rabbit polyclonal antibody (RB10333, 1:200, Thermo Fisher Scientific, Waltham, MA, USA). Donkey Alexa Fluor 488-conjugated anti-rabbit IgG (A11006, Invitrogen, Carlsbad, CA, USA) was utilized as a secondary antibody. In order to detect β_3 integrin expression, the 8 µm B16 melanoma tumor cryosections were incubated with anti-β_3 rabbit monoclonal antibody (ab75872, 1:200, Abcam, Cambridge, UK). Donkey Alexa Fluor 488-conjugated anti-rabbit IgG (A11006, Invitrogen, Carlsbad, CA, USA) was utilized as a secondary antibody. CD45 stainings were performed on the 8 µm B16 melanoma tumor cryosections to examine the invasion of inflammatory cells in B16 tumors. The sections were incubated with a fluorescein isothiocyanate (FITC)-conjugated rat monoclonal anti-CD45 antibody (BD553079, 1:50, BD Biosciences, San Jose, CA, USA). Thereafter, the sections were mounted in ProLong Gold antifade reagent with DAPI (P36935, Invitrogen). All fluorescence stainings (VAP-1, CD31, β_3, and CD45) were scanned with a

fluorescence scanner (Pannoramic MIDI, 3DHistech Ltd.) or an AxioVert 200M microscope (Carl Zeiss Light Microscope) or were imaged using a 3i (Intelligent Imaging Innovations, 3i Inc) Marianas spinning disk confocal microscope with a Yokogawa CSU-W1 scanner and Hamamatsu sCMOS Orca Flash 4.0 camera (Hamamatsu Photonics K.K.), using a tile scan function. Images were analyzed with ImageJ 1.48 software (National Institutes of Health, Bethesda, MD, USA). The results were calculated using automated thresholding and expressed as the percentage of positive staining within the tumor area.

4.7 sVAP-1 measurements

In Study III, the activity and the levels of sVAP-1 were determined from plasma samples, which were taken before PET/CT imaging. In the fluorometric assay determining the activity of sVAP-1, the plasma samples were incubated on a 96-well microplate (Nunc, Roskilde, Denmark) with or without a VAP-1 inhibitor called hydroxylamine for 30 min at 37°C. The VAP-1 substrate benzylamine was added to the wells after the addition of Amplex Red reagent (Molecular Probes, Eugene, OR, USA) and horseradish peroxidase (Sigma Aldrich). The hydrogen peroxidase produced in the wells by sVAP-1 was measured by a standard created with known amounts of hydrogen peroxidase. The amount of the fluorescent end product, resorufin, was measured with a Tecan Infinite M200 plate reader (Tecan, Männedorf, Switzerland) during a period of 1 hour with 5 minute intervals. The specific activities (nmol/mL/h) of sVAP-1 were calculated with a custom-made Excel macro.

An in-house ELISA assay was used to measure the levels of sVAP-1 from the heparin samples. First, the 96-well microtiter plate (MaxiSorp, Nunc, Roskilde, Denmark) was coated with a monoclonal anti-VAP-1 antibody (TK8-18). After blocking, the sample dilutions were added, followed by the detecting biotinylated anti-VAP-1 antibody (TK8-14), streptavidin-horseradish peroxidase (GE Healthcare, Chicago, IL, USA), and finally BM Chemiluminescence ELISA substrate (Roche Diagnostics, Basel, Switzerland). Each reagent was incubated for 1 hour. A linear standard curve was produced with recombinant human VAP-1 protein (R&D Systems, Minneapolis, MN, USA). The luminescence was measured with the Tecan Infinite M200 and the levels (ng/mL) were calculated with an Excel macro.

4.8 Statistical analyses

The statistical analyses were conducted using the GraphPad Prism 7 (GraphPad Software Inc, La Jolla, CA, USA) or IBM SPSS Statistics 23 (IBM, Armonk, NY, USA) software. All results are expressed as mean ± standard deviation (SD) or mean

± standard error of the mean (SEM). Normal distribution of the data was analyzed using the Shapiro-Wilk test. For comparisons between two groups, a Student *t*-test was used for normally distributed data, and nonparametric Mann-Whitney *U* test was used for all other experiments. Comparisons between multiple groups were done by one-way analysis of variance (ANOVA). The *post-hoc* correction methods for ANOVA were Dunnett (I) and Tukey (II). Pearson's and Spearman's correlation coefficients were calculated to assess correlations. A *P* value of less than 0.05 was regarded as statistically significant.

5 Results

5.1 VAP-1 targeting imaging visualizes sites of inflammation in *Borrelia burgdorferi*-infected mice

5.1.1 Characterization of *B. burdorferi*-induced arthritis in mice

All cultured tissue samples of *B. burgdorferi*-infected mice were positive, whereas tissue samples from uninfected control and ceftriaxone-treated infected mice were culture-negative. These results indicate that the infected mice had developed a disseminated *B. burgdorferi* infection.

All of the *B. burgdorferi*-infected mice developed visually distinct tibiotarsal joint swelling and redness, which reached maximum swelling at four weeks post-infection (Figure 4A). The ceftriaxone treatment twice a day for five days did not markedly reduce the swelling of the tibiotarsal joint as compared to that of untreated infected mice, although the joint diameter was significantly higher at 4 and 5 weeks post-infection (Figure 4B). The joint diameters of uninfected mice remained at the same level throughout the follow-up period and differed significantly from the infected and ceftriaxone-treated infected mice.

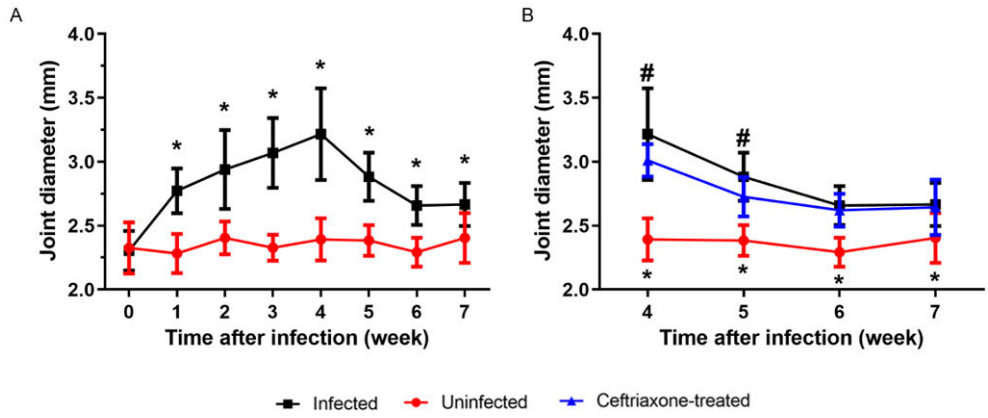

Figure 4. Development of hind tibiotarsal joint swelling in the three study groups. (**A**) Tibiotarsal joint swelling in *B. burgdorferi*-infected mice as compared to the uninfected mice during the 7-week follow-up period. **P* < 0.05 for infected vs. uninfected. (**B**) The effects of ceftriaxone treatment on tibiotarsal joint swelling as compared to the untreated infected and uninfected mice. **P* < 0.05 for ceftriaxone-treated vs. uninfected and #*P* < 0.05 for ceftriaxone-treated vs. infected. Modified and reprinted with permission from Siitonen et al., 2017.

5.1.2 Histology and immunohistochemistry of tibiotarsal joints

The joint inflammation was also studied by HE staining. Histologically, the tibiotarsal joints of infected mice revealed severe signs of inflammation, including the thickening of synovial membrane, proliferation of synovial lining cells, and chronic inflammation. The inflammation status of tibiotarsal joints was scored and the maximum scores were reached at five weeks post-infection in the infected mice group.

The expression of VAP-1 in tibiotarsal joints was verified from uninfected, infected, and ceftriaxone-treated mice. Based on immunohistochemistry staining, VAP-1 was moderately expressed on the synovial tissue vessels of infected mice at two weeks post-infection. The strongest VAP-1 expression was detected at four weeks post-infection in infected mice. The synovium of ceftriaxone-treated mice showed moderate expression of VAP-1, while only occasional VAP-1 positive vessels were observed in the synovium of uninfected mice.

5.1.3 PET/CT imaging

PET/CT imaging with [^{68}Ga]Ga-DOTA-Siglec-9 detected *B. burgdorferi*-induced inflammation in the affected joints of infected mice (Figure 5A). In contrast, low accumulation of [^{68}Ga]Ga-DOTA-Siglec-9 was detected in the joints of uninfected mice. According to the PET/CT imaging, the highest uptake in the affected joints was observed at four weeks post-infection (0.68 ± 0.17), which was significantly higher as compared to uninfected mice (0.36 ± 0.065, $P = 0.0037$) (Figure 5B). In spite of the short-term ceftriaxone treatment, the *B. burgdorferi*-induced arthritis still persisted and

in vivo uptake was equally high as that of untreated infected mice during 4–7 weeks post-infection (Figure 5C). The *ex vivo* measurements of excised tibiotarsal joints 30 min after the injection of [^{68}Ga]Ga-DOTA-Siglec-9 verified the *in vivo* PET/CT imaging results. Furthermore, the *in vivo* [^{68}Ga]Ga-DOTA-Siglec-9 uptake of the individual tibiotarsal joints correlated significantly with the joint swelling ($r = 0.73$, $P < 0.0001$) as well as with the histological scoring of inflammation ($r = 0.61$, $P = 0.020$).

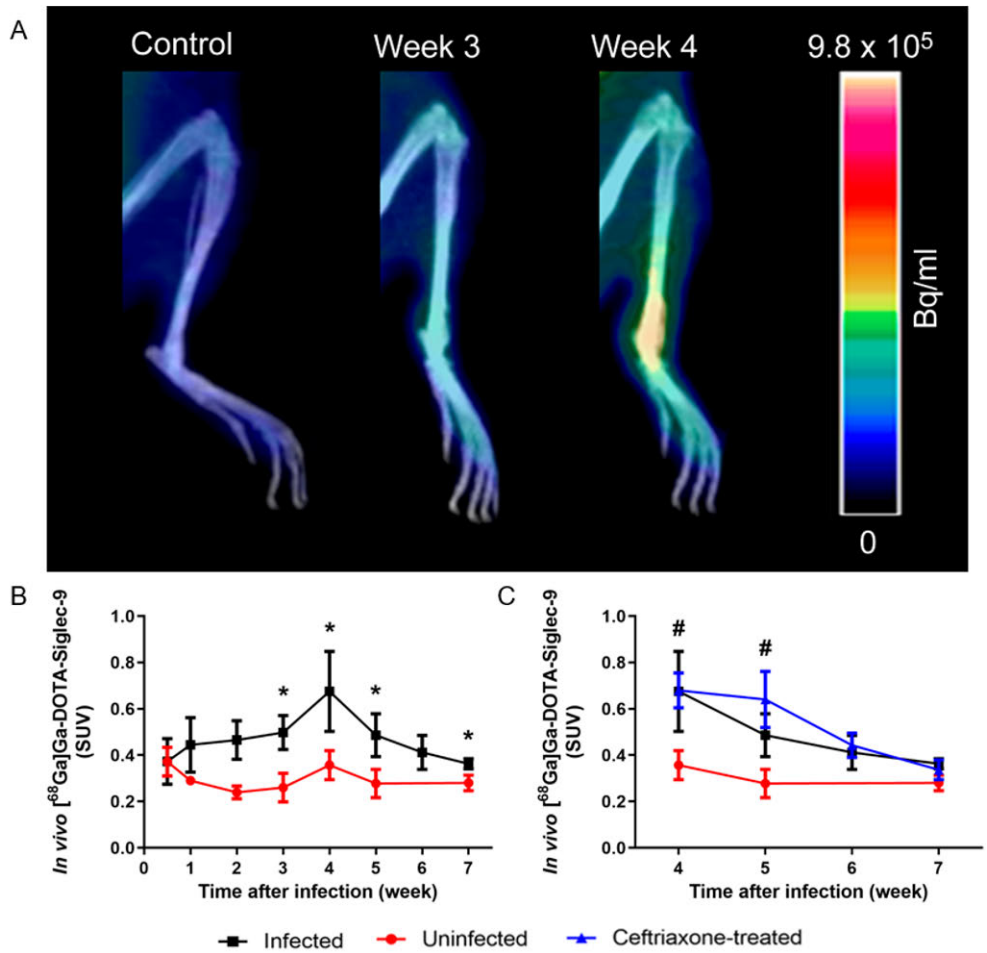

Figure 5. The *in vivo* results of [^{68}Ga]Ga-DOTA-Siglec-9 in mouse tibiotarsal joints. (**A**) Representative coronal PET/CT images of an uninfected mouse and a *B. burgdorferi*-infected mouse showing the increased uptake of [^{68}Ga]Ga-DOTA-Siglec-9 in the tibiotarsal joint of *B. burgdorferi*-infected mouse at weeks 3 and 4 post-infection as compared to an uninfected control mouse. (**B**) Quantified *in vivo* uptake of [^{68}Ga]Ga-DOTA-Siglec-9 in tibiotarsal joints of the infected and uninfected mice during the follow-up period. (C) Quantified *in vivo* uptake of [^{68}Ga]Ga-DOTA-Siglec-9 in tibiotarsal joints of ceftriaxone-treated mice as compared to the untreated infected and uninfected mice from week 4 to week 7 post-infection. $^{*}P < 0.05$ for infected vs. uninfected and $^{\#}P < 0.05$ for ceftriaxone-treated vs. uninfected. Modified and reprinted with permission from Siitonen et al., 2017.

5.2 Imaging of altered $\alpha_v\beta_3$ integrin expression and activity status in inflammation and B16 tumor model

5.2.1 Histology and immunohistochemistry

The HE staining demonstrated that the B16 melanoma tissue was homogenous and viable without large necrotic areas. Luminal expression of VAP-1 in B16 melanoma was proved with i.v. administered anti-VAP-1 antibody followed by immunohistochemical staining with a fluorescent-labeled secondary antibody. Based on the fluorescence staining, the expression of VAP-1 indicative of inflammation was similar between *Sharpin*^{cpdm} and wt mice. Furthermore, CD45 staining did not show differences in the infiltration of immune cells into B16 melanoma between *Sharpin*^{cpdm} and wt mice. The quantitative analysis of CD31 staining revealed that the tumors of *Sharpin*^{cpdm} mice were more vascularized than the tumors of wt mice (percentage of tumor area 2.1 ± 0.11 vs. 1.7 ± 0.15, $P = 0.04$). The β_3 integrin was expressed in both B16 tumor cells and endothelial cells. The quantitative analysis of β_3 integrin staining showed a more elevated β_3 integrin expression in the tumors of *Sharpin*^{cpdm} than those of wt mice, but the difference was not statistically significant ($P = 0.08$).

5.2.2 *Ex vivo* biodistribution and autoradiography

The uptake of [^{68}Ga]Ga-DOTA-E[c(RGDfK)]$_2$, measured as %ID/g, was higher in skin and several other tissues of *Sharpin*^{cpdm} mice than in those of wt littermates. In the competition study, the excess of unlabeled DOTA-E[c(RGDfK)]$_2$ reduced by over 50% the uptake in salivary glands, small intestine, and thymus in *Sharpin*^{cpdm} mice. Moreover, the competition study with the control peptide [^{68}Ga]Ga-DOTA-E[c(RGEfK)]$_2$ provided similar results, and reduced uptake in aorta, salivary glands, small intestine, and thymus was observed in *Sharpin*^{cpdm} mice.

In B16 melanoma bearing mice, the *ex vivo* results of [^{68}Ga]Ga-DOTA-E[c(RGDfK)]$_2$ showed significantly higher uptake in tumor, skin, and secondary lymphoid tissues in *Sharpin*^{cpdm} mice as compared to wt mice. The autoradiography analysis of tumors showed that the uptake in the skin above the tumor was significantly higher for *Sharpin*^{cpdm} mice than wt mice. The uptake of tumor periphery was elevated in *Sharpin*^{cpdm} mice but did not statistically differ from wt mice.

5.2.3 Imaging of B16 tumor-bearing mice with ultrasound and PET/CT

The growth of B16 melanoma was similar between *Sharpin*^{cpdm} and wt mice throughout the study. Contrast-enhanced ultrasound imaging showed comparable blood flow rates in the tumors of *Sharpin*^{cpdm} and wt mice at day 9 or 10 after tumor cell inoculation. However, the B16 primary tumors of *Sharpin*^{cpdm} mice (2/12 tumors) were found to create lymph node metastases at days 9-10 after inoculation, whereas no lymph node metastases were observed in wt mice (0/12 tumors). Similar lymph node metastases were observed in the B16 footpad tumor model at day 14 after tumor cell inoculation where SHARPIN deficiency increased the incidence of lymph node metastasis formation as compared to wt mice (11/16 vs. 7/16 tumors).

B16 melanoma tumors were visualized *in vivo* with [^{68}Ga]Ga-DOTA-E[c(RGDfK)]$_2$ and [^{68}Ga]Ga-DOTA-Siglec-9. The *in vivo* tumor uptake of [^{68}Ga]Ga-DOTA-E[c(RGDfK)]$_2$ increased from day 7 to day 10 after tumor cell inoculation in *Sharpin*^{cpdm} mice, whereas the tumor uptake remained unchanged in wt mice. At day 10 after tumor cell inoculation, the tumor uptake was higher in *Sharpin*^{cpdm} mice than wt littermates (0.47 ± 0.082 vs. 0.22 ± 0.0033 SUV, $P = 0.048$). The experiments of tumor related inflammation in B16 melanoma showed that the tumor uptake of [^{68}Ga]Ga-DOTA-Siglec-9 was significantly higher in *Sharpin*^{cpdm} mice as compared to wt mice at days 7 and 9 after tumor cell inoculation. The *in vivo* tumor uptakes of [^{68}Ga]Ga-DOTA-E[c(RGDfK)]$_2$ and [^{68}Ga]Ga-DOTA-Siglec-9 in wt and *Sharpin*^{cpdm} mice are presented in Table 2.

Table 2. [^{68}Ga]Ga-DOTA-E[c(RGDfK)]$_2$ and [^{68}Ga]Ga-DOTA-Siglec-9 *in vivo* tumor uptakes in *Sharpin*^{cpdm} and wt mice.

	[^{68}Ga]Ga-DOTA-E[c(RGDfK)]$_2$ *Sharpin*^{cpdm}	**[^{68}Ga]Ga-DOTA-E[c(RGDfK)]$_2$ wt**	***P* value**	**[^{68}Ga]Ga-DOTA-Siglec-9 *Sharpin*^{cpdm}**	**[^{68}Ga]Ga-DOTA-Siglec-9 wt**	***P* value**
Day 7	0.27 ± 0.048	0.20 ± 0.011	0.22	0.34 ± 0.020	0.20 ± 0.026	0.0020
Day 9	0.35 ± 0.055	0.23 ± 0.017	0.078	0.32 ± 0.029	0.24 ± 0.021	0.0061
Day 10	0.47 ± 0.082	0.22 ± 0.0033	0.035	ND	ND	

Results are expressed as mean of standardized uptake value ($SUV_{mean;}$ mean ± SEM). ND = not determined

5.3 First-in-human study of VAP-1 targeting tracer

5.3.1 Safety, metabolism, and sVAP-1 measurements of healthy subjects

In healthy male subjects, the i.v. administered [^{68}Ga]Ga-DOTA-Siglec-9 PET tracer was well tolerated and no adverse or pharmacologic effects were observed. The results of clinical laboratory tests and echocardiograms did not show any marked changes after PET imaging when compared to baseline measurements. One out of six healthy subjects was nauseous and got a headache during PET/CT imaging, but it was later found that these symptoms were associated with fasting too long against the instructions. According to the radio-HPLC analysis of plasma samples, the intact tracer and several other peaks were detected. In healthy subjects, the amount of intact tracer was 79.2% ± 5.3% and 4.3% ± 1.6% at 1-min and 10-min post-injection, respectively. In contrast, only one radiometabolite was detected in the analysis of urine samples from healthy subjects.

A soluble form of VAP-1 was analyzed from plasma samples taken prior to PET imaging. The concentration of sVAP-1 in plasma was 874.0 ± 139.9 ng/mL and the enzymatic activity was 10.9 ± 2.2 nmol/L/h. The blood uptake of radiolabeled Siglec-9 did not correlate with the concentration of sVAP-1 (r = -0.58, P = 0.42) or the enzymatic activity (r = -0.88, P = 0.12).

5.3.2 Distribution and radiation dose estimates

The highest uptake was observed in the urinary bladder followed by the kidneys. PET/CT imaging of healthy subjects revealed that i.v. administered [^{68}Ga]Ga-DOTA-Siglec-9 was rapidly excreted through kidneys to urinary bladder (Figure 6). The lowest uptakes of [^{68}Ga]Ga-DOTA-Siglec-9 were observed in the brain, muscle, cortical bone, and trabecular bone. In healthy subjects, there was no detectable uptake of [^{68}Ga]Ga-DOTA-Siglec-9 in the peripheral lymph nodes and tonsils. The liver uptake of [^{68}Ga]Ga-DOTA-Siglec-9 did not correlate with the peptide mass of Siglec-9 (r = 0.08, P = 0.88). Venous blood samples taken during PET imaging revealed rapid radioactivity clearance from blood circulation, which correlated closely with the PET image-derived left ventricle radioactivity.

In healthy subjects, the highest mean normalized residence times in units of hours was found in the urinary bladder contents (0.33 h) and the remainder of the body (0.73 h). The mean effective dose for [^{68}Ga]Ga-DOTA-Siglec-9 according to ICRP 103 was 0.022 mSv/MBq. The most critical and highest absorbed dose was observed in the urinary bladder wall (383 µSv/MBq) followed by the kidneys (54.4 µSv/MBq).

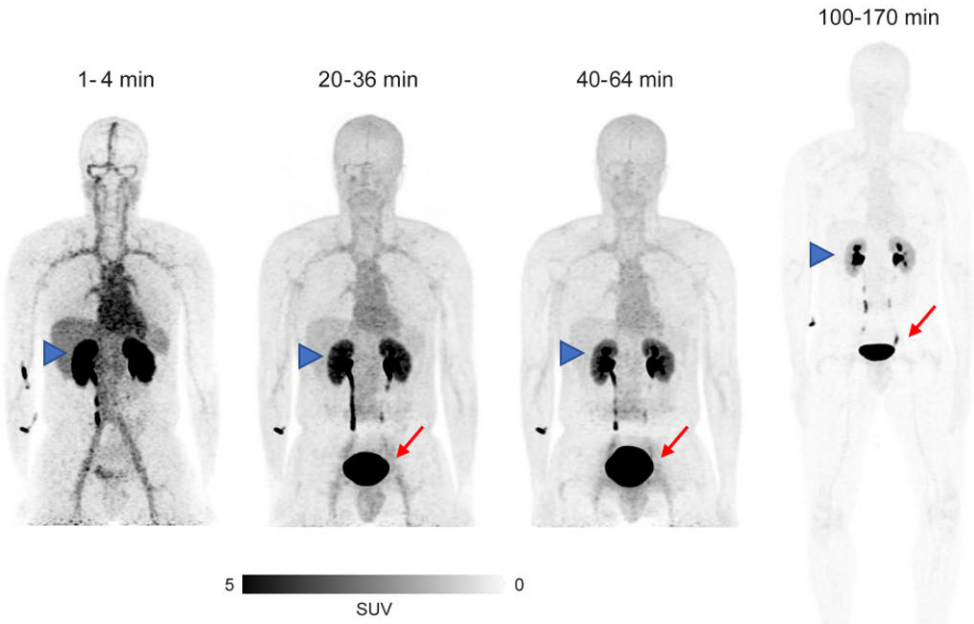

Figure 6. Coronal PET images of a healthy subject after i.v. injection of [^{68}Ga]Ga-DOTA-Siglec-9. Red arrows indicate the urinary bladder and blue arrowheads indicate the kidneys. Modified and reprinted with permission from Viitanen et al., 2020.

5.3.3 Assessment of rheumatoid arthritis

Based on a clinical examination four weeks before PET studies, the disease activity score (DAS28) was 3.3 and the number of tender and swollen joints was five for the male patient with RA. High uptakes of both [^{18}F]FDG and [^{68}Ga]Ga-DOTA-Siglec-9 were clearly detected in the inflamed joints. For both tracers, the highest uptake was observed in the PIP2, PIP3, and DIP3 joints of the right hand (Figure 7). The SUVs for these joints were 1.05, 0.92, and 0.70 with [^{68}Ga]Ga-DOTA-Siglec-9 and 1.46, 1.22, and 1.08 with [^{18}F]FDG.

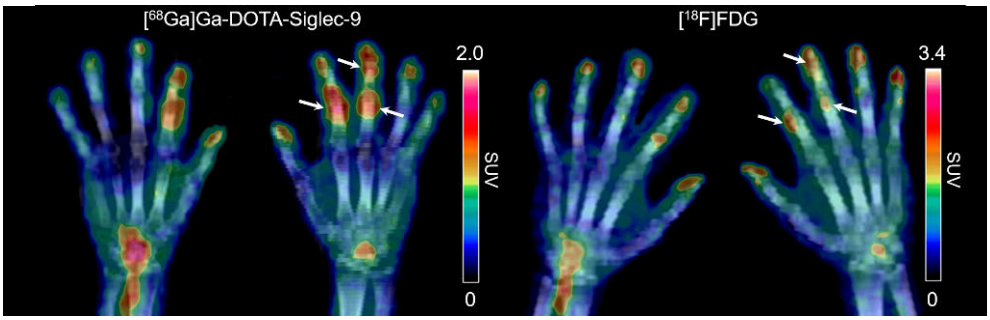

Figure 7. [^{68}Ga]Ga-DOTA-Siglec-9 and [^{18}F]FDG PET/CT images of the hands of a pilot patient with early diagnosed RA. White arrows indicate the three most inflamed joints of the right hand. Modified and reprinted with permission from Viitanen et al., 2020.

6 Discussion

The purpose of this thesis was to evaluate the feasibility of [^{68}Ga]Ga-DOTA-Siglec-9 PET for the imaging of inflammation. In Study I, we showed that VAP-1-targeting [^{68}Ga]Ga-DOTA-Siglec-9 detected *B. burgdorferi* infection-induced inflamed joints in mice and was able to monitor the fluctuating nature of *B. burgdorferi*-induced arthritis. The results of *ex vivo* gamma counting measurements and visible joint swelling were in line with the *in vivo* PET results. Immunohistochemical VAP-1 staining revealed that VAP-1 expression was evident in the synovial tissue of the affected joints. These findings verified that [^{68}Ga]Ga-DOTA-Siglec-9 PET/CT imaging was capable of detecting *B. burgdorferi* infection-induced arthritis at an earlier phase than the joint swelling measurement. In Study II, we demonstrated that an endogenous integrin inhibitor SHARPIN regulates the binding of a radiolabeled cyclic RGD peptide derivative in a B16 melanoma model and mice without tumor allografts. In the B16 melanoma model, the stromal SHARPIN regulated tumor vascularization but was found to regulate tumor vascularization but not to affect the tumor growth or blood flow. Both of the studied tracers, [^{68}Ga]Ga-DOTA-E[c(RGDfK)]$_2$ and [^{68}Ga]Ga-DOTA-Siglec-9, were able to detect increased tumor uptake in SHARPIN deficient mice as compared to wt mice littermates, although the β_3 integrin expression was slightly increased in SHARPIN deficient mice and the immune cell infiltration as well as VAP-1 expression was similar between the mice groups. In Study III, we showed, for the first time, that [^{68}Ga]Ga-DOTA-Siglec-9 was well tolerated and safe in humans. In addition, the biodistribution of [^{68}Ga]Ga-DOTA-Siglec-9 was favorable in terms of further clinical trials. The results of radiation dose estimates revealed that the radiation burden was low and the mean effective dose was comparable to other ^{68}Ga-peptides. Furthermore, [^{68}Ga]Ga-DOTA-Siglec-9 was able to clearly detect the arthritic joints, although only one patient was studied.

6.1 Detection of *B. burgdorferi* infection-induced inflammation

In Study I, the aim was to investigate the capability of VAP-1-targeting [^{68}Ga]Ga-DOTA-Siglec-9 PET to detect *B. burgdorferi* infection-induced joint inflammation and ceftriaxone-treatment induced changes in inflammation during a longitudinal

follow-up period. Study I provided evidence that VAP-1 could be a feasible imaging target to accurately detect *B. burgdorferi* infection-induced arthritis and monitor the development of arthritis over time.

Human tick-borne infection, known as Lyme borreliosis (LB), is caused by the spirochete *B. burgdorferi* sensu lato. Manifestations of the early phase LB can occur in the nervous system and heart whereas late LB usually appears as a chronic skin lesion or as Lyme arthritis (LA). Mice are natural hosts for *B. burgdorferi* spirochetes with symptomless infection. (Bockenstedt & Wormser, 2014; Coburn et al., 2002; Stanek et al., 2012) The dissemination and treatment response of *Borrelia* infection is studied by using C3H mice. *B. burgdorferi*-infected C3H mice develop visually explicit joint symptoms with swelling and leukocyte infiltration, which resemble those of human disease (Barthold et al., 1993). Usually, mice are infected with the dose of 10^4 or 10^7 *B. burgdorferi* bacteria to induce prominent joint manifestations (Barthold et al., 1991, 1993; Bockenstedt et al., 2012; Hodzic et al., 2008). In Study I, the dose of 10^6 *B. burgdorferi* bacteria was selected and used to induce LB. The selected dose was sufficient to develop disseminated infection with explicit joint swelling and therefore no other doses were evaluated.

Traditionally, LB has been studied by means of bacterial culture, polymerase chain reaction, serology, histology, and by measuring the mediolateral diameter of joints in the case of LA. Currently, there are fluorescence- or bioluminescence-based *in vivo* imaging techniques available to monitor LB in mice. In fluorescence-based imaging, a genetically engineered green fluorescent protein expressed in *B. burgdorferi* strain has been reported to detect and visualize disseminated infection from vasculature of infected mice at tissue level by intravital microscopy (Hyde et al., 2011; Moriarty et al., 2008; Norman et al., 2008). The use of *B. burgdorferi* strain expressing luciferase has been reported as being able to monitor the development of LB in mice by means of bioluminescence imaging (Hyde et al., 2011). Both imaging methods have their limitations as they require the use of genetically engineered bacteria and the killing of animals at different time points for the analysis of specific organs. PET imaging offers an alternative for the study of LB since it allows longitudinal whole-animal imaging at multiple time points, thus providing the opportunity to visualize the status of specific tissues. Additionally, PET imaging allows the monitoring of the dissemination of an infection, investigation of therapy responses, and use of wt bacteria.

Currently, the most established PET tracer for the detection of infection and inflammation is a glucose analog, [^{18}F]FDG. It has proved its usefulness in various clinical settings involving, for example, benign and malignant tumors and infectious conditions. (Kircher & Lapa, 2020; Wu et al., 2013) Only a few case reports and one clinical trial have described the use of [^{18}F]FDG PET in patients with LB infection and showed some differences in the metabolism of the brain (Kalina et al., 2005;

Newberg et al., 2002; Plotkin et al., 2005). Recently, TSPO ligand targeting [^{11}C]DPA-713 has been reported to be a potential tool for studying cerebral glial activation in patients with a post-treatment Lyme disease syndrome (Coughlin et al., 2018).

Imaging of bacterial diseases in mice, such as infections caused by *Escherichia coli* and *Mycobacterium tuberculosis*, has identified new radiopharmaceuticals that may replace [^{18}F]FDG and radiolabeled autologous leukocytes in the future (DeMarco et al., 2015; Gowrishankar et al., 2014; Weinstein et al., 2012). Several radiopharmaceuticals have been developed and investigated for the imaging of arthritic synovitis. Methyl-[^{11}C]-choline, [^{11}C]-(*R*)-PK11195, and [^{18}F]fluoro-PEG-folate have shown the most promising results for the imaging of RA (Roivainen et al., 2003; van der Laken et al., 2008; Verweij et al., 2020). Additionally, multiple macrophage-targeted and synovial fibroblast-targeted radiopharmaceuticals have been explored for the imaging of RA in animal models, but their feasibility in terms of human RA is still under investigation (Narayan et al., 2017).

According to our study, [^{68}Ga]Ga-DOTA-Siglec-9 PET/CT detected inflamed joints at an early stage and was able to monitor the fluctuating nature of *B. burgdorferi*-induced arthritis. The maximum uptake of [^{68}Ga]Ga-DOTA-Siglec-9 and the highest joint swelling were observed at four weeks post-infection, whereas no evident uptake of [^{68}Ga]Ga-DOTA-Siglec-9 or joint swelling were identified in the joints of uninfected mice. This result is consistent with previously reported results, where it has been shown that the maximum joint swelling and inflammation is reached 3-4 weeks after infection (Barthold et al., 1991; Salo et al., 2015). In addition, we observed the expression of VAP-1 on synovial tissue of affected joints, which had also previously been reported in patients with treatment-resistant LA (Akin et al., 2001). [^{68}Ga]Ga-DOTA-Siglec-9 showed potential for the imaging of synovial inflammation caused by *B. burgdorferi* infection. Further investigations are needed to evaluate the VAP-1-targeted imaging concept in patients with LA.

6.2 Imaging of SHARPIN regulated integrin activity

Multifunctional Shank-associated RH domain-interacting protein (SHARPIN) is involved in the NF-κB activation, regulation of inflammation, and promotion of tumor growth and metastasis (Jung et al., 2010; Tokunaga et al., 2011). In addition, SHARPIN functions as an endogenous integrin inhibitor by binding to the integrin α-subunit to interfere with the binding of activators to the β-subunit (Rantala et al., 2011). The purpose of Study II was to investigate the role of SHARPIN in tumor growth, invasion, angiogenesis, and metastasis using [^{68}Ga]Ga-DOTA-E[c(RGDfK)]$_2$ and [^{68}Ga]Ga-DOTA-Siglec-9 PET imaging.

Integrins are heterodimeric transmembrane receptors consisting of an α- and a β-subunit, which can form several different integrin receptor combinations. Depending on the αβ subunit combination, integrins can be divided into four receptor groups based on the ligand specificity. The receptor groups are collagen binding integrins, laminin binding integrins, leukocyte specific integrins, and tripeptide sequence RGD binding integrins. (Hynes, 2002; Plow et al., 2000) Several integrins recognize the RGD motif as their ligand, and one of these integrins is $\alpha_v\beta_3$ (Ruoslahti, 1996). Many compounds based on the RGD tripeptide sequence are designed to antagonize the function of $\alpha_v\beta_3$ integrin (Haubner et al., 1997). Peptides mimicking the RGD sequence can be engineered to be integrin heterodimer selective. Modifications of the RGD peptides, such as cyclization, multimerization, and incorporation of a D-amino acid residue, enhance the receptor binding affinity and selectivity to $\alpha_v\beta_3$ integrin (Dijkgraaf et al., 2007, 2011; Kapp et al., 2017).

Angiogenesis is a physiological process where new blood vessels develop and form from existing blood vessels and proliferating endothelial cells. It is known that tumor growth depends on the angiogenesis, which in turn contributes to formation of metastasis. (Carmeliet, 2005) Imaging of the $\alpha_v\beta_3$ integrin expression is useful in the investigation of tumor vasculature because angiogenic endothelial cells have a high $\alpha_v\beta_3$ integrin expression as compared to normal tissue (Brooks, 1996). Besides cancer biology, angiogenesis plays an important role in chronic inflammatory disorders, and $\alpha_v\beta_3$ integrin is upregulated in patients with RA and inflammatory bowel disease (Danese et al., 2006; Wilder, 2002). In Study II, we observed increased uptake of [^{68}Ga]Ga-DOTA-E[c(RGDfK)]$_2$ in several organs of *Sharpin*^{cpdm} mice as compared to wt mice littermates. The *in vivo* competition studies detected reduced uptake and proved the specificity of $\alpha_v\beta_3$ integrin binding in *Sharpin*^{cpdm} mice. However, the competition studies failed to detect the reduced uptake in the skin of *Sharpin*^{cpdm} mice because the skin phenotype is β_1 integrin-dependent (Peuhu et al., 2017). Previously, ^{18}F-labeled galacto-RGD and ^{64}Cu-labeled RGD tetramer have been used in inflammation animal models and showed promising results for the imaging of angiogenesis during chronic inflammation processes (Cao et al., 2007; Pichler et al., 2005). These findings, together with our results, advocate the imaging of $\alpha_v\beta_3$ integrin expression in angiogenesis not only in tumor vasculature but also during chronic inflammation.

Changes in integrin activity are associated with many diseases. Bleeding disorders and immune deficiencies are the results of impaired ability to activate integrin, whereas chronic inflammation and cancer result from increased integrin activity. (Bouvard et al., 2013; Hogg & Bates, 2000; Shattil et al., 2010) It is known that integrins have an effect on tumor growth, angiogenesis, invasion, and metastasis (Desgrosellier & Cheresh, 2010). An endogenous integrin inhibitor SHARPIN is amplified and overexpressed in human breast cancer, hepatocellular carcinoma,

ovarian cancer, prostate cancer, and renal cell carcinoma (De Melo & Tang, 2015; He et al., 2010; Jung et al., 2010; Li et al., 2015). Moreover, SHARPIN enhanced the development of lung metastasis in an animal model of osteosarcoma (Tomonaga et al., 2012). Recently, *in vitro* and *in vivo* data on melanoma have demonstrated that SHARPIN expression is increased and promotes tumor migration and invasion by the upregulating expression of Ras-associated protein-1 and its downstream signaling pathways (Zhou et al., 2020). However, the role of SHARPIN in regulating the tumor stroma has not been fully investigated experimentally, although it is known to regulate stromal architecture in the developing mammary gland (Peuhu et al., 2017).

It is well established that tumor-associated blood vessels are morphologically abnormal and many molecular differences exist between tumor-associated and normal vasculature (Desgrosellier & Cheresh, 2010). In Study II, we observed that stromal SHARPIN did not affect the B16 melanoma growth or blood flow. Nevertheless, angiogenesis was slightly increased in *Sharpin*^{cpdm} mice as compared to tumor-bearing wt mice. Vascular endothelial growth factor A is an angiogenic factor that stimulates proliferation of endothelial cells and promotes their permeability. Increased vascular permeability increases the migration of tumor cells through the endothelium into the blood circulation to form metastases. (Claesson-Welsh & Welsh, 2013) Previously, the increased number of blood vessels and expression of vascular endothelial growth factor A mRNA have been reported in the skin lesions of *Sharpin*^{cpdm} mice (HogenEsch et al., 2016). In line with these findings, we observed that stromal SHARPIN may play a role in reducing the formation of melanoma metastases in the lymph nodes because lymph node metastases were only found in tumor-bearing *Sharpin*^{cpdm} mice. In addition, the tumor uptake of [^{68}Ga]Ga-DOTA-Siglec-9 was increased in *Sharpin*^{cpdm} mice but, unfortunately, the number of VAP-1-positive blood vessels indicating cancer-related inflammation did not differ between *Sharpin*^{cpdm} and wt mice. Similar immunohistochemistry results of human melanoma samples have been reported, in which a weak VAP-1 expression is found in intratumoral vessels (Forster-Horváth et al., 2004). These findings highlight that stromal SHARPIN plays a role in regulating angiogenesis and formation of metastasis.

The ligand binding affinity of integrins is not constant and can be regulated by conformational changes. Conformational changes in integrins occur through a process called inside-out signaling, in which the binding of integrin-activating proteins, such as talins and kindlins, to the cytoplasmic domain causes conformation changes and leads to activation of integrins. (Calderwood, 2004; Hynes, 2002; Shattil et al., 2010) It is known that SHARPIN regulates β_1-integrin activity and inhibits the inside-out integrin activation switch (Rantala et al., 2011). In Study II, a trend was seen that β_3 integrin expression was more positive in tumors of *Sharpin*^{cpdm}

than wt mice. In addition, we observed increased tumor uptake of [^{68}Ga]Ga-DOTA-E[c(RGDfK)]$_2$ in *Sharpin^{cpdm}* tumor-bearing mice at 10 days post-inoculation, which may be a consequence of the higher β_3 integrin expression. Two previous xenograft studies have indicated that anti-angiogenic treatments altered the tumor uptake of $\alpha_v\beta_3$ integrin binding radiotracers, which could not be accounted for by an altered $\alpha_v\beta_3$ integrin expression (Dumont et al., 2009; Rylova et al., 2014). Interestingly, a previous *in vitro* study provided evidence and broadened our understanding that both the $\alpha_v\beta_3$ integrin activation status and expression level have an impact on the binding of $\alpha_v\beta_3$ integrin targeting radiotracers to cells (Andriu et al., 2018). In line with that, we found that SHARPIN deficiency has an impact on the $\alpha_v\beta_3$ integrin activation status and that the cyclic RGD peptide derivative, [^{68}Ga]Ga-DOTA-E[c(RGDfK)]$_2$, can be used to reflect the $\alpha_v\beta_3$ integrin activation. Moreover, our results suggest that the radiolabeled cyclic RGD peptide derivative provides a tool for studying changes in the $\alpha_v\beta_3$ integrin expression and activation, and the use of $\alpha_v\beta_3$ integrin-targeted radiotracers could be extended to the investigation of inflammatory disorders.

6.3 First-in-human study with [^{68}Ga]Ga-DOTA-Siglec-9

Inflammation plays an important role during acute defense against pathogens and other inflammatory stimuli. However, uncontrolled and long-lasting inflammation can eventually lead to pathologic changes in tissues. Early detection of inflammatory lesions is essential for proper diagnosis and effective treatment in many inflammatory diseases. Traditionally, [^{18}F]FDG is the most commonly used PET radiotracer for inflammation imaging, but as it is non-specific, there are challenges in distinguishing between cancer and inflammation. Moreover, [^{68}Ga]Ga-citrate and [^{89}Zr]Zr-transferrin can be used to image inflammation based on the increased expression of transferrin receptor 1 on mononuclear cells, but this receptor is also expressed in cancer cells, which limits its use (Holland et al., 2012; Nanni et al., 2010). Therefore, there is a need for a more inflammation specific PET imaging agent.

VAP-1, an inflammation inducible adhesion molecule, plays an important role during early inflammation through participation in leukocyte trafficking across endothelium (Salmi & Jalkanen, 1992). In addition, the luminal expression of VAP-1 on the endothelial surface remains constant if inflammation continues (Jaakkola et al., 2000). These unique features make VAP-1 a promising target for imaging inflammation. It is well-known that Siglec-9 is a leukocyte ligand for VAP-1 (Aalto et al., 2011). Our research group has shown that ^{68}Ga-labeled DOTA-conjugated Siglec-9 peptide can be used for inflammation imaging in various experimental models, including skin inflammation, osteomyelitis, synovitis, atherosclerosis, acute

lung inflammation, and multiple sclerosis (Aalto et al., 2011; Ahtinen et al., 2014; Elo et al., 2018; Retamal et al., 2016; Silvola et al., 2016; Virtanen et al., 2015). Before introducing [^{68}Ga]Ga-DOTA-Siglec-9 for clinical trials, safety and toxicological studies were performed with precursor DOTA-Siglec-9 in rats. In safety studies, a 1000-fold excess of the planned clinical dose (40 µg per subject) was i.v. injected as a single dose, and the results showed that the dose was well-tolerated and no adverse effects were observed (Chrusciel et al., 2019). In Study III, the injected clinical dose was considerably lower (mean 13.6 µg per subject) because we managed to use a smaller quantity of precursor for radiolabeling. Furthermore, we demonstrated that [^{68}Ga]Ga-DOTA-Siglec-9 was well tolerated and no adverse or clinically observable pharmacologic effects were detected.

The biodistribution and excretion of [^{68}Ga]Ga-DOTA-Siglec-9 have been evaluated in several animal species, such as mice, rats, rabbits, and pigs (Aalto et al., 2011; Retamal et al., 2016; Virtanen et al., 2015, 2017). As shown by the preclinical studies, ^{68}Ga-labeled Siglec-9 peptide is excreted via kidneys to the urinary bladder. In line with these findings, we observed that, in humans, the highest radioactivity concentration was in the urinary bladder and [^{68}Ga]Ga-DOTA-Siglec-9 exhibited fast renal clearance. The radiation exposure of urinary bladder can be reduced by advising the patient to void bladder frequently. The lowest radioactivity concentration was detected in the skeletal muscle, which is in line with the fact that skeletal muscle is VAP-1 negative tissue (Jaakkola et al., 1999). Intermediate uptake of [^{68}Ga]Ga-DOTA-Siglec-9 was observed in the liver, which is consistent with the expression of VAP-1 in the liver (McNab et al., 1996). In summary, the distribution of [^{68}Ga]Ga-DOTA-Siglec-9 was largely consistent with the VAP-1 tissue expression. In addition, we observed plasma protein binding properties that are in line with previously reported values in pigs (Jødal et al., 2019; Retamal et al., 2016).

Conventional radiography is used in routine management of RA to detect anatomical changes, such as bone erosion and cartilage damage. More sensitive imaging techniques, including ultrasound, MRI, and PET, are needed to facilitate an earlier diagnosis of RA. (McQueen, 2013) Previously, we showed that [^{68}Ga]Ga-DOTA-Siglec-9 was able to detect synovitis in an experimental rabbit model and the uptake was comparable to [^{18}F]FDG (Virtanen et al., 2015). In Study III, we demonstrated that [^{68}Ga]Ga-DOTA-Siglec-9 was able to identify inflamed synovium in early RA, although the study only included one patient. Moreover, the uptake of [^{68}Ga]Ga-DOTA-Siglec-9 was slightly lower than that of [^{18}F]FDG. Interestingly, since this was the first time a rheumatic patient was imaged with [^{68}Ga]Ga-DOTA-Siglec-9, it remains to be seen in the future how the optimization of the imaging protocol will affect synovial uptake of [^{68}Ga]Ga-DOTA-Siglec-9. Furthermore, how the findings of [^{68}Ga]Ga-DOTA-Siglec-9 PET/CT affect the treatment of RA patients as compared to [^{18}F]FDG remains to be seen in the future studies.

Currently, the common standard for estimating the effective dose is based on the ICRP 103 recommendation (ICRP, 2007). Previously, human whole-body biodistribution and radiation dosimetry have been evaluated for certain ^{68}Ga-labeled peptides. According to our study, the mean effective dose of [^{68}Ga]Ga-DOTA-Siglec-9 was 0.022 mSv/MBq, calculated according to ICRP 103, which is within the range of the reported values for other ^{68}Ga-labeled peptides as follows: [^{68}Ga]Ga-DOTATATE 0.021 mSv/MBq, [^{68}Ga]Ga-DOTATOC 0.023 mSv/MBq, [^{68}Ga]Ga-DOTANOC 0.025 mSv/MBq, and [^{68}Ga]Ga-DOTA-RGD 0.022 mSv/MBq (Hartmann et al., 2009; Kim et al., 2012; Pettinato et al., 2008; Sandström et al., 2013). In addition, we have earlier reported on the radiation burden and mean effective dose data extrapolated from rats (Virtanen et al., 2017). The mean effective dose reported in rats was 0.024 mSv/MBq, which was practically the same as in humans, taking into account the range of variation. In conclusion, PET imaging of humans with [^{68}Ga]Ga-DOTA-Siglec-9 causes only modest radiation exposure, thus allowing multiple scans to be performed on the same patient over the years.

6.4 Strengths, limitations and future aspects of VAP-1 targeted imaging

PET is a non-invasive and quantitative imaging method that facilitates the visualization and measuring of biological processes *in vivo* with minimal disturbance. In addition, PET imaging provides a useful tool for diagnosing diseases, planning of therapy, and monitoring the treatment efficacy and disease progression. (Phelps, 2000; Rennen et al., 2001) Several new tracers for inflammation imaging have been developed and their ability to detect inflammation has been assessed. PET imaging of inflammation has expanded its feasibility to understanding the mechanisms underlying the pathogenesis of inflammatory diseases and to identifying potential therapeutic targets (Wu et al., 2013). Despite the continuous and long-term efforts to develop inflammation specific tracers, ideal tracers to image inflammation beyond [^{18}F]FDG have not yet been found (Roivainen et al., 2012).

VAP-1 is overexpressed and involved in many inflammatory diseases, such as inflammatory bowel disease, psoriasis, RA, and cancers (Irjala et al., 2001; Madej et al., 2007; Marttila-Ichihara et al., 2009; Salmi et al., 1993; Salmi et al., 1997). VAP-1 is an inflammation-inducible endothelial cell molecule that participates in the leukocyte extravasation cascade. Additionally, VAP-1 plays an important role during early inflammation, and its expression on the surface of endothelial cells remains constant for a longer time, if the inflammation proceeds. (Salmi & Jalkanen, 2019) These features make VAP-1 an ideal target for *in vivo* imaging of inflammation.

Already in 2000, the first proof-of-concept study was performed to indicate the use of VAP-1 as an imaging target with iodinated monoclonal antibodies against VAP-1 in experimental dermatitis and arthritis models (Jaakkola et al., 2000). The next development steps were taken when the crystallographic structure of VAP-1 was resolved. The designed peptides fitting the enzymatic groove were radiolabeled and used to indicate their ability to image bone inflammation, acute sterile skin inflammation and cancer in rats (Autio et al., 2010, 2011; Lankinen et al., 2008). When Siglec-9 was found to be a leukocyte ligand for VAP-1, it was shown that the ^{68}Ga-labeled Siglec-9 motif containing peptide was able to detect VAP-1 in the vasculature of inflamed skin and melanoma tumors in mice (Aalto et al., 2011). In the present thesis, the studies concerning [^{68}Ga]Ga-DOTA-Siglec-9 corroborated the VAP-1 targeting imaging concept and VAP-1 was identified as a promising imaging agent for detecting arthritis caused by *B. burgdorferi* infection as well as for detecting tumor-associated inflammation. Furthermore, for the first time, the toleration and distribution [^{68}Ga]Ga-DOTA-Siglec-9 d in healthy humans was investigated.

However, there are a few practical issues that limit the use of [^{68}Ga]Ga-DOTA-Siglec-9 PET and PET imaging itself. PET imaging requires many resources, such as imaging devices, PET tracers, and specialized staff, which increase the cost of imaging and limit its availability. These issues are likely to limit the use of PET imaging as a diagnostic tool in inflammation imaging. Regarding [^{68}Ga]Ga-DOTA-Siglec-9 PET, the imaging of the abdomen and pelvic area is limited because [^{68}Ga]Ga-DOTA-Siglec-9 is excreted through kidneys to urinary bladder. This issue can be resolved by voiding the bladder often enough and optimizing the imaging protocol. In addition, we observed that the in vivo stability of intravenously injected [^{68}Ga]Ga-DOTA-Siglec-9 peptide is suboptimal in humans. In general, there are several strategies to improve stability of peptide-based radiopharmaceuticals. Commonly used strategies include such as C- or N-terminal modification, use of D- or unnatural amino acids, cyclization of peptide structure, PEGylation or backbone modification (Evans et al., 2020). Our [^{68}Ga]Ga-DOTA-Siglec-9 peptide already includes cyclization, PEGylation and C-terminal modification, but the use of a D-amino acids or unnatural amino acids may help to improve stability and should be studied in the future. In Study III, the number of study subjects was relatively small for the purposes of investigating the safety and distribution of [^{68}Ga]Ga-DOTA-Siglec-9, and the study involved male subjects only. It would be interesting to investigate the distribution of [^{68}Ga]Ga-DOTA-Siglec-9 in female subjects and see if the results differ from those reported in males. VAP-1 has a soluble form in the circulation, but sVAP-1 is not elevated in all inflammatory diseases (Kurkijärvi et al., 1998; Salmi & Jalkanen, 2019). The binding of [^{68}Ga]Ga-DOTA-Siglec-9 to sVAP-1 may cause background signal in cases in which sVAP-1 concentrations are

high. In this thesis, we observed all inflammatory lesions and melanomas from the background tissues, demonstrating that sVAP-1 is not a problem in these indications.

Overall, several experimental animal models have shown that [^{68}Ga]Ga-DOTA-Siglec-9 seems to be a promising PET tracer for the imaging of inflammation (Aalto et al., 2011; Ahtinen et al., 2014; Elo et al., 2018; Retamal et al., 2016; Silvola et al., 2016; Virtanen et al., 2015, 2017). The experimental studies included in this thesis corroborate the ability of [^{68}Ga]Ga-DOTA-Siglec-9 to localize inflammatory process by imaging. VAP-1 is also a potential target molecule for anti-inflammatory therapy. Blocking the functional activity of VAP-1 with mAbs and small molecular inhibitors has been studied and indicated to be effective in several experimental disease models (Bonder et al., 2005; Koskinen et al., 2004; Martelius et al., 2004; Marttila-Ichihara et al., 2006, 2010; Merinen et al., 2005; Tohka et al., 2001). The first-in-human study confirmed the feasibility of [^{68}Ga]Ga-DOTA-Siglec-9 in clinical studies, and the low radiation burden supports the possibility of performing repeated scans per year in the same patient. The repeatability provides the opportunity to investigate the efficacy of novel anti-inflammatory drugs in the future. As the next step, the intention is to investigate the potential of this VAP-1 targeting tracer in patients with RA. In the future, the [^{68}Ga]Ga-DOTA-Siglec-9 PET tracer may potentially be used in various inflammatory diseases besides RA.

7 Conclusions

This thesis investigated the feasibility of [^{68}Ga]Ga-DOTA-Siglec-9 to detect inflammation in mouse models of arthritis and melanoma. The accumulation of [^{68}Ga]Ga-DOTA-E[c(RGDfK)]$_2$ in inflamed areas and melanoma, as well as the effects of stromal SHARPIN on the regulation of tumor growth, metastasis, and vascularization were examined in the SHARPIN deficient mouse model. Furthermore, the first-in-human study investigated the safety, tolerability, distribution, and radiation dosimetry of [^{68}Ga]Ga-DOTA-Siglec-9. The main findings of the studies were the following:

1. [^{68}Ga]Ga-DOTA-Siglec-9 was able to accurately detect *Borrelia burgdorferi* infection-induced arthritis in mice. Longitudinal PET/CT imaging allowed the monitoring of the development of arthritis and the efficacy of antibiotic treatment during the follow-up period.
2. Stromal SHARPIN regulated the binding of [^{68}Ga]Ga-DOTA-E[c(RGDfK)]$_2$ both in a murine B16 melanoma model and in mice without melanoma tumors. In SHARPIN deficient mice, [^{68}Ga]Ga-DOTA-Siglec-9 was able to detect tumor-related inflammation, although the immune cell infiltration and VAP-1 expression were similar between mice. In addition, stromal SHARPIN regulated tumor vascularization and could prevent the formation of metastasis.
3. The first-in-human study showed that [^{68}Ga]Ga-DOTA-Siglec-9 was safe and the radiation burden was low and comparable to other ^{68}Ga-peptides. Furthermore, the ability of [^{68}Ga]Ga-DOTA-Siglec-9 to detect arthritic joints was shown in one patient with early RA.

In summary, the imaging concept of targeting VAP-1 demonstrates potential to detect arthritis caused by *Borrelia burgdorferi*, providing a basis for further evaluation of the method in human patients with Lyme arthritis. The SHARPIN deficiency studies with an $\alpha_v\beta_3$ integrin-targeted tracer provides valuable information of altered integrin activity and suggests that the feasibility of $\alpha_v\beta_3$ integrin-targeted tracers can be expanded to the investigation of changes in the $\alpha_v\beta_3$ integrin expression status and altered integrin activity in both cancer and

inflammatory diseases. Based on the first-in-human study, [^{68}Ga]Ga-DOTA-Siglec-9 targeting VAP-1 appears to be a promising new PET tracer for imaging inflammation.

Acknowledgments

The research for this thesis was carried out at the Turku PET Centre and the Department of Clinical Physiology and Nuclear Medicine in Turku University Hospital and the University of Turku during the years 2014-2020. The former and present Heads of the Department of Clinical Physiology and Nuclear Medicine, Professor Emeritus Jaakko Hartiala and Professor Jukka Kemppainen, and Director of the Turku PET Centre, Professor Juhani Knuuti are warmly thanked for providing the excellent facilities for the research. The study was conducted within the Finnish Centre of Excellence in Cardiovascular and Metabolic Diseases supported by the Academy of Finland, the University of Turku, Turku University Hospital, and Åbo Akademi University. This study was financially supported by the Drug Research Doctoral Programme, University of Turku Graduate School. Grants for this research were received from the Finnish Cultural Foundation, the Varsinais-Suomi Regional Fund and Central Fund, the Instrumentarium Science Foundation, the State Research Funding of Turku University Hospital, Orion Research Foundation, Ida Montin Foundation, Sigrid Jusélius Foundation, Jane and Aatos Erkko Foundation, and the Finnish Foundation for Cardiovascular Research.

I wish to express my profound gratitude to my supervisors, Professor Anne Roivainen and Academician Sirpa Jalkanen. Your passion for science is truly inspiring, and I am deeply grateful for the opportunity to conduct this project under the supervision of such an influential researcher duo. Anne, your talent and high-level expertise in preclinical research context has guided me during this process. Your sympathetic and down-to-earth style of encouraging and supporting a young scientist has given me self-confidence and allowed me to grow as a scientist. I also appreciate the positive atmosphere in your office, which has made it easier for me to come and share the good and bad news about everything. Sirpa, your incredibly great and unique career has been highly inspirational. Your talent and effectiveness as an awarded and recognized scientist as well as your extensive expertise in immunology have been essential in these projects. I am also grateful for your constructive style of guiding me during these years.

I am truly grateful to the reviewers of my thesis, Assistant Professor Olof Eriksson and Adjunct Professor Mirkka Sarparanta. I appreciate your valuable

constructive comments and suggestions, which helped me to improve and complete the thesis. I also wish to thank the Follow-Up Committee members, Associate Professor Jukka Hytönen and Professor Johanna Ivaska for giving me directions and support during this process. In addition, Jukka and Johanna are thanked for a fruitful collaboration and sharing of extensive expertise in their respective fields. The former and present Directors of the Drug Research Doctoral Programme (DRDP), University of Turku, Professor Emeritus Markku Koulu and Associate Professor Eriika Savontaus are warmly thanked. I also want to acknowledge the DRDP Coordinator Eeva Valve, who has answered to my many questions regarding my doctoral studies and also organized annual DRDP meetings for PhD students during these years.

The work behind these projects would not have been successful without teamwork. I owe my sincere gratitude to all my co-authors and collaborators for their valuable contribution during these projects. I warmly thank Associate Professor Jukka Hytönen and Annukka Pietikäinen for introducing me to the research field of Borrelia bacteria and the valuable contribution to my first research article. Jukka, your motivating comments and endless enthusiasm for this study inspired me and made it easier to write the article. Adjunct Professor Mirva Söderström is thanked for providing excellent pathology expertise and analyses. Professor Johanna Ivaska and Adjunct Professor Emilia Peuhu deserve my warmest thanks. You have expanded my knowledge of integrins and challenged me as a researcher in many situations. Elina Mattila is acknowledged for performing melanoma footpad experiments.

I warmly thank Professors Antti Saraste, Pirjo Nuutila, and Juhani Knuuti for their extensive expertise in clinical imaging. I am very grateful to the excellent rheumatologist team in Turku University Hospital, Kirsi Taimen, Markku Mali, Ia Kohonen, Ilpo Koskivirta and Laura Pirilä, for their vital input regarding the recruiting of patients with rheumatoid arthritis, as well as their support with the clinical trial. I would like to thank Petteri Lankinen and Mikko Koivumäki for their invaluable input during the clinical PET imaging studies. Hospital physicists Sami Suilamo and Tuula Tolvanen are warmly thanked for their guidance in the radiation dosimetry, and for having the patience to answer my questions related to the dosimetry study. Vesa Oikonen is thanked for his professional expertise in modeling and pharmacokinetics. Kristiina Santalahti is acknowledged for performing sVAP-1 measurements in the clinical trial.

I am sincerely grateful to Adjunct Professor Anu Autio and Helena Virtanen, who have introduced me to the fascinating fundamentals of VAP-1. It has been a privilege to work with such experienced scientists. I really appreciate your guidance in everything from lab work to data analysis and all the great and hilarious times we have shared in and outside of the lab. I wish to thank our radiochemists, Adjunct

Professor Xiang-Guo Li, Meeri Käkelä, Tiina Saanijoki, Olli Metsälä and Olli Moisio, for providing the tracers. The vital contribution of all of you has been essential, not to mention the availability of radiosynthesis outside normal working hours. Associate Professor Ingrid Dijkgraaf from the University of Maastricht is warmly thanked for productive collaboration and providing extensive expertise in the field of $\alpha_v\beta_3$ integrin PET imaging. Heidi Liljenbäck and Aake Honkaniemi deserve my deepest thanks for high-level assistance and expertise in animal work. Your valuable help and flexibility have been essential in these studies. Special thanks go to Heidi who taught me various technical skills in animal work. I want to thank Erica Nyman, Marja-Riitta Kajaala, and Sari Mäki for your vast and highly skilled contribution to histology and immunohistochemistry stainings. Timo Kattelus is acknowledged for his professional assistance in processing of manuscript figures. Lea Heinonen-Eerola is thanked for the language revision of this thesis.

I wish to express my thanks to the personnel at Turku PET Centre including the physicians, physicists, radiographers, study nurses, laboratory technicians, IT experts, secretaries, and other staff members. Special thanks go to Sanna, Eija, Hanna, Marjo, Minna, Hannele, Anne-Mari, Mia, Marko, Jukka, Kari, Kirsi, Jarna, Marita, Virva, Mika, Tuula, Rami, Marko, Tove, Mirja, and Lenita. Thanks for your sincere help, great discussions and joyful coffee breaks!

I owe my sincere gratitude to my great (former and present) colleagues in Anne's group: Anu, Helena, Johanna, Sanna, Miikka, Max, Mia, Petri, Maria, Heidi, Jenni, Arghavan, Olli, Olli, Maxwell, Meeri, Tiina, Päivi, Aida, Senthil, Andriana, Erika, and Imran. The atmosphere at work has always been friendly and supportive, which made this journey easier. Thanks for sharing the memorable moments in and outside of the office as well as during congress trips. Special thanks to Mia Ståhle with whom I have studied and worked side by side for more than a decade. We have shared a lot of thoughts in science and real life, thanks for a long-lasting friendship. Heartfelt thanks to my dear colleagues and friends outside Anne's group: Simona Malaspina, Minna Lahesmaa, Miikka Honka, Sanna Laurila, Eleni Rebelos, Prince Dadson, Kerttu Seppälä, and Iida Stenström. The peer support and great dinners with good Italian red wine have been essential, and I appreciate your friendship very much.

I sincerely want to thank my wonderful friends in my life. Special thanks to the "Terbio girls", Sofia, Norma, Mia, and Mari, for the peer support and fun that we have shared from the first university lectures until today. Friends outside science, Johanna, Iina, Susanna, and Heidi, thank you for a lifelong friendship. You have truly believed in me and kept me sane during all these years. My dance team Fimosa and the girls I coach also deserve big thanks for helping me to leave all stress and worries behind during these years.

I express my deepest gratitude to my parents Riitta and Veijo for their endless love, encouragement, and support throughout my life and doctoral studies. You have

never questioned my choices although they are not familiar to you. I am grateful to my wonderful brothers Mikko and Jussi and their lovely families. You have supported me whatever I have done, believed in me, and pushed me forward gently like a princess. Most of all, I want to thank my beloved husband Sami. Your love and support have made this journey easier. Thank you for being there for me, sharing the life with me, and making me smile every day. I look forward to our future adventures which will certainly be as awesome as what we already have experienced together. A heartfelt thank you to my whole family!

Turku, January 2021

Riikka Viitanen

References

Aalto, K., Autio, A., Kiss, E. A., Elima, K., Nymalm, Y., Veres, T. Z., Marttila-Ichihara, F., Elovaara, H., Saanijoki, T., Crocker, P. R., Maksimow, M., Bligt, E., Salminen, T. A., Salmi, M., Roivainen, A., & Jalkanen, S. (2011). Siglec-9 is a novel leukocyte ligand for vascular adhesion protein-1 and can be used in PET imaging of inflammation and cancer. *Blood*, *118*(13), 3725–3733.

Aalto, K., Havulinna, A. S., Jalkanen, S., Salomaa, V., & Salmi, M. (2014). Soluble vascular adhesion protein-1 predicts incident major adverse cardiovascular events and improves reclassification in a finnish prospective cohort study. *Circulation: Cardiovascular Genetics*, *7*(4), 529–535.

Abella, A., García-Vicente, S., Viguerie, N., Ros-Baró, A., Camps, M., Palacín, M., Zorzano, A., & Marti, L. (2004). Adipocytes release a soluble form of VAP-1/SSAO by a metalloprotease-dependent process and in a regulated manner. *Diabetologia*, *47*(3), 429–438.

Ahtinen, H., Kulkova, J., Lindholm, L., Eerola, E., Hakanen, A. J., Moritz, N., Söderström, M., Saanijoki, T., Jalkanen, S., Roivainen, A., & Aro, H. T. (2014). (68)Ga-DOTA-Siglec-9 PET/CT imaging of peri-implant tissue responses and staphylococcal infections. *EJNMMI Research*, *4*, 45.

Airenne, T. T., Nymalm, Y., Kidron, H., Smith, D. J., Pihlavisto, M., Salmi, M., Jalkanen, S., Johnson, M. S., & Salminen, T. A. (2005). Crystal structure of the human vascular adhesion protein-1: Unique structural features with functional implications. *Protein Science*, *14*(8), 1964–1974.

Akin, E., Aversa, J., & Steere, A. C. (2001). Expression of adhesion molecules in synovia of patients with treatment-resistant lyme arthritis. *Infection and Immunity*, *69*(3), 1774–1780.

Ambrosini, V., Zompatori, M., De Luca, F., Antonia, D., Allegri, V., Nanni, C., Malvi, D., Tonveronachi, E., Fasano, L., Fabbri, M., & Fanti, S. (2010). 68Ga-DOTANOC PET/CT Allows Somatostatin Receptor Imaging in Idiopathic Pulmonary Fibrosis: Preliminary Results. *Journal of Nuclear Medicine*, *51*(12), 1950–1955.

Anders, H. J., & Vielhauer, V. (2011). Renal co-morbidity in patients with rheumatic diseases. *Arthritis Research and Therapy*, *13*(3), 222.

Andriu, A., Crockett, J., Dall'Angelo, S., Piras, M., Zanda, M., & Fleming, I. N. (2018). Binding of αvβ3 Integrin-Specific Radiotracers Is Modulated by Both Integrin Expression Level and Activation Status. *Molecular Imaging and Biology*, *20*(1), 27–36.

Antonov, A. S., Antonova, G. N., Munn, D. H., Mivechi, N., Lucas, R., Catravas, J. D., & Verin, A. D. (2011). αVβ3 integrin regulates macrophage inflammatory responses via PI3 kinase/Akt-dependent NF-κB activation. *Journal of Cellular Physiology*, *226*(2), 469–476.

Arndtz, K., Corrigan, M., Rowe, A., Kirkham, A., Barton, D., Fox, R. P., Llewellyn, L., Athwal, A., Wilkhu, M., Chen, Y. Y., Weston, C., Desai, A., Adams, D. H., & Hirschfield, G. M. (2017). Investigating the safety and activity of the use of BTT1023 (Timolumab), in the treatment of patients with primary sclerosing cholangitis (BUTEO): A single-arm, two-stage, open-label, multi-centre, phase II clinical trial protocol. *BMJ Open*, *7*(6), e015081.

Arvilommi, A. M., Salmi, M., Kalimo, K., & Jalkanen, S. (1996). Lymphocyte binding to vascular endothelium in inflamed skin revisited: A central role for vascular adhesion protein-1 (VAP-1). *European Journal of Immunology*, *26*(4), 825–833.

Aspinall, A. I., Curbishley, S. M., Lalor, P. F., Weston, C. J., Blahova, M., Liaskou, E., Adams, R. M., Holt, A. P., & Adams, D. H. (2010). CX3CR1 and vascular adhesion protein-1-dependent

recruitment of CD16+ monocytes across human liver sinusoidal endothelium. *Hepatology*, *51*(6), 2030–2039.

Autio, A., Henttinen, T., Sipilä, H. J., Jalkanen, S., & Roivainen, A. (2011). Mini-PEG spacering of VAP-1-targeting 68Ga-DOTAVAP-P1 peptide improves PET imaging of inflammation. *EJNMMI Research*, *1*(1), 10.

Autio, A., Ujula, T., Luoto, P., Salomäki, S., Jalkanen, S., & Roivainen, A. (2010). PET imaging of inflammation and adenocarcinoma xenografts using vascular adhesion protein 1 targeting peptide 68Ga-DOTAVAP-P1: comparison with 18F-FDG. *European Journal of Nuclear Medicine and Molecular Imaging*, *37*(10), 1918–1925.

Avraamides, C. J., Garmy-Susini, B., & Varner, J. A. (2008). Integrins in angiogenesis and lymphangiogenesis. *Nature Reviews. Cancer*, *8*(8), 604–617

Bansal, G. J. (2006). Digital radiography. A comparison with modern conventional imaging. *Postgraduate Medical Journal*, *82*(969), 425–428.

Barthold, S. W., de Souza, M. S., Janotka, J. L., Smith, A. L., & Persing, D. H. (1993). Chronic Lyme borreliosis in the laboratory mouse. *The American Journal of Pathology*, *143*(3), 959–971.

Barthold, S. W., Persing, D. H., Armstrong, A. L., & Peeples, R. A. (1991). Kinetics of Borrelia burgdorferi dissemination and evolution of disease after intradermal inoculation of mice. *The American Journal of Pathology*, *139*(2), 263–273.

Bauer, S., Jendro, M. C., Wadle, A., Kleber, S., Stenner, F., Dinser, R., Reich, A., Faccin, E., Gödde, S., Dinges, H., Müller-Ladner, U., & Renner, C. (2006). Fibroblast activation protein is expressed by rheumatoid myofibroblast-like synoviocytes. *Arthritis Research and Therapy*, *8*(6), R171.

Beer, A. J., Haubner, R., Sarbia, M., Goebel, M., Luderschmidt, S., Grosu, A. L., Schnell, O., Niemeyer, M., Kessler, H., Wester, H. J., Weber, W. A., & Schwaiger, M. (2006). Positron emission tomography using [18F]Galacto-RGD identifies the level of integrin αvβ3 expression in man. *Clinical Cancer Research*, *12*(13), 3942–3949.

Beer, A. J., Niemeyer, M., Carlsen, J., Sarbia, M., Ñahrig, J., Watzlowik, P., Wester, H. J., Harbeck, N., & Schwaiger, M. (2008). Patterns of αvβ3 expression in primary and metastatic human breast cancer as shown by 18F-galacto-RGD PET. *Journal of Nuclear Medicine*, *49*(2), 255–259.

Beer, A. J., & Schwaiger, M. (2008). Imaging of integrin alphavbeta3 expression. *Cancer and Metastasis Reviews*, 27(4), 631–644.

Bockenstedt, L. K., Gonzalez, D. G., Haberman, A. M., & Belperron, A. A. (2012). Spirochete antigens persist near cartilage after murine Lyme borreliosis therapy. *The Journal of Clinical Investigation*, *122*(7), 2652–2660.

Bockenstedt, L. K., & Wormser, G. P. (2014). Review: unraveling Lyme disease. *Arthritis & Rheumatology*, *66*(9), 2313–2323.

Boellaard, R., Delgado-Bolton, R., Oyen, W. J. G., Giammarile, F., Tatsch, K., Eschner, W., Verzijlbergen, F. J., Barrington, S. F., Pike, L. C., Weber, W. A., Stroobants, S., Delbeke, D., Donohoe, K. J., Holbrook, S., Graham, M. M., Testanera, G., Hoekstra, O. S., Zijlstra, J., Visser, E., … Krause, B. J. (2015). FDG PET/CT: EANM procedure guidelines for tumour imaging: version 2.0. *European Journal of Nuclear Medicine and Molecular Imaging*, *42*(2), 328–354.

Boerman, O. C., Rennen, H., Oyen, W. J. G., & Corstens, F. H. M. (2001). Radiopharmaceuticals to image infection and inflammation. *Seminars in Nuclear Medicine*, *31*(4), 286–295.

Bonder, C. S., Norman, M. U., Swain, M. G., Zbytnuik, L. D., Yamanouchi, J., Santamaria, P., Ajuebor, M., Salmi, M., Jalkanen, S., & Kubes, P. (2005). Rules of recruitment for Th1 and Th2 lymphocytes in inflamed liver: A role for alpha-4 integrin and vascular adhesion protein-1. *Immunity*, *23*(2), 153–163.

Bornhöfft, K. F., Goldammer, T., Rebl, A., & Galuska, S. P. (2018). Siglecs: A journey through the evolution of sialic acid-binding immunoglobulin-type lectins. *Developmental and Comparative Immunology*, *86*, 219–231.

Bouvard, D., Pouwels, J., De Franceschi, N., & Ivaska, J. (2013). Integrin inactivators: balancing cellular functions in vitro and in vivo. *Nature Reviews Molecular Cell Biology*, *14*(7), 432–444.

Boyman, O., & Sprent, J. (2012). The role of interleukin-2 during homeostasis and activation of the immune system. *Nature Reviews Immunology*, *12*(3), 180–190.

Braeuer, R. R., Watson, I. R., Wu, C.-J., Mobley, A. K., Kamiya, T., Shoshan, E., & Bar-Eli, M. (2014). Why is melanoma so metastatic? *Pigment Cell & Melanoma Research*, *27*(1), 19–36.

Brooks, P. C. (1996). Role of integrins in angiogenesis. *European Journal of Cancer*, *32A*(14), 2423–2429.

Brooks, P. C., Clark, R., & Cheresh, D. (1994). Requirement of vascular integrin alpha v beta 3 for angiogenesis. *Science*, *264*(5158), 569–571.

Bruce, T. O. (2008). Comorbid depression in rheumatoid arthritis: Pathophysiology and clinical implications. *Current Psychiatry Reports*, *10*(3), 258–264.

Bruijnen, S. T. G., Verweij, N. J. F., Gent, Y. Y. J., Huisman, M. C., Windhorst, A. D., Kassiou, M., van de Ven, P. M., Lammertsma, A. A., Hoekstra, O. S., Voskuyl, A. E., & van der Laken, C. J. (2019). Imaging disease activity of rheumatoid arthritis by macrophage targeting using second generation translocator protein positron emission tomography tracers. *PLoS ONE*, *14*(9), e0222844.

Bruijnen, S., Tsang-A-Sjoe, M., Raterman, H., Ramwadhdoebe, T., Vugts, D., van Dongen, G., Huisman, M., Hoekstra, O., Tak, P. P., Voskuyl, A., & van der Laken, C. (2016). B-cell imaging with zirconium-89 labelled rituximab PET-CT at baseline is associated with therapeutic response 24weeks after initiation of rituximab treatment in rheumatoid arthritis patients. *Arthritis Research and Therapy*, *18*(1), 266.

Buchmann, I., Henze, M., Engelbrecht, S., Eisenhut, M., Runz, A., Schäfer, M., Schilling, T., Haufe, S., Herrmann, T., & Haberkorn, U. (2007). Comparison of 68Ga-DOTATOC PET and 111In-DTPAOC (Octreoscan) SPECT in patients with neuroendocrine tumours. *European Journal of Nuclear Medicine and Molecular Imaging*, *34*(10), 1617–1626.

Calderwood, D. A. (2004). Integrin activation. *Journal of Cell Science*, *117*(5), 657–666.

Canat, X., Guillaumont, A., Bouaboula, M., Poinot-Chazel, C., Derocq, J. M., Carayon, P., Le Fur, G., & Casellas, P. (1993). Peripheral benzodiazepine receptor modulation with phagocyte differentiation. *Biochemical Pharmacology*, *46*(3), 551–554.

Cao, Q., Cai, W., Li, Z. B., Chen, K., He, L., Li, H. C., Hui, M., & Chen, X. (2007). PET imaging of acute and chronic inflammation in living mice. *European Journal of Nuclear Medicine and Molecular Imaging*, *34*(11), 1832–1842.

Carmeliet, P. (2005). Angiogenesis in life, disease and medicine. *Nature*, *438*(7070), 932–936.

Caronni, N., Savino, B., & Bonecchi, R. (2015). Myeloid cells in cancer-related inflammation. *Immunobiology*, *220*(2), 249–253.

Carrega, P., Morandi, B., Costa, R., Frumento, G., Forte, G., Altavilla, G., Ratto, G. B., Mingari, M. C., Moretta, L., & Ferlazzo, G. (2008). Natural killer cells infiltrating human nonsmall-cell lung cancer are enriched in CD56brightCD16- cells and display an impaired capability to kill tumor cells. *Cancer*, *112*(4), 863–875.

Cavaillon, J.-M., & Singer, M. (2018). *Inflammation: from molecular and cellular mechanisms to the clinic*. Wiley-VCH.

Chaudhari, A. J., Bowen, S. L., Burkett, G. W., Packard, N. J., Godinez, F., Joshi, A. A., Naguwa, S. M., Shelton, D. K., Hunter, J. C., Boone, J. M., Buonocore, M. H., & Badawi, R. D. (2010). High-resolution 18F-FDG PET with MRI for monitoring response to treatment in rheumatoid arthritis. *European Journal of Nuclear Medicine and Molecular Imaging*, *37*(5), 1047.

Chavakis, E., Eun, Y. C., & Chavakis, T. (2009). Novel aspects in the regulation of the leukocyte adhesion cascade. *Thrombosis and Haemostasis*, *102*(2), 191–197.

Chrapko, B., Chrapko, M., Nocuń, A., Stefaniak, B., Zubilewicz, T., & Drop, A. (2016). Role of 18F-FDG PET/CT in the diagnosis of inflammatory and infectious vascular disease. *Nuclear Medicine Review*, *19*(1), 28–36.

Chrusciel, P., Yatkin, E., Li, X. G., Jaakkola, U. M., Knuuti, J., Jalkanen, S., & Roivainen, A. (2019). Safety Study of Single-Dose Intravenously Administered DOTA-Siglec-9 Peptide in Sprague Dawley Rats. *International Journal of Toxicology*, *38*(1), 4–11.

Claesson-Welsh, L., & Welsh, M. (2013). VEGFA and tumour angiogenesis. *Journal of Internal Medicine*, *273*(2), 114–127.

Clemente, C. G., Mihm, M. C., Bufalino, R., Zurrida, S., Collini, P., & Cascinelli, N. (1996). Prognostic value of tumor infiltrating lymphocytes in the vertical growth phase of primary cutaneous melanoma. *Cancer*, *77*(7), 1303–1310.

Coburn, J., Medrano, M., & Cugini, C. (2002). Borrelia burgdorferi and its tropisms for adhesion molecules in the joint. *Current Opinion in Rheumatology*, *14*(4), 394–398.

Connolly, C. M., & Donohoe, K. J. (2017). Nuclear Medicine Imaging of Infection. *Seminars in Roentgenology*, *52*(2), 114–119.

Coughlin, J. M., Yang, T., Rebman, A. W., Bechtold, K. T., Du, Y., Mathews, W. B., Lesniak, W. G., Mihm, E. A., Frey, S. M., Marshall, E. S., Rosenthal, H. B., Reekie, T. A., Kassiou, M., Dannals, R. F., Soloski, M. J., Aucott, J. N., & Pomper, M. G. (2018). Imaging glial activation in patients with post-treatment Lyme disease symptoms: A pilot study using [11C]DPA-713 PET. *Journal of Neuroinflammation*, *15*(1), 1–7.

Coussens, L. M., & Werb, Z. (2002). Inflammation and cancer. *Nature*, 420(6917), 860–867.

Cybulsky, M. I., Iiyama, K., Li, H., Zhu, S., Chen, M., Iiyama, M., Davis, V., Gutierrez-Ramos, J. C., Connelly, P. W., & Milstone, D. S. (2001). A major role for VCAM-1, but not ICAM-1, in early atherosclerosis. *Journal of Clinical Investigation*, *107*(10), 1255–1262

Dalm, V. A. S. H., Van Hagen, P. M., Van Koetsveld, P. M., Achilefu, S., Houtsmuller, A. B., Pols, D. H. J., Van Der Lely, A. J., Lamberts, S. W. J., & Hofland, L. J. (2003). Expression of somatostatin, cortistatin, and somatostatin receptors in human monocytes, macrophages, and dendritic cells. *American Journal of Physiology - Endocrinology and Metabolism*, *285*(2), E344–E353.

Dancey, A. L., Mahon, B. S., & Rayatt, S. S. (2008). A review of diagnostic imaging in melanoma. *Journal of Plastic, Reconstructive and Aesthetic Surgery*, *61*(11), 1275–1283.

Danese, S., Sans, M., de la Motte, C., Graziani, C., West, G., Phillips, M. H., Pola, R., Rutella, S., Willis, J., Gasbarrini, A., & Fiocchi, C. (2006). Angiogenesis as a Novel Component of Inflammatory Bowel Disease Pathogenesis. *Gastroenterology*, *130*(7), 2060–2073.

Dash, A., & Chakravarty, R. (2019). Radionuclide generators: the prospect of availing PET radiotracers to meet current clinical needs and future research demands. *American Journal of Nuclear Medicine and Molecular Imaging*, *9*(1), 30–66.

De Melo, J., & Tang, D. (2015). Elevation of SIPL1 (SHARPIN) Increases Breast Cancer Risk. *PloS One*, *10*(5), e0127546.

DeMarco, V. P., Ordonez, A. A., Klunk, M., Prideaux, B., Wang, H., Zhuo, Z., Tonge, P. J., Dannals, R. F., Holt, D. P., Lee, C. K. K., Weinstein, E. A., Dartois, V., Dooley, K. E., & Jain, S. K. (2015). Determination of [11C]rifampin pharmacokinetics within Mycobacterium tuberculosis-infected mice by using dynamic positron emission tomography bioimaging. *Antimicrobial Agents and Chemotherapy*, *59*(9), 5768–5774.

Desgrosellier, J. S., & Cheresh, D. A. (2010). Integrins in cancer: Biological implications and therapeutic opportunities. *Nature Reviews Cancer*, *10*(1), 9–22.

Di Gialleonardo, V., Signore, A., Glaudemans, A. W. J. M., Dierckx, R. A. J. O., & De Vries, E. F. J. (2012). N-(4-18F-fluorobenzoyl)interleukin-2 for PET of human-activated T lymphocytes. *Journal of Nuclear Medicine*, *53*(5), 679–686.

Di Gialleonardo, V., Signore, A., Willemsen, A. T. M., Sijbesma, J. W. A., Dierckx, R. A. J. O., & De Vries, E. F. J. (2012). Pharmacokinetic modelling of N-(4-[18F]fluorobenzoyl) interleukin-2 binding to activated lymphocytes in an xenograft model of inflammation. *European Journal of Nuclear Medicine and Molecular Imaging*, *39*(10), 1551–1560.

Dieu-Nosjean, M. C., Antoine, M., Danel, C., Heudes, D., Wislez, M., Poulot, V., Rabbe, N., Laurans, L., Tartour, E., De Chaisemartin, L., Lebecque, S., Fridman, W. H., & Cadranel, J. (2008). Long-

term survival for patients with non-small-cell lung cancer with intratumoral lymphoid structures. *Journal of Clinical Oncology*, *26*(27), 4410–4417.

Dijkgraaf, I., Kruijtzer, J. A. W., Liu, S., Soede, A. C., Oyen, W. J. G., Corstens, F. H. M., Liskamp, R. M. J., & Boerman, O. C. (2007). Improved targeting of the alpha(v)beta (3) integrin by multimerisation of RGD peptides. *European Journal of Nuclear Medicine and Molecular Imaging*, *34*(2), 267–273.

Dijkgraaf, I., Yim, C.-B., Franssen, G. M., Schuit, R. C., Luurtsema, G., Liu, S., Oyen, W. J. G., & Boerman, O. C. (2011). PET imaging of $\alpha v\beta_3$ integrin expression in tumours with ^{68}Ga-labelled mono-, di- and tetrameric RGD peptides. *European Journal of Nuclear Medicine and Molecular Imaging*, *38*(1), 128–137.

Dumont, R. A., Deininger, F., Haubner, R., Maecke, H. R., Weber, W. A., & Fani, M. (2011). Novel 64Cu- and 68Ga-labeled RGD conjugates show improved PET imaging of αvβ3 integrin expression and facile radiosynthesis. *Journal of Nuclear Medicine*, *52*(8), 1276–1284.

Dumont, R. A., Hildebrandt, I., Su, H., Haubner, R., Reischl, G., Czernin, J. G., Mischel, P. S., & Weber, W. A. (2009). Noninvasive imaging of alphaVbeta3 function as a predictor of the antimigratory and antiproliferative effects of dasatinib. *Cancer Research*, *69*(7), 3173–3179.

Eckl, J., Buchner, A., Prinz, P. U., Riesenberg, R., Siegert, S. I., Kammerer, R., Nelson, P. J., & Noessner, E. (2012). Transcript signature predicts tissue NK cell content and defines renal cell carcinoma subgroups independent of TNM staging. *Journal of Molecular Medicine*, *90*(1), 55–66.

Elinav, E., Nowarski, R., Thaiss, C. A., Hu, B., Jin, C., & Flavell, R. A. (2013). Inflammation-induced cancer: crosstalk between tumours, immune cells and microorganisms. *Nature Reviews. Cancer*, *13*(11), 759–771.

Elmore, B. O., Bollinger, J. A., & Dooley, D. M. (2002). Human kidney diamine oxidase: Heterologous expression, purification, and characterization. *Journal of Biological Inorganic Chemistry*, *7*(6), 565–579.

Elo, P., Tadayon, S., Liljenbäck, H., Teuho, J., Käkelä, M., Koskensalo, K., Saunavaara, V., Virta, J., Veres, T. Z., Kiviniemi, A., Saraste, A., Marjamäki, P., Airas, L., Jalkanen, S., & Roivainen, A. (2018). Vascular adhesion protein-1 is actively involved in the development of inflammatory lesions in rat models of multiple sclerosis. *Journal of Neuroinflammation*, *15*(1), 128.

Enrique-Tarancón, G., Marti, L., Morin, N., Lizcano, J. M., Unzeta, M., Sevilla, L., Camps, M., Palacín, M., Testar, X., Carpéné, C., & Zorzano, A. (1998). Role of semicarbazide-sensitive amine oxidase on glucose transport and GLUT4 recruitment to the cell surface in adipose cells. *Journal of Biological Chemistry*, *273*(14), 8025–8032.

Eo, J. S., & Jeong, J. M. (2016). Angiogenesis Imaging Using 68Ga-RGD PET/CT: Therapeutic Implications. *Seminars in Nuclear Medicine*, *46*(5), 419–427.

Evans, B. J., King, A. T., Katsifis, A., Matesic, L., & Jamie, J. F. (2020). Methods to Enhance the Metabolic Stability of Peptide-Based PET Radiopharmaceuticals. *Molecules*, *25*(10).

Evans, R., Patzak, I., Svensson, L., De Filippo, K., Jones, K., McDowall, A., & Hogg, N. (2009). Integrins in immunity. *Journal of Cell Science*, *122*(2), 215–225.

Ferjančič, Š., Gil-Bernabé, A. M., Hill, S. A., Allen, P. D., Richardson, P., Sparey, T., Savory, E., McGuffog, J., & Muschel, R. J. (2013). VCAM-1 and VAP-1 recruit myeloid cells that promote pulmonary metastasis in mice. *Blood*, *121*(16), 3289–3297.

Fidler, I. J., & Nicolson, G. L. (1977). Fate of recirculating B16 melanoma metastatic variant cells in parabiotic syngeneic recipients: brief communication. *Journal of the National Cancer Institute*, *58*(6), 1867–1872.

Finney, J., Moon, H. J., Ronnebaum, T., Lantz, M., & Mure, M. (2014). Human copper-dependent amine oxidases. *Archives of Biochemistry and Biophysics*, *546*, 19–32.

Forster-Horváth, C., Döme, B., Paku, S., Ladányi, A., Somlai, B., Jalkanen, S., & Tímár, J. (2004). Loss of vascular adhesion protein-1 expression in intratumoral microvessels of human skin melanoma. *Melanoma Research*, *14*(2), 135–140.

Fridlender, Z. G., Sun, J., Kim, S., Kapoor, V., Cheng, G., Ling, L., Worthen, G. S., & Albelda, S. M. (2009). Polarization of Tumor-Associated Neutrophil Phenotype by TGF-β: "N1" versus "N2" TAN. *Cancer Cell*, *16*(3), 183–194.

Gaemperli, O., Shalhoub, J., Owen, D. R. J., Lamare, F., Johansson, S., Fouladi, N., Davies, A. H., Rimoldi, O. E., & Camici, P. G. (2012). Imaging intraplaque inflammation in carotid atherosclerosis with 11C-PK11195 positron emission tomography/computed tomography. *European Heart Journal*, *33*(15), 1902–1910.

Garin-Chesa, P., Old, L. J., & Rettig, W. J. (1990). Cell surface glycoprotein of reactive stromal fibroblasts as a potential antibody target in human epithelial cancers. *Proceedings of the National Academy of Sciences of the United States of America*, *87*(18), 7235–7239.

Garner, H., & de Visser, K. E. (2020). Immune crosstalk in cancer progression and metastatic spread: a complex conversation. *Nature Reviews Immunology*, *20*(8), 483–497.

Gent, Y. Y. J., ter Wee, M. M., Voskuyl, A. E., den Uyl, D., Ahmadi, N., Dowling, C., van Kuijk, C., Hoekstra, O. S., Boers, M., Lems, W. F., & van der Laken, C. J. (2015). Subclinical synovitis detected by macrophage PET, but not MRI, is related to short-term flare of clinical disease activity in early RA patients: An exploratory study. *Arthritis Research and Therapy*, *17*(1), 266.

Gent, Y. Y. J., Weijers, K., Molthoff, C. F. M., Windhorst, A. D., Huisman, M. C., Kassiou, M., Jansen, G., Lammertsma, A. A., & Van der Laken, C. J. (2014). Promising potential of new generation translocator protein tracers providing enhanced contrast of arthritis imaging by positron emission tomography in a rat model of arthritis. *Arthritis Research and Therapy*, *16*(2), R70.

Gentles, A. J., Newman, A. M., Liu, C. L., Bratman, S. V., Feng, W., Kim, D., Nair, V. S., Xu, Y., Khuong, A., Hoang, C. D., Diehn, M., West, R. B., Plevritis, S. K., & Alizadeh, A. A. (2015). The prognostic landscape of genes and infiltrating immune cells across human cancers. *Nature Medicine*, *21*(8), 938–945.

Giesel, F. L., Kratochwil, C., Lindner, T., Marschalek, M. M., Loktev, A., Lehnert, W., Debus, J., Jäger, D., Flechsig, P., Altmann, A., Mier, W., & Haberkorn, U. (2019). 68Ga-FAPI PET/CT: Biodistribution and preliminary dosimetry estimate of 2 DOTA-containing FAP-targeting agents in patients with various cancers. *Journal of Nuclear Medicine*, *60*(3), 386–392.

Gonzalez, H., Hagerling, C., & Werb, Z. (2018). Roles of the immune system in cancer: From tumor initiation to metastatic progression. *Genes and Development*, *32*(19–20), 1267–1284.

Gotthardt, M., Bleeker-Rovers, C. P., Boerman, O. C., & Oyen, W. J. G. (2010). Imaging of inflammation by PET, conventional scintigraphy, and other imaging techniques. *Journal of Nuclear Medicine*, *51*(12), 1937–1949.

Gowrishankar, G., Namavari, M., Jouannot, E. B., Hoehne, A., Reeves, R., Hardy, J., & Gambhir, S. S. (2014). Investigation of 6-[18F]-fluoromaltose as a novel PET tracer for imaging bacterial infection. *PLoS ONE*, *9*(9), 6–11.

Grover, V. P. B., Tognarelli, J. M., Crossey, M. M. E., Cox, I. J., Taylor-Robinson, S. D., & McPhail, M. J. W. (2015). Magnetic Resonance Imaging: Principles and Techniques: Lessons for Clinicians. *Journal of Clinical and Experimental Hepatology*, *5*(3), 246–255.

Guhlmann, A., Brecht-Krauss, D., Suger, G., Glatting, G., Kotzerke, J., Kinzl, L., & Reske, S. N. (1998). Chronic osteomyelitis: Detection with FDG PET and correlation with histopathologic findings. *Radiology*, *206*(3), 749–754.

Guo, Q., Wang, Y., Xu, D., Nossent, J., Pavlos, N. J., & Xu, J. (2018). Rheumatoid arthritis: Pathological mechanisms and modern pharmacologic therapies. *Bone Research*, *6*(1), 15.

Halama, N., Braun, M., Kahlert, C., Spille, A., Quack, C., Rahbari, N., Koch, M., Weitz, J., Kloor, M., Zoernig, I., Schirmacher, P., Brand, K., Grabe, N., & Falk, C. S. (2011). Natural killer cells are scarce in colorectal carcinoma tissue despite high levels of chemokines and cytokines. *Clinical Cancer Research*, *17*(4), 678–689.

Hamacher, K., Coenen, H., & Stöcklin, G. (1986). Efficient Stereospecific Synthesis of No-Carrier-Added 2-[18F]-Fluoro-2-Deoxy-D-Glucose Using Aminopolyether Supported Nucleophilic Substitution. *Journal of Nuclear Medicine*, *27*(2), 235–238.

Hartimath, S. V, Draghiciu, O., van de Wall, S., Manuelli, V., Dierckx, R. A. J. O., Nijman, H. W., Daemen, T., & de Vries, E. F. J. (2017). Noninvasive monitoring of cancer therapy induced activated T cells using [18F]FB-IL-2 PET imaging. *OncoImmunology*, *6*(1), e1248014.

Hartmann, H., Zöphel, K., Freudenberg, R., Oehme, L., Andreeff, M., Wunderlich, G., Eisenhofer, G., & Kotzerke, J. (2009). Radiation exposure of patients during 68Ga-DOTATOC PET/CT examinations. *NuklearMedizin*, *48*(5), 201–207.

Haubner, R., Finsinger, D., & Kessler, H. (1997). Stereoisomeric Peptide Libraries and Peptidomimetics for Designing Selective Inhibitors of the αvβ3 Integrin for a New Cancer Therapy. *Angewandte Chemie International Edition in English*, *36*(1314), 1374–1389.

Haubner, R., Weber, W. A., Beer, A. J., Vabuliene, E., Reim, D., Sarbia, M., Becker, K. F., Goebel, M., Hein, R., Wester, H. J., Kessler, H., & Schwaiger, M. (2005). Noninvasive visualization of the activated αvβ3 integrin in cancer patients by positron emission tomography and [18F]Galacto-RGD. *PLoS Medicine*, *2*(3), e70.

He, L., Ingram, A., Rybak, A. P., & Tang, D. (2010). Shank-interacting protein-like 1 promotes tumorigenesis via PTEN inhibition in human tumor cells. *The Journal of Clinical Investigation*, *120*(6), 2094–2108.

Histed, S. N., Lindenberg, M. L., Mena, E., Turkbey, B., Choyke, P. L., & Kurdziel, K. A. (2012). Review of functional/anatomical imaging in oncology. *Nuclear Medicine Communications*, *33*(4), 349–361.

Hodzic, E., Feng, S., Holden, K., Freet, K. J., & Barthold, S. W. (2008). Persistence of Borrelia burgdorferi following antibiotic treatment in mice. *Antimicrobial Agents and Chemotherapy*, *52*(5), 1728–1736.

Hofman, M. S., Eddie Lau, W. F., & Hicks, R. J. (2015). Somatostatin receptor imaging with 68Ga DOTATATE PET/CT: Clinical utility, normal patterns, pearls, and pitfalls in interpretation. *Radiographics*, *35*(2), 500–516.

Hofmann, M., Maecke, H., Börner, A. R., Weckesser, E., Schöffski, P., Oei, M. L., Schumacher, J., Henze, M., Heppeler, A., Meyer, G. J., & Knapp, W. H. (2001). Biokinetics and imaging with the somatostatin receptor PET radioligand 68Ga-DOTATOC: Preliminary data. *European Journal of Nuclear Medicine*, *28*(12), 1751–1757.

HogenEsch, H., Gijbels, M. J., Offerman, E., van Hooft, J., van Bekkum, D. W., & Zurcher, C. (1993). A spontaneous mutation characterized by chronic proliferative dermatitis in C57BL mice. *The American Journal of Pathology*, *143*(3), 972–982.

HogenEsch, H., Sola, M., Stearns, T. M., Silva, K. A., Kennedy, V. E., & Sundberg, J. P. (2016). Angiogenesis in the skin of SHARPIN-deficient mice with chronic proliferative dermatitis. *Experimental and Molecular Pathology*, *101*(3), 303–307.

Hogg, N., & Bates, P. A. (2000). Genetic analysis of integrin function in man: LAD-1 and other syndromes. *Matrix Biology*, *19*(3), 211–222.

Holland, J. P., Evans, M. J., Rice, S. L., Wongvipat, J., Sawyers, C. L., & Lewis, J. S. (2012). Annotating MYC status with 89Zr-transferrin imaging. *Nature Medicine*, *18*(10), 1586–1591.

Hu, Z., Zhao, P., Zhang, K., Zang, L., Liao, H., & Ma, W. (2016). Evaluation of Serum Vascular Adhesion Protein-1 as a Potential Biomarker in Thyroid Cancer. *International Journal of Endocrinology*, *2016*, 6312529.

Hyde, J. A., Weening, E. H., Chang, M., Trzeciakowski, J. P., Höök, M., Cirillo, J. D., & Skare, J. T. (2011). Bioluminescent imaging of Borrelia burgdorferi in vivo demonstrates that the fibronectin-binding protein BBK32 is required for optimal infectivity. *Molecular Microbiology*, *82*(1), 99–113.

Hynes, R. O. (2002). Integrins: Bidirectional, Allosteric Signaling Machines. *Cell*, *110*(6), 673–687.

ICRP. (2007). The 2007 Recommendations of the International Commission on Radiological Protection. ICRP publication 103. *Annals of the ICRP*, *37*(2–4), 1–332.

Imamura, Y., Kubota, R., Wang, Y., Asakawa, S., Kudoh, J., Mashima, Y., Oguchi, Y., & Shimizu, N. (1997). Human retina-specific amine oxidase (RAO): cDNA cloning, tissue expression, and chromosomal mapping. *Genomics*, *40*(2), 277–283.

Irjala, H., Salmi, M., Alanen, K., Grenman, R., & Jalkanen, S. (2001). Vascular Adhesion Protein 1 Mediates Binding of Immunotherapeutic Effector Cells to Tumor Endothelium. *The Journal of Immunology*, *166*(11), 6937–6943.

Israel, I., Richter, D., Stritzker, J., Ooschot, M., Donat, U., Buck, A., & Samnick, S. (2014). PET Imaging with [68Ga]NOTA-RGD for Prostate Cancer: A Comparative Study with [18F]Fluorodeoxyglucose and [18F]Fluoroethylcholine. *Current Cancer Drug Targets*, *14*(4), 371–379.

Jaakkola, K., Kaunismäki, K., Tohka, S., Yegutkin, G., Vänttinen, E., Havia, T., Pelliniemi, L. J., Virolainen, M., Jalkanen, S., & Salmi, M. (1999). Human vascular adhesion protein-1 in smooth muscle cells. *The American Journal of Pathology*, *155*(6), 1953–1965.

Jaakkola, K., Nikula, T., Holopainen, R., Vähäsilta, T., Matikainen, M. T., Laukkanen, M. L., Huupponen, R., Halkola, L., Nieminen, L., Hiltunen, J., Parviainen, S., Clark, M. R., Knuuti, J., Savunen, T., Kääpä, P., Voipio-Pulkki, L. M., & Jalkanen, S. (2000). In vivo detection of vascular adhesion protein-1 in experimental inflammation. *The American Journal of Pathology*, *157*(2), 463–471.

Jacobs, P., Bissonnette, R., & Guenther, L. C. (2011). Socioeconomic burden of immune-mediated inflammatory diseases - Focusing on work productivity and disability. *Journal of Rheumatology Supplement*, *88*, 55–61.

Jalkanen, S., Karikoski, M., Mercier, N., Koskinen, K., Henttinen, T., Elima, K., Salmivirta, K., & Salmi, M. (2007). The oxidase activity of vascular adhesion protein-1 (VAP-1) induces endothelial E- and P-selectins and leukocyte binding. *Blood*, *110*(6), 1864–1870.

Jamar, F., Buscombe, J., Chiti, A., Christian, P. E., Delbeke, D., Donohoe, K. J., Israel, O., Martin-Comin, J., & Signore, A. (2013). EANM/SNMMI guideline for 18F-FDG use in inflammation and infection. *Journal of Nuclear Medicine*, *54*(4), 647–658.

James, M. L., Hoehne, A., Mayer, A. T., Lechtenberg, K., Moreno, M., Gowrishankar, G., Ilovich, O., Natarajan, A., Johnson, E. M., Nguyen, J., Quach, L., Han, M., Buckwalter, M., Chandra, S., & Gambhir, S. S. (2017). Imaging B cells in a mouse model of multiple sclerosis using 64Cu-rituximab PET. *Journal of Nuclear Medicine*, *58*(11), 1845–1851.

Jensen, S. B., Käkelä, M., Jødal, L., Moisio, O., Alstrup, A. K. O., Jalkanen, S., & Roivainen, A. (2017). Exploring the radiosynthesis and in vitro characteristics of [68Ga]Ga-DOTA-Siglec-9. *Journal of Labelled Compounds and Radiopharmaceuticals*, *60*(9), 439–449.

Jødal, L., Roivainen, A., Oikonen, V., Jalkanen, S., Hansen, S. B., Afzelius, P., Alstrup, A. K. O., Nielsen, O. L., & Jensen, S. B. (2019). Kinetic modelling of [68Ga]Ga-DOTA-siglec-9 in porcine osteomyelitis and soft tissue infections. *Molecules*, *24*(22), 4094.

Jung, J., Kim, J. M., Park, B., Cheon, Y., Lee, B., Choo, S. H., Koh, S. S., & Lee, S. (2010). Newly identified tumor-associated role of human Sharpin. *Molecular and Cellular Biochemistry*, *340*(1–2), 161–167.

Kaitaniemi, S., Elovaara, H., Grön, K., Kidron, H., Liukkonen, J., Salminen, T., Salmi, M., Jalkanen, S., & Elima, K. (2009). The unique substrate specificity of human AOC2, a semicarbazide-sensitive amine oxidase. *Cellular and Molecular Life Sciences*, *66*(16), 2743–2757.

Kalina, P., Decker, A., Kornel, E., & Halperin, J. J. (2005). Lyme disease of the brainstem. *Neuroradiology*, *47*(12), 903–907.

Kapp, T. G., Rechenmacher, F., Neubauer, S., Maltsev, O. V, Cavalcanti-Adam, E. A., Zarka, R., Reuning, U., Notni, J., Wester, H. J., Mas-Moruno, C., Spatz, J., Geiger, B., & Kessler, H. (2017). A comprehensive evaluation of the activity and selectivity profile of ligands for RGD-binding integrins. *Scientific Reports*, *7*, 39805.

Kemik, O., Sümer, A., Kemik, A. S., Itik, V., Dulger, A. C., Purisa, S., & Tuzun, S. (2010). Human vascular adhesion protein-1 (VAP-1): Serum levels for hepatocellular carcinoma in non-alcoholic and alcoholic fatty liver disease. *World Journal of Surgical Oncology*, *8*(1), 83.

Kgoebane, K., Ally, M. M. T. M., Duim-Beytell, M. C., & Suleman, F. E. (2018). The role of imaging in rheumatoid arthritis. *South African Journal of Radiology*, *22*(1), 1316.

Khalil, M. M., Tremoleda, J. L., Bayomy, T. B., & Gsell, W. (2011). Molecular SPECT Imaging: An Overview. *International Journal of Molecular Imaging*, *2011*, 796025.

Kim, J., & Bae, J. S. (2016). Tumor-associated macrophages and neutrophils in tumor microenvironment. *Mediators of Inflammation*, *2016*, 6058147.

Kim, J. H., Lee, J. S., Kang, K. W., Lee, H. Y., Han, S. W., Kim, T. Y., Lee, Y. S., Jeong, J. M., & Lee, D. S. (2012). Whole-body distribution and radiation dosimetry of 68Ga-NOTA-RGD, a positron emission tomography agent for angiogenesis imaging. *Cancer Biotherapy and Radiopharmaceuticals*, *27*(1), 65–71.

Kircher, M., & Lapa, C. (2020). Infection and Inflammation Imaging: Beyond FDG. *PET Clinics*, *15*(2), 215–229.

Kivi, E., Elima, K., Aalto, K., Nymalm, Y., Auvinen, K., Koivunen, E., Otto, D. M., Crocker, P. R., Salminen, T. A., Salmi, M., & Jalkanen, S. (2009). Human Siglec-10 can bind to vascular adhesion protein-1 and serves as its substrate. *Blood*, *114*(26), 5385–5392.

Kobayashi, H., Boelte, K., & Lin, P. C. (2007). Endothelial Cell Adhesion Molecules and Cancer Progression. *Current Medicinal Chemistry*, *14*(4), 377–386.

Koskinen, K., Vainio, P. J., Smith, D. J., Pihlavisto, M., Ylä-Herttuala, S., Jalkanen, S., & Salmi, M. (2004). Granulocyte transmigration through the endothelium is regulated by the oxidase activity of vascular adhesion protein-1 (VAP-1). *Blood*, *103*(9), 3388–3395.

Koutroubakis, I. E., Petinaki, E., Vardas, E., Dimoulios, P., Roussomoustakaki, M., Maniatis, A. N., & Kouroumalis, E. A. (2002). Circulating soluble vascular adhesion protein 1 in patients with inflammatory bowel disease. *European Journal of Gastroenterology and Hepatology*, *14*(4), 405–408.

Kratochwil, C., Flechsig, P., Lindner, T., Abderrahim, L., Altmann, A., Mier, W., Adeberg, S., Rathke, H., Röhrich, M., Winter, H., Plinkert, P. K., Marme, F., Lang, M., Kauczor, H. U., Jäger, D., Debus, J., Haberkorn, U., & Giesel, F. L. (2019). 68Ga-FAPI PET/CT: Tracer uptake in 28 different kinds of cancer. *Journal of Nuclear Medicine*, *60*(6), 801–805.

Kubota, K., Ito, K., Morooka, M., Mitsumoto, T., Kurihara, K., Yamashita, H., Takahashi, Y., & Mimori, A. (2009). Whole-body FDG-PET/CT on rheumatoid arthritis of large joints. *Annals of Nuclear Medicine*, *23*(9), 783–791.

Kumar, V., Abbas, A. K., & Aster, J. C. (2017). *Basic Pathology* (10th ed.). Elsevier.

Kurkijärvi, R., Adams, D. H., Leino, R., Möttönen, T., Jalkanen, S., & Salmi, M. (1998). Circulating form of human vascular adhesion protein-1 (VAP-1): increased serum levels in inflammatory liver diseases. *The Journal of Immunology*, *161*(3), 1549–1557.

Kurkijärvi, R., Jalkanen, S., Isoniemi, H., & Salmi, M. (2001). Vascular adhesion protein-1 (VAP-1) mediates lymphocyte-endothelial interactions in chronic kidney rejection. *European Journal of Immunology*, *31*(10), 2876–2884.

Kurkijarvi, R., Yegutkin, G. G., Gunson, B. K., Jalkanen, S., Salmi, M., & Adams, D. H. (2000). Circulating soluble vascular adhesion protein 1 accounts for the increased serum monoamine oxidase activity chronic liver disease. *Gastroenterology*, *119*(4), 1096–1103.

Lalor, P. F., Edwards, S., McNab, G., Salmi, M., Jalkanen, S., & Adams, D. H. (2002). Vascular Adhesion Protein-1 Mediates Adhesion and Transmigration of Lymphocytes on Human Hepatic Endothelial Cells. *The Journal of Immunology*, *169*(2), 983–992.

Lalor, P. F., Sun, P. J., Weston, C. J., Martin-Santos, A., Wakelam, M. J. O., & Adams, D. H. (2007). Activation of vascular adhesion protein-1 on liver endothelium results in an NF-κB-dependent increase in lymphocyte adhesion. *Hepatology*, *45*(2), 465–474.

Lamare, F., Hinz, R., Gaemperli, O., Pugliese, F., Mason, J. C., Spinks, T., Camici, P. G., & Rimoldi, O. E. (2011). Detection and quantification of large-vessel inflammation with 11C-(R)-PK11195 PET/CT. *Journal of Nuclear Medicine*, *52*(1), 33–39.

Lankinen, P., Mäkinen, T. J., Pöyhönen, T. A., Virsu, P., Salomäki, S., Hakanen, A. J., Jalkanen, S., Aro, H. T., & Roivainen, A. (2008). (68)Ga-DOTAVAP-P1 PET imaging capable of demonstrating the phase of inflammation in healing bones and the progress of infection in osteomyelitic bones. *European Journal of Nuclear Medicine and Molecular Imaging*, *35*(2), 352–364.

Laverman, P., van der Geest, T., Terry, S. Y. A., Gerrits, D., Walgreen, B., Helsen, M. M., Nayak, T. K., Freimoser-Grundschober, A., Waldhauer, I., Hosse, R. J., Moessner, E., Umana, P., Klein, C., Oyen, W. J. G., Koenders, M. I., & Boerman, O. C. (2015). Immuno-PET and Immuno-SPECT of Rheumatoid Arthritis with Radiolabeled Anti-Fibroblast Activation Protein Antibody Correlates with Severity of Arthritis. *Journal of Nuclear Medicine*, *56*(5), 778–783.

Levy, M. T., McCaughan, G. W., Abbott, C. A., Park, J. E., Cunningham, A. M., Muller, E., Rettig, W. J., & Gorrell, M. D. (1999). Fibroblast activation protein: A cell surface dipeptidyl peptidase and gelatinase expressed by stellate cells at the tissue remodelling interface in human cirrhosis. *Hepatology*, *29*(6), 1768–1778.

Ley, K., Laudanna, C., Cybulsky, M. I., & Nourshargh, S. (2007). Getting to the site of inflammation: the leukocyte adhesion cascade updated. *Nature Reviews. Immunology*, *7*(9), 678–689.

Li, J., Lai, Y., Cao, Y., Du, T., Zeng, L., Wang, G., Chen, X., Chen, J., Yu, Y., Zhang, S., Zhang, Y., Huang, H., & Guo, Z. (2015). SHARPIN overexpression induces tumorigenesis in human prostate cancer LNCaP, DU145 and PC-3 cells via NF-κB/ERK/Akt signaling pathway. *Medical Oncology*, *32*(2), 444.

Li, Y. I., Hung, J. S., Yu, T. Y., Liou, J. M., Wei, J. N., Kao, H. L., Chuang, L. M., Shun, C. T., Lee, P. H., Lai, H. S., Su, C. Y., Li, H. Y., & Liang, J. T. (2014). Serum vascular adhesion protein-1 predicts all-cause mortality and cancer-related mortality in subjects with colorectal cancer. *Clinica Chimica Acta*, *428*, 51–56.

Liaskou, E., Karikoski, M., Reynolds, G. M., Lalor, P. F., Weston, C. J., Pullen, N., Salmi, M., Jalkanen, S., & Adams, D. H. (2011). Regulation of mucosal addressin cell adhesion molecule 1 expression in human and mice by vascular adhesion protein 1 amine oxidase activity. *Hepatology*, *53*(2), 661–672.

Libby, P. (2006). Inflammation and cardiovascular disease mechanisms. *American Journal of Clinical Nutrition*, *83*(2), 456S-460S.

Lindner, T., Loktev, A., Altmann, A., Giesel, F., Kratochwil, C., Debus, J., Jäger, D., Mier, W., & Haberkorn, U. (2018). Development of quinoline-based theranostic ligands for the targeting of fibroblast activation protein. *Journal of Nuclear Medicine*, *59*(9), 1415–1422.

Llopis, E., Kroon, H. M., Acosta, J., & Bloem, J. L. (2017). Conventional Radiology in Rheumatoid Arthritis. *Radiologic Clinics of North America*, *55*(5), 917–941.

Loktev, A., Lindner, T., Burger, E. M., Altmann, A., Giesel, F., Kratochwil, C., Debus, J., Marmé, F., Jäger, D., Mier, W., & Haberkorn, U. (2019). Development of fibroblast activation protein-targeted radiotracers with improved tumor retention. *Journal of Nuclear Medicine*, *60*(10), 1421–1429.

Loktev, A., Lindner, T., Mier, W., Debus, J., Altmann, A., Jäger, D., Giesel, F., Kratochwil, C., Barthe, P., Roumestand, C., & Haberkorn, U. (2018). A tumor-imaging method targeting cancer-associated fibroblasts. *Journal of Nuclear Medicine*, *59*(9), 1423–1429.

Loose, D., Signore, A., Staelens, L., Bulcke, K. Vanden, Vermeersch, H., Dierckx, R. A., Bonanno, E., & Van De Wiele, C. (2008). 123I-Interleukin-2 uptake in squamous cell carcinoma of the head and neck carcinoma. *European Journal of Nuclear Medicine and Molecular Imaging*, *35*(2), 281–286.

Lopes de Carvalho, L., Bligt-Lindén, E., Ramaiah, A., Johnson, M. S., & Salminen, T. A. (2019). Evolution and functional classification of mammalian copper amine oxidases. *Molecular Phylogenetics and Evolution*, *139*, 106571.

MacRitchie, N., Frleta-Gilchrist, M., Sugiyama, A., Lawton, T., McInnes, I. B., & Maffia, P. (2020). Molecular imaging of inflammation - Current and emerging technologies for diagnosis and treatment. *Pharmacology and Therapeutics*, *211*, 107550.

Madej, A., Reich, A., Orda, A., & Szepietowski, J. C. (2007). Vascular adhesion protein-1 (VAP-1) is overexpressed in psoriatic patients. *Journal of the European Academy of Dermatology and Venereology*, *21*(1), 72–78.

Mantovani, A., Allavena, P., Sica, A., & Balkwill, F. (2008). Cancer-related inflammation. *Nature*, *454*(7203), 436–444.

Mantovani, A., Sozzani, S., Locati, M., Allavena, P., & Sica, A. (2002). Macrophage polarization: Tumor-associated macrophages as a paradigm for polarized M2 mononuclear phagocytes. *Trends in Immunology*, *23*(11), 549–555.

Martelius, T., Salaspuro, V., Salmi, M., Krogerus, L., Höckerstedt, K., Jalkanen, S., & Lautenschlager, I. (2004). Blockade of vascular adhesion protein-1 inhibits lymphocyte infiltration in rat liver allograft rejection. *American Journal of Pathology*, *165*(6), 1993–2001.

Martin, K. H., & Dayton, P. A. (2013). Current status and prospects for microbubbles in ultrasound theranostics. *Wiley Interdisciplinary Reviews: Nanomedicine and Nanobiotechnology*, *5*(4), 329–345.

Marttila-Ichihara, F., Auvinen, K., Elima, K., Jalkanen, S., & Salmi, M. (2009). Vascular adhesion protein-1 enhances tumor growth by supporting recruitment of Gr-1+CD11b+ myeloid cells into tumors. *Cancer Research*, *69*(19), 7875–7883.

Marttila-Ichihara, F., Castermans, K., Auvinen, K., Oude Egbrink, M. G. A., Jalkanen, S., Griffioen, A. W., & Salmi, M. (2010). Small-molecule inhibitors of vascular adhesion protein-1 reduce the accumulation of myeloid cells into tumors and attenuate tumor growth in mice. *The Journal of Immunology*, *184*(6), 3164–3173.

Marttila-Ichihara, F., Smith, D. J., Stolen, C., Yegutkin, G. G., Elima, K., Mercier, N., Kiviranta, R., Pihlavisto, M., Alaranta, S., Pentikäinen, U., Pentikäinen, O., Fülöp, F., Jalkanen, S., & Salmi, M. (2006). Vascular amine oxidases are needed for leukocyte extravasation into inflamed joints in vivo. *Arthritis and Rheumatism*, *54*(9), 2852–2862.

Maula, S. M., Salminen, T., Kaitaniemi, S., Nymalm, Y., Smith, D. J., & Jalkanen, S. (2005). Carbohydrates located on the top of the "cap" contribute to the adhesive and enzymatic functions of vascular adhesion protein-1. *European Journal of Immunology*, *35*(9), 2718–2727.

McNab, G., Reeves, J. L., Salmi, M., Hubscher, S., Jalkanen, S., & Adams, D. H. (1996). Vascular adhesion protein 1 mediates binding of T cells to human hepatic endothelium. *Gastroenterology*, *110*(2), 522–528.

McQueen, F. M. (2013). Imaging in early rheumatoid arthritis. *Best Practice & Research. Clinical Rheumatology*, *27*(4), 499–522.

Medzhitov, R. (2008). Origin and physiological roles of inflammation. *Nature*, *454*(7203), 428–435.

Meier, R., Krug, C., Golovko, D., Boddington, S., Piontek, G., Rudelius, M., Sutton, E. J., Baur-Melnyk, A., Jones, E. F., & Daldrup-Link, H. E. (2010). Indocyanine green - Enhanced imaging of antigen-induced arthritis with an integrated optical imaging/radiography system. *Arthritis and Rheumatism*, *62*(8), 2322–2327.

Merinen, M., Irjala, H., Salmi, M., Jaakkola, I., Hänninen, A., & Jalkanen, S. (2005). Vascular adhesion protein-1 is involved in both acute and chronic inflammation in the mouse. *American Journal of Pathology*, *166*(3), 793–800.

Miller, A., & Mihm, M. J. (2006). Melanoma. *The New England Journal of Medicine*, *355*, 51–65.

Mizui, M. (2019). Natural and modified IL-2 for the treatment of cancer and autoimmune diseases. *Clinical Immunology*, *206*, 63–70.

Moriarty, T. J., Norman, M. U., Colarusso, P., Bankhead, T., Kubes, P., & Chaconas, G. (2008). Real-time high resolution 3D imaging of the lyme disease spirochete adhering to and escaping from the vasculature of a living host. *PLoS Pathogens*, *4*(6), e1000090.

Murray, P. J., Allen, J. E., Biswas, S. K., Fisher, E. A., Gilroy, D. W., Goerdt, S., Gordon, S., Hamilton, J. A., Ivashkiv, L. B., Lawrence, T., Locati, M., Mantovani, A., Martinez, F. O., Mege, J. L., Mosser, D. M., Natoli, G., Saeij, J. P., Schultze, J. L., Shirey, K. A., … Wynn, T. A. (2014). Macrophage Activation and Polarization: Nomenclature and Experimental Guidelines. *Immunity*, *41*(1), 14–20.

Muylle, K., Flamen, P., Vugts, D. J., Guiot, T., Ghanem, G., Meuleman, N., Bourgeois, P., Vanderlinden, B., van Dongen, G. A. M. S., Everaert, H., Vaes, M., & Bron, D. (2015). Tumour targeting and radiation dose of radioimmunotherapy with 90Y-rituximab in CD20+ B-cell lymphoma as predicted by 89Zr-rituximab immuno-PET: impact of preloading with unlabelled rituximab. *European Journal of Nuclear Medicine and Molecular Imaging*, *42*(8), 1304–1314.

Nahrendorf, M., Keliher, E., Panizzi, P., Zhang, H., Hembrador, S., Figueiredo, J. L., Aikawa, E., Kelly, K., Libby, P., & Weissleder, R. (2009). 18F-4V for PET-CT Imaging of VCAM-1 Expression in Atherosclerosis. *JACC: Cardiovascular Imaging*, *2*(10), 1213–1222.

Nakamura, K., & Smyth, M. J. (2017). Targeting cancer-related inflammation in the era of immunotherapy. *Immunology and Cell Biology*, *95*(4), 325–332.

Nanni, C., Errani, C., Boriani, L., Fantini, L., Ambrosini, V., Boschi, S., Rubello, D., Pettinato, C., Mercuri, M., Gasbarrini, A., & Fanti, S. (2010). 68Ga-citrate PET/CT for evaluating patients with infections of the bone: Preliminary results. *Journal of Nuclear Medicine*, *51*(12), 1932–1936.

Narayan, N., Owen, D. R., & Taylor, P. C. (2017). Advances in positron emission tomography for the imaging of rheumatoid arthritis. *Rheumatology*, *68*, S236-40.

Newberg, A., Hassan, A., & Alavi, A. (2002). Cerebral metabolic changes associated with Lyme disease. *Nuclear Medicine Communications*, *23*(8), 773–777.

Nieminen, M., Henttinen, T., Merinen, M., Marttila-Ichihara, F., Eriksson, J. E., & Jalkanen, S. (2006). Vimentin function in lymphocyte adhesion and transcellular migration. *Nature Cell Biology*, *8*(2), 156–162.

Nobashi, T., Nakamoto, Y., Kubo, T., Ishimori, T., Handa, T., Tanizawa, K., Sano, K., Mishima, M., & Togashi, K. (2016). The utility of PET/CT with 68Ga-DOTATOC in sarcoidosis: comparison with 67Ga-scintigraphy. *Annals of Nuclear Medicine*, *30*(8), 544–552.

Norman, M. U., Moriarty, T. J., Dresser, A. R., Millen, B., Kubes, P., & Chaconas, G. (2008). Molecular mechanisms involved in vascular interactions of the Lyme disease pathogen in a living host. *PLoS Pathogens*, *4*(10), e1000169.

Nourshargh, S., & Alon, R. (2014). Leukocyte Migration into Inflamed Tissues. *Immunity*, *41*(5), 694–707.

Nourshargh, S., Hordijk, P. L., & Sixt, M. (2010). Breaching multiple barriers: Leukocyte motility through venular walls and the interstitium. *Nature Reviews Molecular Cell Biology*, *11*(5), 366–378.

Nurmohamed, M. T., Heslinga, M., & Kitas, G. D. (2015). Cardiovascular comorbidity in rheumatic diseases. *Nature Reviews Rheumatology*, *11*(12), 693–704.

Oh, U., Fujita, M., Ikonomidou, V. N., Evangelou, I. E., Matsuura, E., Harberts, E., Ohayon, J., Pike, V. W., Zhang, Y., Zoghbi, S. S., Innis, R. B., & Jacobson, S. (2011). Translocator protein PET imaging for glial activation in multiple sclerosis. *Journal of Neuroimmune Pharmacology*, *6*(3), 354–361.

Pannecoeck, R., Serruys, D., Benmeridja, L., Delanghe, J. R., Van Geel, N., Speeckaert, R., & Speeckaert, M. M. (2015). Vascular adhesion protein-1: Role in human pathology and application as a biomarker. *Critical Reviews in Clinical Laboratory Sciences*, *52*(6), 284–300.

Papadopoulos, V., & Lecanu, L. (2009). Translocator protein (18 kDa) TSPO: An emerging therapeutic target in neurotrauma. *Experimental Neurology*, *219*(1), 53–57.

Parkin, J., & Cohen, B. (2001). An overview of the immune system. *Lancet*, *357*(9270), 1777–1789.

Perera, R. H., Hernandez, C., Zhou, H., Kota, P., Burke, A., & Exner, A. A. (2015). Ultrasound imaging beyond the vasculature with new generation contrast agents. *Wiley Interdisciplinary Reviews: Nanomedicine and Nanobiotechnology*, *7*(4), 593–608.

Pettinato, C., Sarnelli, A., Di Donna, M., Civollani, S., Nanni, C., Montini, G., Di Pierro, D., Ferrari, M., Marengo, M., & Bergamini, C. (2008). 68Ga-DOTANOC: Biodistribution and dosimetry in patients affected by neuroendocrine tumors. *European Journal of Nuclear Medicine and Molecular Imaging*, *35*(1), 72–79.

Peuhu, E., Kaukonen, R., Lerche, M., Saari, M., Guzmán, C., Rantakari, P., De Franceschi, N., Wärri, A., Georgiadou, M., Jacquemet, G., Mattila, E., Virtakoivu, R., Liu, Y., Attieh, Y., Silva, K. A., Betz, T., Sundberg, J. P., Salmi, M., Deugnier, M.-A., … Ivaska, J. (2017). SHARPIN regulates collagen architecture and ductal outgrowth in the developing mouse mammary gland. *The EMBO Journal*, *36*(2), 165–182.

Peuhu, E., Salomaa, S. I., De Franceschi, N., Potter, C. S., Sundberg, J. P., & Pouwels, J. (2017). Integrin beta 1 inhibition alleviates the chronic hyperproliferative dermatitis phenotype of SHARPIN-deficient mice. *PLoS ONE*, *12*(10), e0186628.

Phelps, M. E. (2000). PET: the merging of biology and imaging into molecular imaging. *Journal of Nuclear Medicine*, *41*(4), 661–681.

Pichler, B. J., Kneilling, M., Haubner, R., Braumüller, H., Schwaiger, M., Röcken, M., & Weber, W. A. (2005). Imaging of delayed-type hypersensitivity reaction by PET and 18F-galacto-RGD. *Journal of Nuclear Medicine*, *46*(1), 184–189.

Plotkin, M., Hautzel, H., Krause, B. J., Mohr, S., Langen, K. J., & Müller, H.-W. (2005). Fluorine-18-labeled fluorodeoxyglucose-positron emission tomography studies of acute brainstem Lyme neuroborreliosis. *Journal of Neurosurgery*, *102*(5), 927–929.

Plow, E. F., Haas, T. A., Zhang, L., Loftus, J., & Smith, J. W. (2000). Ligand binding to integrins. *Journal of Biological Chemistry*, *275(29)*, 21785–21788.

Pugliese, F., Gaemperli, O., Kinderlerer, A. R., Lamare, F., Shalhoub, J., Davies, A. H., Rimoldi, O. E., Mason, J. C., & Camici, P. G. (2010). Imaging of vascular inflammation with [11C]-PK11195 and positron emission tomography/computed tomography angiography. *Journal of the American College of Cardiology*, *56*(8), 653–661.

Rahmim, A., & Zaidi, H. (2008). PET versus SPECT: strengths, limitations and challenges. *Nuclear Medicine Communications*, *29*(3), 193–207.

Rantala, J. K., Pouwels, J., Pellinen, T., Veltel, S., Laasola, P., Mattila, E., Potter, C. S., Duffy, T., Sundberg, J. P., Kallioniemi, O., Askari, J. A., Humphries, M. J., Parsons, M., Salmi, M., & Ivaska, J. (2011). SHARPIN is an endogenous inhibitor of β1-integrin activation. *Nature Cell Biology*, *13*(11), 1315–1324.

Rennen, H. J., Boerman, O. C., Oyen, W. J., & Corstens, F. H. (2001). Imaging infection/inflammation in the new millennium. *European Journal of Nuclear Medicine*, *28*(2), 241–252.

Retamal, J., Sörensen, J., Lubberink, M., Suarez-Sipmann, F., Borges, J. B., Feinstein, R., Jalkanen, S., Antoni, G., Hedenstierna, G., Roivainen, A., Larsson, A., & Velikyan, I. (2016). Feasibility of (68)Ga-labeled Siglec-9 peptide for the imaging of acute lung inflammation: a pilot study in a porcine model of acute respiratory distress syndrome. *American Journal of Nuclear Medicine and Molecular Imaging*, *6*(1), 18–31.

Rettig, W. J., Garin-Chesa, P., Healey, J. H., Su, S. L., Ozer, H. L., Schwab, M., Albino, A. P., & Old, L. J. (1993). Regulation and Heteromeric Structure of the Fibroblast Activation Protein in Normal and Transformed Cells of Mesenchymal and Neuroectodermal Origin. *Cancer Research*, *53*(14), 3327–3335.

Reubi, J. C., Schär, J. C., Waser, B., Wenger, S., Heppeler, A., Schmitt, J. S., & Mäcke, H. R. (2000). Affinity profiles for human somatostatin receptor subtypes SST1-SST5 of somatostatin radiotracers selected for scintigraphic and radiotherapeutic use. *European Journal of Nuclear Medicine*, *27*(3), 273–282.

Roivainen, A., Jalkanen, S., & Nanni, C. (2012). Gallium-labelled peptides for imaging of inflammation. *European Journal of Nuclear Medicine and Molecular Imaging*, *39 Suppl 1*, S68-77.

Roivainen, A., Parkkola, R., Yli-Kerttula, T., Lehikoinen, P., Viljanen, T., Möttönen, T., Nuutila, P., & Minn, H. (2003). Use of Positron Emission Tomography With Methyl-11C-Choline and 2-18F-Fluoro-2-Deoxy-D-Glucose in Comparison With Magnetic Resonance Imaging for the Assessment of Inflammatory Proliferation of Synovium. *Arthritis and Rheumatism*, *48*(11), 3077–3084.

Rossin, R., Muro, S., Welch, M. J., Muzykantov, V. R., & Schustery, D. P. (2008). In vivo imaging of 64Cu-labeled polymer nanoparticles targeted to the lung endothelium. *Journal of Nuclear Medicine*, *49*(1), 103–111.

Ruoslahti, E. (1996). RGD and other recognition sequences for integrins. *Annual Review of Cell and Developmental Biology*, *12*, 697–715.

Rylova, S. N., Barnucz, E., Fani, M., Braun, F., Werner, M., Lassmann, S., Maecke, H. R., & Weber, W. A. (2014). Does Imaging αvβ3 Integrin Expression with PET Detect Changes in Angiogenesis During Bevacizumab Therapy? *Journal of Nuclear Medicine*, *55*(11), 1878–1884.

Salmi, M., & Jalkanen, S. (1992). A 90-kilodalton endothelial cell molecule mediating lymphocyte binding in humans. *Science*, *257*(5075), 1407–1409.

Salmi, M., & Jalkanen, S. (1996). Human vascular adhesion protein 1 (VAP-1) is a unique sialoglycoprotein that mediates carbohydrate-dependent binding of lymphocytes to endothelial cells. *Journal of Experimental Medicine*, *183*(2), 569–579.

Salmi, M., & Jalkanen, S. (2001). VAP-1: an adhesin and an enzyme. *Trends in Immunology*, *22*(4), 211–216.

Salmi, M., & Jalkanen, S. (2005). Cell-surface enzymes in control of leukocyte trafficking. *Nature Reviews. Immunology*, *5*(10), 760–771.

Salmi, M., & Jalkanen, S. (2011). Homing-associated molecules CD73 and VAP-1 as targets to prevent harmful inflammations and cancer spread. *FEBS Letters*, *585*(11), 1543–1550.

Salmi, M., & Jalkanen, S. (2019). Vascular adhesion protein-1: A cell surface amine oxidase in translation. *Antioxidants and Redox Signaling*, *30*(3), 314–332.

Salmi, M., Kalimo, K., & Jalkanen, S. (1993). Induction and function of vascular adhesion protein-1 at sites of inflammation. *Journal of Experimental Medicine*, *178*(6), 2255–2260.

Salmi, M., Rajala, P., & Jalkanen, S. (1997). Homing of mucosal leukocytes to joints: Distinct endothelial ligands in synovium mediate leukocyte-subtype specific adhesion. *Journal of Clinical Investigation*, *99*(9), 2165–2172.

Salmi, M., Yegutkin, G. G., Lehvonen, R., Koskinen, K., Salminen, T., & Jalkanen, S. (2001). A cell surface amine oxidase directly controls lymphocyte migration. *Immunity*, *14*(3), 265–276.

Salo, J., Jaatinen, A., Söderström, M., Viljanen, M. K., & Hytönen, J. (2015). Decorin binding proteins of Borrelia burgdorferi promote arthritis development and joint specific post-treatment DNA persistence in mice. *PloS One*, *10*(3), e0121512.

Sandström, M., Velikyan, I., Garske-Román, U., Sörensen, J., Eriksson, B., Granberg, D., Lundqvist, H., Sundin, A., & Lubberink, M. (2013). Comparative biodistribution and radiation dosimetry of 68Ga-DOTATOC and 68Ga-DOTATATE in patients with neuroendocrine tumors. *Journal of Nuclear Medicine*, *54*(10), 1755–1759.

Sasada, T., Kimura, M., Yoshida, Y., Kanai, M., & Takabayashi, A. (2003). CD4+CD25+ regulatory T cells in patients with gastrointestinal malignancies: Possible involvement of regulatory T cells in disease progression. *Cancer*, *98*(5), 1089–1099.

Schnell, O., Krebs, B., Carlsen, J., Miederer, I., Goetz, C., Goldbrunner, R. H., Wester, H. J., Haubner, R., Pöpperl, G., Holtmannspötter, M., Kretzschmar, H. A., Kessler, H., Tonn, J. C., Schwaiger, M., & Beer, A. J. (2009). Imaging of integrin αvβ3 expression in patients with malignant glioma by [18F]Galacto-RGD positron emission tomography. *Neuro-Oncology*, *11*(6), 861–870.

Schwelberger, H. G. (2007). The origin of mammalian plasma amine oxidases. *Journal of Neural Transmission*, *114*(6), 757–762.

Serhan, C. N., Ward, P. A., & Gilroy, D. W. (2010). *Fundamentals of Inflammation*. Cambridge University Press.

Seymour, R. E., Hasham, M. G., Cox, G. A., Shultz, L. D., Hogenesch, H., Roopenian, D. C., & Sundberg, J. P. (2007). Spontaneous mutations in the mouse Sharpin gene result in multiorgan inflammation, immune system dysregulation and dermatitis. *Genes and Immunity*, *8*(5), 416–421.

Shattil, S. J., Kim, C., & Ginsberg, M. H. (2010). The final steps of integrin activation: the end game. *Nature Reviews. Molecular Cell Biology*, *11*(4), 288–300.

Shetty, S., Weston, C. J., Oo, Y. H., Westerlund, N., Stamataki, Z., Youster, J., Hubscher, S. G., Salmi, M., Jalkanen, S., Lalor, P. F., & Adams, D. H. (2011). Common Lymphatic Endothelial and Vascular Endothelial Receptor-1 Mediates the Transmigration of Regulatory T Cells across Human Hepatic Sinusoidal Endothelium. *The Journal of Immunology*, *186*(7), 4147–4155.

Signore, A., Annovazzi, A., Barone, R., Bonanno, E., D'Alessandria, C., Chianelli, M., Mather, S. J., Bottoni, U., Panetta, C., Innocenzi, D., Scopinaro, F., & Calvieri, S. (2004). 99mTc-interleukin-2 scintigraphy as a potential tool for evaluating tumor-infiltrating lymphocytes in melanoma lesions: A validation study. *Journal of Nuclear Medicine*, *45*(10), 1647–1652.

Signore, A., Chianelli, M., Annovazzi, A., Rossi, M., Maiuri, L., Greco, M., Ronga, G., Britton, K. E., & Picarelli, A. (2000). Imaging active lymphocytic infiltration in coeliac disease with iodine-123-interleukin-2 and the response to diet. *European Journal of Nuclear Medicine*, *27*(1), 18–24.

Signore, A., & Glaudemans, A. W. J. M. (2011). The molecular imaging approach to image infections and inflammation by nuclear medicine techniques. *Annals of Nuclear Medicine*, *25*(10), 681–700.

Signore, A, Picarelli, A., Annovazzi, A., Britton, K. E., Grossman, A. B., Bonanno, E., Maras, B., Barra, D., & Pozzilli, P. (2003). 123I-Interleukin-2: biochemical characterization and in vivo use for imaging autoimmune diseases. *Nuclear Medicine Communications*, *24*(3), 305–316.

Silvola, J., Autio, A., Luoto, P., Jalkanen, S., & Roivainen, A. (2010). Preliminary evaluation of novel 68Ga-DOTAVAP-PEG-P2 peptide targeting vascular adhesion protein-1. *Clinical Physiology and Functional Imaging*, *30*(1), 75–78.

Silvola, J., Virtanen, H., Siitonen, R., Hellberg, S., Liljenbäck, H., Metsälä, O., Ståhle, M., Saanijoki, T., Käkelä, M., Hakovirta, H., Ylä-Herttuala, S., Saukko, P., Jauhiainen, M., Veres, T. Z., Jalkanen, S., Knuuti, J., Saraste, A., & Roivainen, A. (2016). Leukocyte trafficking-associated vascular adhesion protein 1 is expressed and functionally active in atherosclerotic plaques. *Scientific Reports*, *6*, 35089.

Smith, D. J., Salmi, M., Bono, P., Hellman, J., Leu, T., & Jalkanen, S. (1998). Cloning of vascular adhesion protein 1 reveals a novel multifunctional adhesion molecule. *Journal of Experimental Medicine*, *188*(1), 17–27.

Smolen, J. S., Aletaha, D., & McInnes, I. B. (2016). Rheumatoid arthritis. *Lancet*, *388*(10055), 2023–2038.

Solé, M., Hernandez-Guillamon, M., Boada, M., & Unzeta, M. (2008). p53 phosphorylation is involved in vascular cell death induced by the catalytic activity of membrane-bound SSAO/VAP-1. *Biochimica et Biophysica Acta - Molecular Cell Research*, *1783*(6), 1085–1094.

Som, P., Atkins, H. L., Bandoypadhyay, D., Fowler, J. S., Macgregor, R. R., Matsui, K., Oster, Z. H., Sacker, D. F., Shiue, C. Y., Turner, H., Wan, C.-N., Wolf, A. P., & Zabinski, S. V. (1980). A Fluorinated Glucose Analog, 2-fluoro-2-deoxy-D-glucose (F-18): Nontoxic Tracer for Rapid Tumor Detection. *Journal of Nuclear Medicine*, *21*(7), 670–675.

Speiser, D. E., Ho, P. C., & Verdeil, G. (2016). Regulatory circuits of T cell function in cancer. *Nature Reviews Immunology*, *16*(10), 599–611.

Stabin, M. G., & Siegel, J. A. (2003). Physical models and dose factors for use in internal dose assessment. *Health Physics*, *85*(3), 294–310.

Stabin, M. G., & Siegel, J. A. (2018). RADAR dose estimate report: A compendium of radiopharmaceutical dose estimates based on OLINDA/EXM version 2.0. *Journal of Nuclear Medicine*, *59*(1), 154–160.

Stanek, G., Wormser, G. P., Gray, J., & Strle, F. (2012). Lyme borreliosis. *Lancet*, *379*(9814), 461–473.

Sudoł-Szopińska, I., Zaniewicz-Kaniewska, K., Warczyńska, A., Matuszewska, G., Saied, F., & Kunisz, W. (2012). The pathogenesis of rheumatoid arthritis in radiological studies. Part II: Imaging studies in rheumatoid arthritis. *Journal of Ultrasonography*, *12*(50), 319–328.

Synowiecki, M. A., Perk, L. R., & Nijsen, J. F. W. (2018). Production of novel diagnostic radionuclides in small medical cyclotrons. *EJNMMI Radiopharmacy and Chemistry*, *3*(1), 3.

Tarkin, J. M., Joshi, F. R., Evans, N. R., Chowdhury, M. M., Figg, N. L., Shah, A. V, Starks, L. T., Martin-Garrido, A., Manavaki, R., Yu, E., Kuc, R. E., Grassi, L., Kreuzhuber, R., Kostadima, M. A., Frontini, M., Kirkpatrick, P. J., Coughlin, P. A., Gopalan, D., Fryer, T. D., … Rudd, J. H. F. (2017). Detection of Atherosclerotic Inflammation by 68Ga-DOTATATE PET Compared to [18F]FDG PET Imaging. *Journal of the American College of Cardiology*, *69*(14), 1774–1791.

Tohka, S., Laukkanen, M., Jalkanen, S., & Salmi, M. (2001). Vascular adhesion protein 1 (VAP-1) functions as a molecular brake during granulocyte rolling and mediates recruitment in vivo. *The FASEB Journal*, *15*(2), 373–382.

Toiyama, Y., Miki, C., Inoue, Y., Kawamoto, A., & Kusunoki, M. (2009). Circulating form of human vascular adhesion protein-1 (VAP-1): Decreased serum levels in progression of colorectal cancer and predictive marker of lymphatic and hepatic metastasis. *Journal of Surgical Oncology*, *99*(6), 368–372.

Tokunaga, F., Nakagawa, T., Nakahara, M., Saeki, Y., Taniguchi, M., Sakata, S., Tanaka, K., Nakano, H., & Iwai, K. (2011). SHARPIN is a component of the NF-κB-activating linear ubiquitin chain assembly complex. *Nature*, *471*(7340), 633–636.

Tomonaga, M., Hashimoto, N., Tokunaga, F., Onishi, M., Myoui, A., Yoshikawa, H., & Iwai, K. (2012). Activation of nuclear factor-kappa B by linear ubiquitin chain assembly complex contributes to lung metastasis of osteosarcoma cells. *International Journal of Oncology*, *40*(2), 409–417.

Toms, J., Kogler, J., Maschauer, S., Daniel, C., Schmidkonz, C., Kuwert, T., & Prante, O. (2020). Targeting Fibroblast Activation Protein: Radiosynthesis and Preclinical Evaluation of an 18F-labeled FAP Inhibitor. *Journal of Nuclear Medicine*, jnumed.120.242958.

Tosolini, M., Kirilovsky, A., Mlecnik, B., Fredriksen, T., Mauger, S., Bindea, G., Berger, A., Bruneval, P., Fridman, W. H., Pagès, F., & Galon, J. (2011). Clinical impact of different classes of infiltrating T cytotoxic and helper cells (Th1, Th2, Treg, Th17) in patients with colorectal cancer. *Cancer Research*, *71*(4), 1263–1271.

Ujula, T., Salomäki, S., Virsu, P., Lankinen, P., Mäkinen, T. J., Autio, A., Yegutkin, G. G., Knuuti, J., Jalkanen, S., & Roivainen, A. (2009). Synthesis, 68Ga labeling and preliminary evaluation of DOTA peptide binding vascular adhesion protein-1: a potential PET imaging agent for diagnosing osteomyelitis. *Nuclear Medicine and Biology*, *36*(6), 631–641.

Vakal, S., Jalkanen, S., Dahlström, K. M., & Salminen, T. A. (2020). Human copper-containing amine oxidases in drug design and development. *Molecules*, *25*(6), 1293.

van der Geest, T., Laverman, P., Gerrits, D., Walgreen, B., Helsen, M. M., Klein, C., Nayak, T. K., Storm, G., Metselaar, J. M., Koenders, M. I., & Boerman, O. C. (2017). Liposomal treatment of experimental arthritis can be monitored noninvasively with a radiolabeled anti-fibroblast activation protein antibody. *Journal of Nuclear Medicine*, *58*(1), 151–155.

van der Laken, C. J., Elzinga, E. H., Kropholler, M. A., Molthoff, C. F. M., Van Der Heijden, J. W., Maruyama, K., Boellaard, R., Dijkmans, B. A. C., Lammertsma, A. A., & Voskuyl, A. E. (2008). Noninvasive imaging of macrophages in rheumatoid synovitis using 11C-(R)-PK11195 and positron emission tomography. *Arthritis and Rheumatism*, *58*(11), 3350–3355.

van der Veen, E. L., Suurs, F. V, Cleeren, F., Bormans, G., Elsinga, P. H., Hospers, G. A. P., Lub-de Hooge, M. N., de Vries, E. G. E., de Vries, E. F. J., & F Antunes, I. (2020). Development and evaluation of interleukin-2-derived radiotracers for PET imaging of T-cells in mice. *Journal of Nuclear Medicine*, *61*(9), 1355–1360.

Varasteh, Z., Mohanta, S., Robu, S., Braeuer, M., Li, Y., Omidvari, N., Topping, G., Sun, T., Nekolla, S. G., Richter, A., Weber, C., Habenicht, A., Haberkorn, U. A., & Weber, W. A. (2019). Molecular

imaging of fibroblast activity after myocardial infarction using a 68Ga-labeled fibroblast activation protein inhibitor, FAPI-04. *Journal of Nuclear Medicine*, *60*(12), 1743–1749.

Varela, M. L., Mogildea, M., Moreno, I., & Lopes, A. (2018). Acute Inflammation and Metabolism. *Inflammation*, *41*(4), 1115–1127.

Verweij, N. J. F., Yaqub, M., Bruijnen, S. T. G., Pieplenbosch, S., ter Wee, M. M., Jansen, G., Chen, Q., Low, P. S., Windhorst, A. D., Lammertsma, A. A., Hoekstra, O. S., Voskuyl, A. E., & van der Laken, C. J. (2020). First in man study of [18F]fluoro-PEG-folate PET: a novel macrophage imaging technique to visualize rheumatoid arthritis. *Scientific Reports*, *10*(1), 1047.

Vesalainen, S., Lipponen, P., Talja, M., & Syrjänen, K. (1994). Histological grade, perineural infiltration, tumour-infiltrating lymphocytes and apoptosis as determinants of long-term prognosis in prostatic adenocarcinoma. *European Journal of Cancer*, *30*(12), 1797–1803.

Vestweber, D. (2015). How leukocytes cross the vascular endothelium. *Nature Reviews Immunology*, *15*(11), 692–704.

Virchow, R. (1881). An address on the value of pathological experiments. *British Medical Journal*, *2*(1075), 198–203.

Virtanen, H., Autio, A., Siitonen, R., Liljenbäck, H., Saanijoki, T., Lankinen, P., Mäkilä, J., Käkelä, M., Teuho, J., Savisto, N., Jaakkola, K., Jalkanen, S., & Roivainen, A. (2015). 68Ga-DOTA-Siglec-9 – a new imaging tool to detect synovitis. *Arthritis Research & Therapy*, *17*(1), 308.

Virtanen, H., Silvola, J. M. U., Autio, A., Li, X.-G., Liljenbäck, H., Hellberg, S., Siitonen, R., Ståhle, M., Käkelä, M., Airaksinen, A. J., Helariutta, K., Tolvanen, T., Veres, T. Z., Saraste, A., Knuuti, J., Jalkanen, S., & Roivainen, A. (2017). Comparison of 68Ga-DOTA-Siglec-9 and 18F-Fluorodeoxyribose-Siglec-9: Inflammation Imaging and Radiation Dosimetry. *Contrast Media & Molecular Imaging*, *2017*, 7645070.

Vivier, E., Ugolini, S., Blaise, D., Chabannon, C., & Brossay, L. (2012). Targeting natural killer cells and natural killer T cells in cancer. *Nature Reviews Immunology*, *12*(4), 239–252.

Watabe, T., Liu, Y., Kaneda-Nakashima, K., Shirakami, Y., Lindner, T., Ooe, K., Toyoshima, A., Nagata, K., Shimosegawa, E., Haberkorn, U., Kratochwil, C., Shinohara, A., Giesel, F., & Hatazawa, J. (2020). Theranostics Targeting Fibroblast Activation Protein in the Tumor Stroma: 64Cu- and 225Ac-Labeled FAPI-04 in Pancreatic Cancer Xenograft Mouse Models. *Journal of Nuclear Medicine*, *61*(4), 563–569.

Weiner, R. E., Sasso, D. E., Gionfriddo, M. A., Thrall, R. S., Syrbu, S., Smilowitz, H. M., & Vento, J. (2001). Early detection of oleic acid-induced lung injury in rats using 111In-labeled anti-rat intercellular adhesion molecule-1. *Journal of Nuclear Medicine*, *42*(7), 1109–1115.

Weiner, R. E., Sasso, D. E., Gionfriddo, M. A., Syrbu, S. I., Smilowitz, H. M., Vento, J., & Thrall, R. S. (1998). Early detection of bleomycin-induced lung injury in rat using indium-111-labeled antibody directed against intercellular adhesion molecule-1. *Journal of Nuclear Medicine*, *39*(4), 723–728.

Weinstein, E. A., Liu, L., Ordonez, A. A., Wang, H., Hooker, J. M., Tonge, P. J., & Jain, S. K. (2012). Noninvasive determination of 2-[18F]-fluoroisonicotinic acid hydrazide pharmacokinetics by positron emission tomography in Mycobacterium tuberculosis-infected mice. *Antimicrobial Agents and Chemotherapy*, *56*(12), 6284–6290.

Werner, S. G., Langer, H. E., Ohrndorf, S., Bahner, M., Schott, P., Schwenke, C., Schirner, M., Bastian, H., Lind-Albrecht, G., Kurtz, B., Burmester, G. R., & Backhaus, M. (2012). Inflammation assessment in patients with arthritis using a novel in vivo fluorescence optical imaging technology. *Annals of the Rheumatic Diseases*, *71*(4), 504–510.

Wild, D., Mäcke, H. R., Waser, B., Reubi, J. C., Ginj, M., Rasch, H., Müller-Brand, J., & Hofmann, M. (2005). 68Ga-DOTANOC: A first compound for PET imaging with high affinity for somatostatin receptor subtypes 2 and 5. *European Journal of Nuclear Medicine and Molecular Imaging*, *32*(6), 724.

Wild, D., Schmitt, J. S., Ginj, M., Mäcke, H. R., Bernard, B. F., Krenning, E., De Jong, M., Wenger, S., & Reubi, J. C. (2003). DOTA-NOC, a high-affinity ligand of somatostatin receptor subtypes 2,

3 and 5 for labelling with various radiometals. *European Journal of Nuclear Medicine and Molecular Imaging*, *30*(10), 1338–1347.

Wilder, R. L. (2002). Integrin alpha V beta 3 as a target for treatment of rheumatoid arthritis and related rheumatic diseases. *Annals of the Rheumatic Diseases*, *61*(Suppl 2), ii96–99.

Wu, C., Li, F., Niu, G., & Chen, X. (2013). PET imaging of inflammation biomarkers. *Theranostics*, *3*(7), 448–466.

Yasuda, H., Toiyama, Y., Ohi, M., Mohri, Y., Miki, C., & Kusunoki, M. (2011). Serum soluble vascular adhesion protein-1 is a valuable prognostic marker in gastric cancer. *Journal of Surgical Oncology*, *103*(7), 695–699.

Yegutkin, G. G., Salminen, T., Koskinen, K., Kurtis, C., McPherson, M. J., Jalkanen, S., & Salmi, M. (2004). A peptide inhibitor of vascular adhesion protein-1 (VAP-1) blocks leukocyte-endothelium interactions under shear stress. *European Journal of Immunology*, *34*(8), 2276–2285.

Yoon, J. T., Longtine, M. S., Marquez-Nostra, B. V, & Wahl, R. L. (2018). Evaluation of next-generation anti-CD20 antibodies labeled with 89ZR in human lymphoma xenografts. *Journal of Nuclear Medicine*, *59*(8), 1219–1224.

Yoong, K. F., McNab, G., Hübscher, S. G., & Adams, D. H. (1998). Vascular adhesion protein-1 and ICAM-1 support the adhesion of tumor-infiltrating lymphocytes to tumor endothelium in human hepatocellular carcinoma. *The Journal of Immunology*, *160*(8), 3978–3988.

Zern, B. J., Chacko, A. M., Liu, J., Greineder, C. F., Blankemeyer, E. R., Radhakrishnan, R., & Muzykantov, V. (2013). Reduction of nanoparticle avidity enhances the selectivity of vascular targeting and PET detection of pulmonary inflammation. *ACS Nano*, *7*(3), 2461–2469.

Zettlitz, K. A., Tavaré, R., Knowles, S. M., Steward, K. K., Timmerman, J. M., & Wu, A. M. (2017). ImmunoPET of malignant and normal B cells with 89Zr- and 124I-labeled obinutuzumab antibody fragments reveals differential CD20 internalization in vivo. *Clinical Cancer Research*, *23*(23), 7242–7252.

Zhang, J. Q., Nicoll, G., Jones, C., & Crocker, P. R. (2000). Siglec-9, a novel sialic acid binding member of the immunoglobulin superfamily expressed broadly on human blood leukocytes. *Journal of Biological Chemistry*, *275*(29), 22121–22126.

Zhang, Y. Z., & Li, Y. Y. (2014). Inflammatory bowel disease: Pathogenesis. *World Journal of Gastroenterology*, *20*(1), 91–99.

Zhou, S., Liang, Y., Zhang, X., Liao, L., Yang, Y., Ouyang, W., & Xu, H. (2020). SHARPIN Promotes Melanoma Progression via Rap1 Signaling Pathway. *Journal of Investigative Dermatology*, *140*(2), 395-403.

Zhu, Z., Yin, Y., Zheng, K., Li, F., Chen, X., Zhang, F., & Zhang, X. (2014). Evaluation of synovial angiogenesis in patients with rheumatoid arthritis using 68Ga-PRGD2 PET/CT: A prospective proof-of-concept cohort study. *Annals of the Rheumatic Diseases*, *73*(6), 1269–1272.

UNIVERSITY OF TURKU

Painosalama Oy, Turku, Finland 2021

ISBN 978-951-29-8359-9 (PRINT)
ISBN 978-951-29-8360-5 (PDF)
ISSN 0355-9483 (Print)
ISSN 2343-3213 (Online)